Technische Universität München
III. Medizinische Klinik am Klinikum rechts der Isar

The Role of Bone Marrow Mesenchymal Stem Cells in Myelodysplastic Syndrome and Acute Myeloid Leukemia

Marie-Theresa Weickert

Vollständiger Abdruck der von der Fakultät für Medizin der
Technischen Universität München zur Erlangung des akademischen Grades
eines Doktors der Naturwissenschaften (Dr. rer. nat.) genehmigten Dissertation.

Vorsitzender: Prof. Dr. Jürgen Ruland

Prüfer der Dissertation:

1. apl. Prof. Dr. Katharina S. Götze
2. Prof. Dr. Bernhard Küster

Die Dissertation wurde am 10.08.2020 bei der Technischen Universität München eingereicht und durch die Fakultät für Medizin am 16.02.2021 angenommen.

Table of Contents

1 Abstract

Myelodysplastic syndrome (MDS) and acute myeloid leukemia (AML) are two hematopoietic disorders that, despite intensive research and therapeutic advances over the last two decades, remain with a poor prognosis, especially for elderly patients. The origin of these diseases is thought to be the accumulation of specific driver mutations and cytogenetic aberrations in hematopoietic precursor cells in the bone marrow (BM). However, more and more evidence accumulates that alterations in the surrounding, non-hematopoietic microenvironment (BM niche) can contribute to or initiate the malignant transformation of the hematopoietic compartment and promote disease progression. One of the key components of the BM niche are mesenchymal stems cells (MSC) that give rise to osteoblasts and adipocytes. All of these different cell types provide a complex signaling network towards the hematopoietic cells and are crucial in regulating their function. Adipo-osteogenic balance was shown to play an important role in the regulation of hematopoiesis. Knockout or overexpression of certain factors in niche cells in mice were shown to trigger the development of *de novo* AML and MDS. Furthermore, analyses of bone marrow from patients with MDS and AML revealed alterations in the genetic profile and function of these MSC.

To further elucidate the role of BM niche cells in the pathogenesis of MDS and AML, we performed functional and molecular analyses of MSC isolated from MDS and AML patients. First, we established a detailed flow cytometric protocol for the prospective isolation of the specifically defined, small MSC population of uncultivated whole bone marrow from patients newly diagnosed with MDS and AML as well as age-matched healthy donor controls. The isolated MDS and AML MSC showed a strongly reduced capacity to form CFU-F (colony-formation unit-fibroblast), an altered phenotype as well as reduced survival rates upon passaging indicating cellular stress. Expression analysis of selected target genes involved in adipo- and osteogenic differentiation as well as Wnt- and Notch-signaling pathways showed significantly reduced levels of *DLK1*, an adipogenic inhibitor, in MDS and AML MSC samples that we also observed on protein level using immunoblotting. Additionally, we found increased expression of the activating Notch ligand *JAGGED1* in AML MSC and several MDS MSC samples that is consistent with previous findings in mice showing upregulated JAGGED1 in solid and hematologic cancers contributing to tumorigenesis. Matching our observation of decreased *DLK1* levels in primary MDS and AML MSC, functional analysis showed significantly increased *in vitro* adipogenic differentiation potential in malignant MSC.

Overall, our data showed an altered molecular and functional profile in MSC from MDS and AML patients indicating a shift towards the adipogenic lineage that is likely to provide a disease-promoting microenvironment.

2 Zusammenfassung

Myelodysplastisches Syndrom (MDS) und akute myeloische Leukämie (AML) sind zwei hämatopoetische Erkrankungen, die trotz intensiver Forschung und deutlicher therapeutischer Fortschritte in den letzten zwei Jahrzehnten vor allem bei älteren Patienten immer noch eine schlechte Prognose bedeuten. Als Ursprung dieser Erkrankungen wird die Ansammlung spezifischer Mutationen (sog. Treiber-Mutationen) und zytogenetischer Aberrationen in den hämatopoetischen Vorläuferzellen im Knochenmark (KM) gesehen. Es mehren sich jedoch immer mehr Hinweise darauf, dass auch Veränderungen in der nicht-hämatopoetischen Mikroumgebung (KM-Nische) zur malignen Transformation der hämatopoetischen Zellen beitragen oder diese initiieren und somit das Fortschreiten der Erkrankung fördern können. Eine der Schlüsselkomponenten der KM-Nische sind mesenchymale Stammzellen (MSC), welche sich zu Osteoblasten und Adipozyten differenzieren können. Alle diese verschiedenen Zelltypen kommunizieren mittels eines komplexen Signalnetzwerks mit den hämatopoetischen Zellen und sind entscheidend für deren funktionelle Regulation. Es wurde gezeigt, dass das adipo-osteogene Gleichgewicht eine wichtige Rolle bei der Regulation der Hämatopoese spielt. Weiterhin wurde demonstriert, dass Überexpression oder Ausschalten bestimmter Faktoren in Nischenzellen bei Mäusen zur Entwicklung von *de novo* AML und MDS führen kann. Darüber hinaus zeigten Knochenmarksanalysen genetische und funktionelle Veränderungen in MSCs von Patienten mit MDS und AML.

Um die Rolle von KM-Nischenzellen bei der Pathogenese von MDS und AML genauer zu erforschen, wurden in dieser Studie funktionelle und molekulare Analysen von MSC durchgeführt, welche direkt aus dem Knochenmark von MDS- und AML-Patienten isoliert wurden. Zuerst wurde ein detailliertes durchflusszytometrisches Protokoll für die prospektive Isolierung der spezifisch definierten, kleinen MSC-Population aus unkultiviertem Knochenmark von Patienten erstellt, welche eine Erstdiagnose mit MDS und AML erhalten hatten. Als Kontrollen wurde gesundes Spender-KM aus der gleichen Alterspopulation verwendet. Untersuchungen der isolierten MDS- und AML-MSC zeigten eine stark reduzierte Kapazität zur Bildung von CFU-F (Colony-Formation Unit-Fibroblast), einen veränderten Phänotyp sowie reduzierte Überlebensraten nach Passagieren der Zellen, was auf zellulären Stress hinweist. Expressionsanalysen ausgewählter Zielgene, die an der adipo- und osteogenen Differenzierung sowie an Wnt- und Notch-Signalwegen beteiligt sind, zeigte signifikant reduzierte Werte von *DLK1*, einem adipogenen Inhibitor, in MDS- und AML-MSC-Proben, die auch auf Proteinebene mittels Immunoblotting beobachtet wurden. Zusätzlich zeigte sich eine erhöhte Expression des aktivierenden Notch-Liganden *JAGGED1* in AML MSC und mehreren MDS MSC-Proben, was mit vorangegangenen Studien in Mäusen übereinstimmt, welch zeigten, dass eine erhöhte JAGGED1-Expression in soliden und hämatologischen Krebsarten zur Tumorgenese beitrug. In Übereinstimmung mit den verringerten *DLK1*-Leveln in primärem MDS- und AML-MSC zeigten *in vitro* Funktionsanalysen ein signifikant erhöhtes adipogenes Differenzierungspotenzial in malignen MSC. Zusammengefasst zeigen die Daten dieser Studie ein verändertes molekulares und funktionelles Profil in MSC von MDS- und AML-Patienten, was auf eine Verschiebung in

Richtung eines verstärkt adipogen gerichteten MSC-Zellpools hinweist, welcher einen wesentlichen Faktor zu einer krankheitsfördernden Mikroumgebung beitragen könnte.

3 Introduction

3.1 The hematopoietic system

Hematopoietic cells in the blood are crucial for oxygen supply to all body cells, wound healing, and fighting of pathogens. Due to the complexity of these tasks, there are different kinds of specified blood and immune cells, that differ greatly in their morphology and functions. Despite this complexity, the different types of mature blood cells derive from multipotent hematopoietic stem cells (HSC), that form the apex of the hematopoietic hierarchy (see Figure 1). HSC fulfil the two criteria of stem cells, that were first postulated by Till and McCulloch in the 1960s: First, they can regenerate themselves upon cell division (self-renewal), and second, they are able to generate all types of functionally specified blood cells (multipotency) [1–3]. In the classic model of hematopoiesis, HSC terminate their self-renewal capacity in favor of differentiation into more committed multipotent progenitors (MPP) [4]. Subsequently, MPPs differentiate in a stepwise manner towards a specific cell lineage type (see Figure 1).

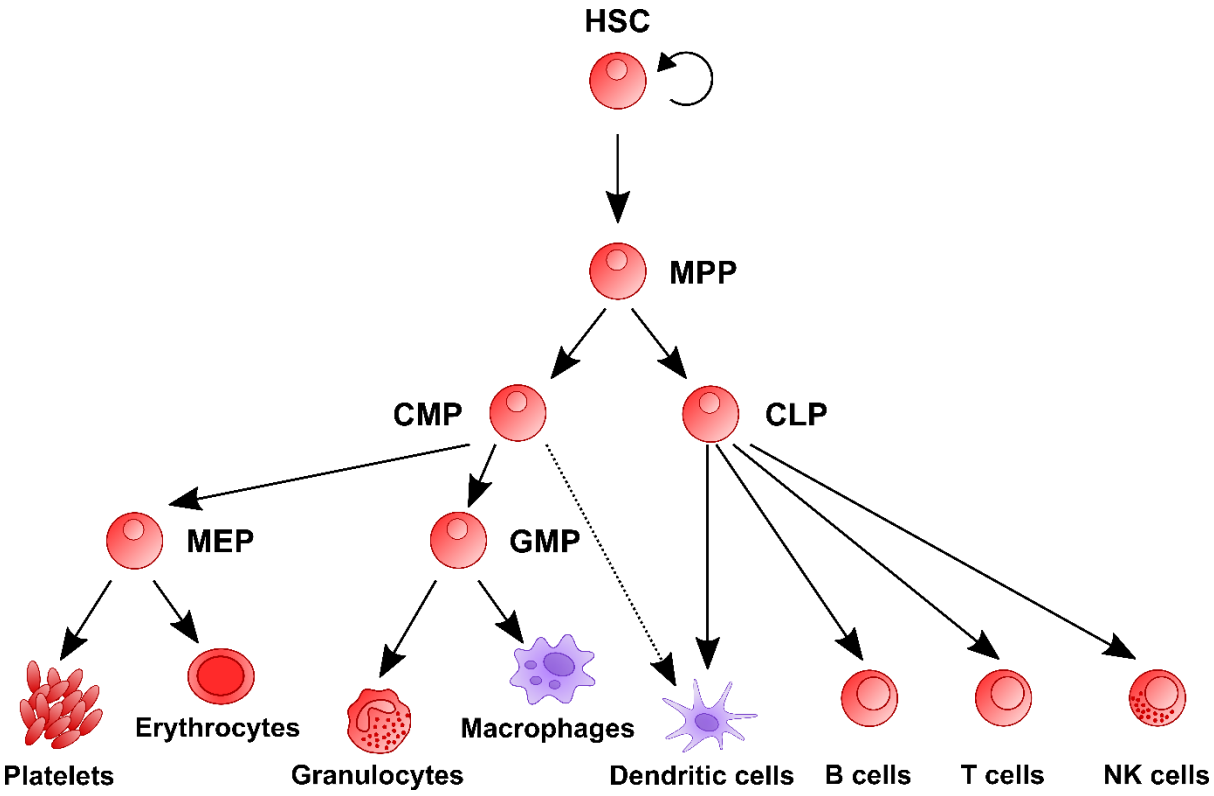

Figure 1: Current model of the hematopoietic hierarchy.

The hematopoietic stem cell (HSC) resides at the apex of the hematopoietic hierarchy and possess both the ability to self-renew, as well as to give rise to all kinds of blood cells (multipotency). In course of differentiation, the HSC first loses its self-renewal capacity, becoming a multipotent progenitor (MPP), before gradually acquiring the identity of a specific mature blood cell lineage in a stepwise manner. In this process of lineage commitment, MPP are thought to give rise to two main lineage committed progenitors: the common myeloid progenitors (CMP), and the common lymphoid progenitors (CLP). CMP then give rise to two myeloid subgroup precursors: the megakaryocyte/erythrocyte precursors (MEP), which can finally differentiate into erythrocytes and megakaryocytes that form the platelets, and the granulocyte/macrophage precursors (GMP) that can give

rise to granulocytes and macrophages. Furthermore, CMP are thought to give rise to a subgroup of dendritic cells. CLP can differentiate into dendritic cells, B cells, T cells, as well as natural killer cells (NK cells).

Due to the limited life-span of terminally differentiated blood cells, there is on the one hand the need of constant reproduction of these cells, with a rate of about 1 million mature blood cells per second [4,5]. On the other hand, under steady-state conditions over 90 % of the multipotent HSC remain in a quiescent state in G_0 phase to preserve their long-term proliferation potential and genomic stability over the whole lifetime of an individual [4,6–8]. As a consequence, the organism has to find a balance between preserving a pool of undifferentiated HSC over the whole lifetime of an individual whilst still keeping up a sufficient production of differentiated, mature blood cells.

With increasing age, HSC are increased in frequency but less quiescent, functionally impaired, can accumulate genetic lesions and DNA damage by ROS, and are skewed towards the myeloid lineage [9–14]. These events are thought to favor the event of clonal hematopoiesis and selection of "pre-leukemic" HSC clones, which bear an increased risk of subsequent malignant transformation [11,15,16].

3.2 Myelodysplastic syndrome and acute myeloid leukemia

3.2.1 Myelodysplastic syndrome

Myelodysplastic syndrome (MDS) is a heterogeneous clonal disorder of the hematopoietic system that occurs mainly in elderly patients (median 68 – 75 years) with an incidence of 3 – 4/100,000 individuals (US population) that increases with age. MDS is characterized by an insufficient hematopoiesis and presence of dysplastic cells of hematopoietic lineages in the bone marrow, as well as one or more cytopenia(s) in the periphery, and bear an increased risk of transformation into acute myeloid leukemia (AML). Patients typically suffer from anemia, bleeding, and infections [17].

MDS is classified by scoring systems of the World Health Organization (WHO), the international prognostic scoring system (IPSS), or the revised IPSS (IPSS-R) according to factors such as dysplasia of one or more hematopoietic cell lineages, peripheral cytopenias, percentage of BM blasts, and molecular and cytogenetic characteristics (see Table 1). The scoring systems are used to assign the patients to specific risk subgroups in order to personalize the treatment as much as possible to the individual patient [18–20]. Median survival rates according to the IPSS risk subgroups are 5.7 years for low risk, 3.5 years for INT-1, 1.2 years for INT-2, and 0.4 years for high risk [20,21]. Treatment goals for lower risk patients are improvement of cytopenia with subsequent reduction of transfusion needs and infection rates, prevention of progress to a higher risk group or AML, and improvement of survival. The goal for higher risk patients is the prolonging of survival. Current treatment strategies include supply with hematopoietic growth factors, hypomethylating agents, immunomodulatory drugs, chemotherapy, and allogeneic stem cell transplantation. Management of MDS is hampered by the fact that older patients are no candidates for intensive chemotherapy or

treatment regimens concerning treatment-related mortality due to poor performance status and higher comorbidity scores within the elderly. Furthermore, patients with transition of MDS to AML have reduced response rates to therapy compared to patients with *de novo* AML [17,20].

Table 1: WHO classification of myelodysplastic/myeloproliferative neoplasms (MDS/MPN), and myelodysplastic syndrome (MDS) (Arber et al., 2016).

Myelodysplastic/myeloproliferative neoplasms (MDS/MPN)
Chronic myelomonocytic leukemia (CMML)
Atypical chronic myeloid leukemia (aCML), BCR-ABL12
Juvenile myelomonocytic leukemia (JMML)
MDS/MPN with ring sideroblasts and thrombocytosis (MDS/MPN-RS-T)
MDS/MPN, unclassifiable
Myelodysplastic syndrome (MDS)
MDS with single lineage dysplasia
MDS with ring sideroblasts (MDS-RS)
MDS-RS and single lineage dysplasia
MDS-RS and multilineage dysplasia
MDS with multilineage dysplasia
MDS with excess blasts
MDS with isolated del(5q)
MDS, unclassifiable
Provisional entity: Refractory cytopenia of childhood

3.2.2 Acute myeloid leukemia

Acute myeloid leukemia is a highly heterogeneous clonal disorder of the hematopoietic system, where undifferentiated blasts of the myeloid lineage proliferate heavily in the BM and displace healthy hematopoiesis [22,23]. Clinical symptoms of AML patients are similar to that of MDS patients, but disease progression is highly accelerated [24,25]. AML can occur as a *de novo* disease, as a secondary AML (sAML) from prior hematologic malignancies like MDS or myeloproliferative neoplasms (MPN), or after exposure to chemotherapeutics or radiation therapy (therapy-induced AML; tAML) [23]. With a case number of about 80 %, AML is the most common form of acute leukemias in adults [25]. AML has an incidence of 3.4 – 5/100,000 individuals in the US population, with a median age of 68 years at diagnosis [25,26]. Incidence is increasing with age, with about 1.3/100,000 individuals in patients < 65 years, up to 12.2/100,000 individuals in patients older than 65 years [23,24]. From formerly being a terminal disease, AML curative rates have been improved to 35 – 40 % in patients ≤ 60 years. However, the prognosis for patients older than 60 years is still poor with only 5 – 15 % being cured [27]. Another problem is that elderly and frail patients are more likely to not being eligible for intensive chemotherapy, being mirrored in a median survival of only 5 – 10 months [22].

Classification of AML is done according to the risk-scoring system of the WHO [18]. For that, blood and bone marrow smears are assessed, with the key factor of

≥ 20 % myeloid blasts needed for initial diagnosis. Furthermore, patients are screened for specific surface markers and typical chromosomal and molecular genetic lesions that are needed for classification of specific risk subgroups (see Table 2). Other important factors are age, general performance, and co-morbidities [28]. As for MDS, sub-classification of AML is essential for applying a tailored treatment to the individual patient [18,28]. Initially, patients are assessed for tolerance of an intensive induction chemotherapy, which is normally a "7+3" regimen (continuous infusion of cytarabine for 7 days and anthracycline for 3 days). In case of complete remission (< 5 % blasts in the BM) patients are administered with a post-remission-therapy that includes standard chemotherapy or hematopoietic stem cell transplantation (HSCT), depending on their risk status, to erase minimum residual disease (MDR) and prevent disease relapse [22,28]. Although the majority of the patients reach complete remission, the relapse rate within 3 years remains very high [29].

Table 2: WHO classification of acute myeloid leukemia and related neoplasms (Arber et al., 2016).

Acute myeloid leukemia (AML) and related neoplasms
AML with recurrent genetic abnormalities
AML with t(8;21)(q22;q22.1);RUNX1-RUNX1T1
AML with inv(16)(p13.1q22) or t(16;16)(p13.1;q22);CBFB-MYH11
APL with PML-RARA
AML with t(9;11)(p21.3;q23.3);MLLT3-KMT2A
AML with t(6;9)(p23;q34.1);DEK-NUP214
AML with inv(3)(q21.3q26.2) or t(3;3)(q21.3;q26.2); GATA2, MECOM
AML (megakaryoblastic) with t(1;22)(p13.3;q13.3);RBM15-MKL1
Provisional entity: AML with BCR-ABL1
AML with mutated NPM1
AML with biallelic mutations of CEBPA
Provisional entity: AML with mutated RUNX1
AML with myelodysplasia-related changes
Therapy-related myeloid neoplasms
AML, NOS
AML with minimal differentiation
AML without maturation
AML with maturation
Acute myelomonocytic leukemia
Acute monoblastic/monocytic leukemia
Pure erythroid leukemia
Acute megakaryoblastic leukemia
Acute basophilic leukemia
Acute panmyelosis with myelofibrosis
Myeloid sarcoma
Myeloid proliferations related to Down syndrome
Transient abnormal myelopoiesis (TAM)
Myeloid leukemia associated with Down syndrome

3.2.3 Disease origins

The origin of the malignant clones is thought to be the accumulation of sets of specific driver mutations and cytogenetic alterations within the hematopoietic precursors [30–33]. In course of disease progression, the malignant clones gain advantage by superior survival and proliferation over the healthy HSC in a dynamic process called clonal evolution and take over the BM [34,35].

Genome analysis of MDS patients by sequencing revealed the acquisition of several somatic mutations of genes involved in RNA splicing, DNA modification and repair, regulation of transcription, signal transduction, and chromatin modification [33,36,37], with 78 – 89 % of the MDS patients carrying one or more oncogenic mutations [37,38]. Furthermore, chromosomal lesions are present in over 50 % of MDS patients, which are important for disease risk stratification and therefore prognosis and clinical outcome of the individual patient. For example, deletion at chromosome 5 or 11 is normally associated with a favorable outcome, whereas monosomy 7 or complex karyotypes (>3 abnormalities) indicate a poor prognosis [19]. In MDS, it is supposed that early driver mutations in genes, typically involved in RNA splicing, are setting the course for disease evolution and clinical features, with a negative correlation of disease-free survival and number of driver mutations [37,38].

Similarly, sequencing analysis of AML patients showed a very heterogeneous cytogenetic and mutational landscape. Chromosomal aberrations were found in 50 % of patients, with certain abnormalities associated with favorable (e. g. t(8;21)) or poor (e. g. complex karyotypes) outcome [22,35]. Mutations in cytogenetically normal (CN) patients are important for risk classification and therapeutic decisions. Recurrent driver mutations in this class are categorized according to the affected functions into nine groups: Activated signaling (e. g. receptor tyrosine kinases), DNA methylation, chromatin modifiers, tumor suppressors, nucleophosmin 1 (NPM1), myeloid transcription factors, transcription factor-fusions, cohesin complex, and spliceosome complex [39]. The current model of clonal evolution in AML is the co-occurrence of two non-synonymous driver mutations that act synergistically to induce leukemia by activation of specific epigenetic and transcriptional events [34,35].

Next to the acquisition of driver mutations in the HSC pool, there is increasing evidence that not only the hematopoietic compartment but also the surrounding bone marrow (BM) microenvironment is involved in development and progression of hematopoietic malignancies, supporting the “bad seed in bad soil” hypothesis, which was first described by Stephen Paget in 1889, stating that a tumor cell (the “seed”) needs an appropriate environment (the “soil”) to form metastases [40,41].

3.3 The bone marrow niche

The BM microenvironment, also called the BM niche, consists of a variety of different cells, amongst them mesenchymal stem cells (MSC) that can differentiate into osteoblasts and adipocytes, endothelial cells, neuronal cells, and pericytes. Pericytes derive from mesenchymal origin and include a variety of stroma cells with high redundancy (about 90 %), such as pericytic MSC, Nestin-expressing cells, and CXCL12-abundant reticular (CAR)

cells [42–45]. Crosstalk of hematopoietic stem cells (HSC) with the surrounding niche via secreted factors or by direct interactions is crucial for regulation of hematopoietic function (see Figure 2). Since the first description of the bone marrow niche concept in 1978 by R. Schofield [46], research on its components and their interplay led to the current model that specific niche subregions harbor HSC with distinct states of activation.

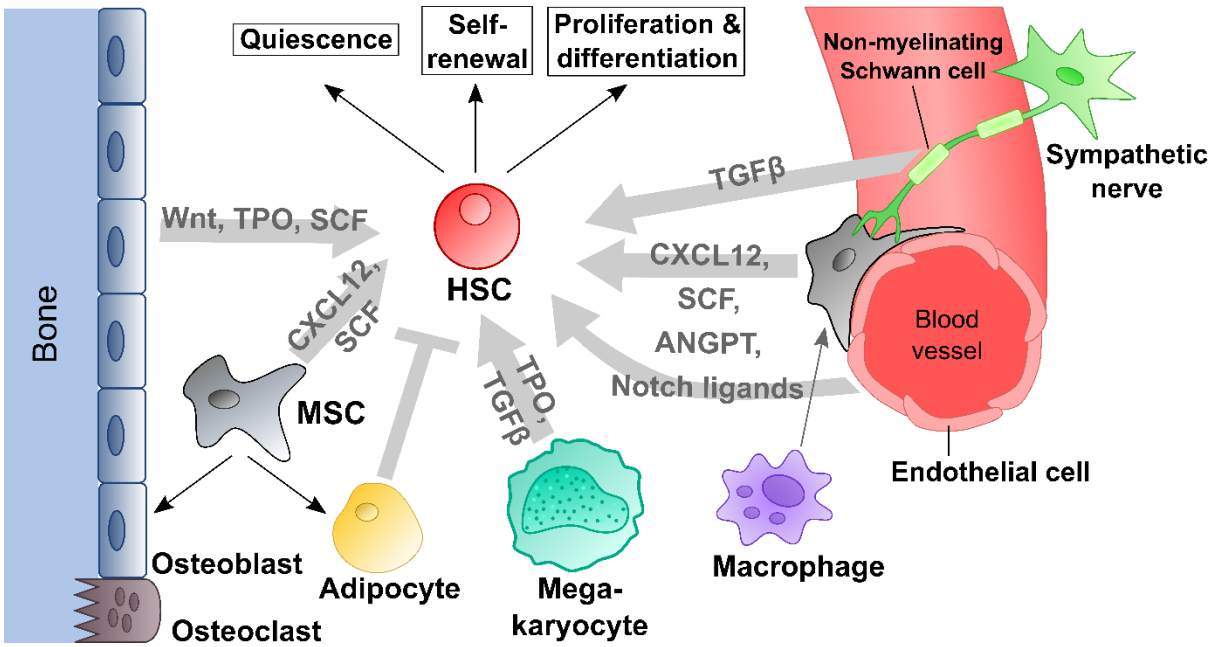

Figure 2: Model of the bone marrow niche.

Within the bone marrow, hematopoietic stem cells (HSC) interact with their microenvironment, the bone marrow niche, that comprises a variety of different non-hematopoietic cells such as osteoblasts, mesenchymal stem cells (MSC), endothelial cells, macrophages, megakaryocytes, adipocytes, and non-myelinating Schwann cells around sympathetic neurons. The niche provides complex signaling cues via soluble ligands and direct cell-cell-interactions that regulate HSC activity, proliferation, and differentiation, depending on the localization of the HSC in distinct sub-niches near the inner bone surface (endosteal niche), or close to blood vessels (arteriolar and sinusoidal perivascular niches). ANGPT, angiopoietin; CXCL12, C-X-C motif chemokine 12; SCF, stem cell factor; TGFβ, transforming growth factor β; TPO, thrombopoietin; Wnt, Wnt pathway ligands.

In the endosteal niche, close to the inner bone surface, HSC closely interact with bone-lining osteoblasts, MSC, and pericytes, which keep them in a deeply quiescent (dormant) state by producing maintenance and quiescence factors such as thrombopoietin (TPO), vascular cell adhesion molecule 1 (VCAM-1), stem cell factor (SCF), and angiopoietin (ANGPT) [44,47]. Most HSC, however, are located close to blood vessels in so-called perivascular niches. Along arterioles, that can also be located near the endosteum, the perivascular arteriolar niche comprises quiescent HSC, endothelial cells, pericytic mesenchymal stem and progenitor cells (MSPC), Nestin-expressing pericytes, as well as sympathetic neurons that regulate circadian CXCL12 release by pericytes. Furthermore, non-myelinating Schwann cells along the neuronal axons, and megakaryocytes express transforming growth factor beta (TGFβ), which also contributes to HSC quiescence [42,43,45]. In contrast, activated HSC and hematopoietic progenitors are mostly located in the perivascular sinusoidal niche close to sinusoid vessels that are more distant from the endosteum. Non-hematopoietic compartments of this niche

include CXCL12- and SCF-producing pericytic MSPC, CAR cells, and Nestin-expressing cells, as well as endothelial cells, and TPO-producing megakaryocytes. Furthermore, there are macrophages that support the production and release of CXCL12 by pericytes [42–45].
Next to these sub-niches, adipocytes are located all over the bone marrow cavity. Initially thought of as mere space fillers, it turned out that adipocytes have an inhibitory effect on HSC number, although more detailed studies are needed to unravel the underlying molecular mechanisms [42,48].

3.4 Mesenchymal stem cells

The current concept of MSC is founded on the work of Friedenstein and colleagues in the 1960s and 1970s, who found a subset of non-hematopoietic stroma cells with osteogenic potential in the BM by performing heterotopic BM transplantations [49–53]. Seeded at clonal density *in vitro*, single BM cells were able to clonally form adherent colonies with fibroblastic morphology (colony-forming unit-fibroblast, CFU-F) that had the potential to differentiate into skeletal tissues, such as osteoblasts, adipocytes, and chondroblasts [52,54–56]. *In vivo* transplantation assays showed that a single BM stroma cell was able to initiate the formation of several types of skeletal tissues [50,57–59]. These demonstrations of multipotency and self-renewal led to the introduction of the term “osteogenic” or “stromal” stem cell by Friedenstein and Owen, which was substituted by “mesenchymal stem cell” in 1991 by Caplan [58–60]. This new term occurred at the same time as another, different MSC concept, in which “mesenchymal” also referred to progeny of non-skeletal identity (e. g. smooth muscle cells, and myocard), which led to confusion in the field, and is not yet formally proven *in vivo* and therefore still controversial [57]. However, the term “mesenchymal stem cell” gained a high popularity and is now mainly used for non-hematopoietic BM cells that fulfil the following minimal key criteria for multipotent mesenchymal stromal cells postulated by the International Society for Cellular Therapy: (1) MSC must be plastic-adherent in *in vitro* culture; (2) MSC must be positive for expression of the surface markers CD105, CD73, and CD90, and negative for CD45, CD34, CD14 or CD11b, CD79a or CD19, and HLA-DR expression; (3) MSC must possess *in vitro* differentiation potential into osteoblastic, adipocytic, and chondrocytic lineage [61]. Supporting this, Sacchetti and colleagues were the first to proof *bona fide* MSC in humans, by showing that prospectively surface marker-isolated MSC, which were able to form multipotent CFU-F *in vitro*, are the counterparts of *in situ* perivascular BM stroma cells, and are able to form niche structures with invading hematopoiesis in serial heterotopic transplants [62].

3.5 The role of the BM niche in malignant transformation

Not only mutations in the hematopoietic compartment, but also aberrations in the surrounding BM niche cells can support or induce malignant transformation of HSC. In 2010, Raaijmakers and colleagues showed in a mouse model that deletion of the *Dicer1* gene in osteoprogenitors results in development of MDS with partial transition to sAML, accompanied by a downregulation of the *Shwachman-Bodian-Diamond syndrome* (*Sbds*)

gene. In humans, inactivating mutations of *SBDS* are frequently observed in the eponymous clinical syndrome, which displays BM failure and increased risk of developing MDS and sAML. Deletion of *Sbds* in mouse osteoprogenitors recapitulated the *Dicer1*-knockout findings, including BM failure and myelodysplasia, indicating a niche-based induction of tumorigenesis [63]. Four years later, Kode and co-workers showed that constitutively active β-catenin expression in mouse osteoblasts led to the development of AML, mediated by increased Notch pathway signaling. Matching that, they found increased levels of nuclear β-catenin and increased β-catenin signaling in osteoblasts as well as increased Notch signaling in hematopoietic cells in 38 % of patients with AML or MDS [64,65]. In humans, supporting evidence for niche-induced oncogenesis are mainly the rare cases of donor-derived leukemia upon BM transplantation, where a dysregulated recipient niche is thought to support the malignant transformation of a genetically predisposed but yet unobtrusive HSC clone from the donor [66,67]. Next to that, there are data that indicate a remodeling of the healthy towards a disease-promoting niche during malignant transformation. Several studies showed abnormalities in MSC from MDS and AML patient samples on molecular and functional level, such as chromosomal aberrations, alterations in transcriptome and epigenetics, as well as changes in cytokine secretion, support of HSC, and differentiation potential (reviewed in [45,66,68,69]).

The adipo-osteogenic balance of the niche is important for proper regulation of hematopoietic function [70,71]. As mentioned before, osteoblasts are an important niche component and regulate HSC activity, proliferation and localization by expression of soluble factors such as TPO and CXCL12, or membrane-bound ligands for direct cell-cell-interaction like osteopontin [40]. In the last decade, several studies were published that showed an inhibitory effect of adipocytes on healthy HSC. In 2009, Naveiras and colleagues were the first to proof that adipocytes are negative regulators of hematopoiesis [48]. Furthermore, it was shown that an increased amount of adipocytes due to obesity or in course of ageing has a negative impact on hematopoietic regeneration [72,73]. Matching these observations are findings showing that inhibition of adipogenesis improves hematopoietic recovery upon chemotherapy [74]. In addition, it was recently shown that adipocyte metabolism is re-programmed in AML, conferring a selective advantage to the leukemic blasts by promoting their survival and proliferation [75].

However, conflicting data exist about the differentiation potential in MSC from MDS and AML patients. There are publications showing no change in adipo- and osteogenic differentiation potential at all, whereas others showed increase or decrease of one or both pathways (reviewed in [40]). Further research is needed for evaluation of the role of adipo-/osteogenic differentiation of the BM niche in course of hematopoietic malignancies and its consequences on HSC regulation.

3.6 The adipogenic inhibitor Delta-like 1

Delta-like 1 (DLK1), also called preadipocyte factor 1 (Pref-1), is a cell surface transmembrane glycoprotein that belongs to the Notch/Delta/Serrate family of epidermal growth factor (EGF)-like repeat-containing proteins, and is a known inhibitor of adipogenesis [76].

In humans, it is located on chromosome 14 and is maternally imprinted, which means that only the paternally inherited allele is expressed. The DLK1 protein consists of an extracellular domain with a signal sequence, six EGF-like-repeats, a juxtamembrane domain containing a proteolytic cleavage site, a helical single-pass transmembrane domain, and a short cytoplasmic tail [77–79]. DLK1 can be cleaved by the TNFα-converting enzyme (TACE)-protease to generate a soluble ligand [80,81]. Controversial data exist if the soluble or only the membrane-tethered form of DLK1 is crucial for inhibition of adipogenesis [80–83]. In contrast to other Notch/Delta/Serrate family members, it lacks the typical DSL domain that is essential for the interaction with Notch receptors via the EGF-like repeats, and was therefore initially thought to be an orphan Notch ligand [84,85]. However, there are contrary findings concerning its mode of action. On the one hand, DLK1 was shown to operate Notch-independently by interacting with fibronectin on the surface of cells, transmitting the signal into the cell via integrins, where it comes to activation of the mitogen activated protein (MAP)-kinase cascade. This leads to SRY-box 9 (SOX9)-mediated blocking of the promoter regions of early adipogenic transcription factors like CEBPβ/δ (CCAAT/enhancer binding protein β/δ), thereby inhibiting progress of adipogenic differentiation by keeping the cell in a pre-adipocytic state [86,87]. On the other hand, it was shown that DLK1 interacts specifically with NOTCH1 via specific regions in their EGF-like-repeat domains. The DLK1-NOTCH1-interaction leads to inhibition of Notch signaling with decreased levels of its downstream target HES-1, resulting in an inhibition of adipogenesis [88–91]. Furthermore, interaction of DLK1 with the insulin-like growth factor binding protein 1 (IGFBP1) was reported in 3T3-L1 cells, modulating their adipogenic differentiation potential by regulation of insulin-like growth factor 1 (IGF-1) release [92].

3.7 Aim of this study

Although extensively studied, the treatment management of MDS and AML remains difficult, especially for elderly patients being ineligible for intensive chemotherapy regimens facing high mortality rates. More and more evidence accumulates that BM-MSC from malignant niches display distinct features to be altered from healthy BM-MSC and that these differences are likely to be contributing or even able to initiate the formation of leukemic stem cells [40,64,93–97]. Therapeutically targeting the niche, next to chemotherapy for clearing the malignant HSC clone, could be of great importance to improve patient prognosis and outcome. However, the involved pathways and detailed mechanisms in malignant transformation of the niche in MDS and AML as well as their consequences on healthy and leukemic hematopoietic cells remain mostly elusive, yet.

To shed more light on this issue, this study aims in a detailed analysis of MSC from primary BM samples of patients with MDS and AML in order to investigate differences on molecular and cellular level, giving more insight in the biological pathways involved in the transformation of healthy to leukemic niche cells. In contrast to other studies, which often use MSC selected only by their ability of plastic-adherence, a detailed flow cytometric sorting approach based on positive and negative surface marker expression will be used for prospective isolation of the rare MSC population from whole BM samples of patients newly diagnosed with MDS and AML, as well as age-matched healthy donor samples. The isolated

healthy and malignant MSC will be characterized according to their compliance with the minimal MSC key criteria, and analyzed for possible differences concerning their subpopulation frequency, CFU-F frequency, and survival upon passaging.

Transcriptome analysis of freshly isolated, uncultured MSC from healthy and malignant samples will be conducted to identify new dysregulated pathways and target genes when comparing healthy to malignant conditions. Furthermore, expression levels of likely altered genes, such as key regulators of the adipo-/osteogenic differentiation pathways including *DLK1*, as well as genes involved in Wnt and Notch pathway signaling, will be compared in healthy and malignant MSC samples. Functional analyses of the malignant MSC will be performed to get more clues about possible new target molecules involved in regulation of the adipo-osteogenic differentiation potential in context of malignant transformation.

4 Material and Methods

4.1 Material

4.1.1 Laboratory instruments and equipment

Table 3: Laboratory instruments and equipment.

Instrument	Name	Company
Flow Cytometer	CyAn ADP LxP8	Beckmann Coulter, California, USA
Cell Sorter	MoFlo Legacy	Beckmann Coulter, California, USA
Microscope	Axiovert 25	Zeiss, Jena, Germany
Camera of Microscope	Axiocam ICc1	Zeiss, Jena, Germany
Centrifuge		Heraeus Holding GmbH, Hanau, Germany
Thermal Cycler	PTC 100 Peltier	Bio-Rad, Philadelphia, USA
Cell Incubator	Hera Cell 240	Heraeus Instruments, Hanau, Germany
Real-time PCR System	StepOne Plus	Thermo Fisher, Massachusetts, USA
Spectrophotometer	ND-1000 (NanoDrop)	Thermo Fisher, Massachusetts, USA
Microplate Reader	ELx800 Universal Micro-plate Reader	BioTek Instruments Inc., Vermont, USA
Immunoblotting System	Mini Trans-Blot, Wet/Tank Blotting System	Bio-Rad, Philadelphia, USA
Bioanalyzer	2100Bioanalyzer	Agilent Technologies, CA, USA
Sequencing Platform	Illumina HiSeq1500	Illumina, CA, USA

4.1.2 Reagents and commercial kits

Table 4: Reagents and commercial kits.

Reagent/Kit	Company
Biocoll (1,077 g/L)	Merck, Darmstadt, Germany
FCS (Batch-No. 0742C)	Merck, Darmstadt, Germany
Trypsin (0.5 %)	Thermo Scientific, Massachusetts, USA
PBS (1x)	Thermo Scientific, Massachusetts, USA
HEPES 1M	Thermo Scientific, Massachusetts, USA
HBSS (10x)	Thermo Scientific, Massachusetts, USA
Penicillin-Streptomycin	Thermo Scientific, Massachusetts, USA
Oil Red O	Sigma-Aldrich, Missouri, USA
Alizarin Red	Sigma-Aldrich, Missouri, USA
RNeasy Micro Kit	Qiagen, Hilden, Germany
RNeasy Mini Kit	Qiagen, Hilden, Germany
Omni Script RT Kit	Qiagen, Hilden, Germany

Power SYBR™ Green PCR Master Mix	Thermo Scientific, Massachusetts, USA
DC Protein Assay Kit II	Bio-Rad, California, USA
4-15% Mini-PROTEAN TGX Stain-Free Protein Gel	Bio-Rad, California, USA
SuperSignal West chemiluminescent substrate	Thermo Scientific, Massachusetts, USA
StemMACS HSC-CFU complete with Epo	Miltenyi Biotech, Bergisch Gladbach, Germany
BIT 9500 Serum Substitute	Stemcell Technologies
Biocoll Solution (1.077 g/ml)	Biochrom GmbH, Berlin, Germany
Ciprofloxacin	Life Tech, California, USA
Penicillin-Streptomycin (1:100)	Life Tech, California, USA
α-MEM (1g/L Glucose, Cat. No. M4526)	Sigma-Aldrich, Missouri, USA
α-MEM, GlutaMAX	Life Tech, California, USA
IMDM, GlutaMAX	Life Tech, California, USA
Heparin 5000 U/ml	Biochrom GmbH, Berlin, Germany
L-Glutamine 200 mM	Sigma-Aldrich, Missouri, USA
DMSO	Sigma-Aldrich, Missouri, USA
Murine recombinant DLK1 (Cat. No. 8545-PR-050)	R&D Systems, Minnesota, USA
CD34 MicroBead Kit, human (Cat. No. 130-046-702)	Miltenyi Biotech, Bergisch Gladbach, Germany

4.1.3 Buffers, solutions and media

Table 5: Buffers, solutions and media.

Name	Ingredients
HF2 buffer	20 ml heat-inactivated FCS 10 ml 1M HEPES 100 ml HBSS (100x) 10 ml Penicillin-Streptomycin ($1e^4$ U/ml) 860 ml ddH_2O (0.22 µm sterile filtered)
Human MSC medium	α-MEM (1g/L Glucose, M4526, Sigma-Aldrich) 2 mM L-Glutamine 10 U/L Heparin (preservative-free, Merck) 20 U/ml Penicillin-Streptomycin (0.22 µm sterile filtered) Add freshly to cell culture: 10 % (v/v) pHPL
Propidium iodide (1 mg/ml)	Dissolve 5 mg propidium iodide powder in 1 ml DMSO Dilute 1:5 in ddH_2O
Adipogenic induction medium	Human MSC medium 1 µM Dexamethasone 60 µM Indomethacin 0.5 mM IBMX 10 µM Insulin

	(0.22 µm sterile filtered)
Osteogenic induction medium	Human MSC medium 1 nM Dexamethasone 0.1 mM L-ascorbic acid-2-phosphate at day 7: add 10 mM β-Glycerolphosphate (0.22 µm sterile filtered)
Oil Red O solution	0.5 g Oil Red O powder 25 ml Acetone 25 ml 70% Ethanol
1x Transfer buffer	3.5 L ddH_2O 1 L Methanol 0.5 L 10x running buffer
10x Running buffer	576 g Glycine 120 g TRIS 40 g SDS ad 4 L ddH_2O
10x TBS	84 g NaCl 24.2 g Tris ad 1 L ddH_2O adjust pH = 7.6
TBS-T	1x TBS 0,1 % Tween 20
Strip buffer	10 % Methanol 10 % Acetic acid ddH_2O
0.1 % gelatin solution	1 % gelatin powder ddH_2O autoclave to sterilize and dissolve dilute 1:10 in ddH_2O
SFM + 5GF medium	20 % BIT 9500 Serum Substitute 80 % IMDM GlutaMAX 10 µM ß-Mercaptoethanol 1:250 Ciprofloxacine 4 µg/ml LDL 100 ng/ml SCF 100 ng/ml FLT3-Ligand 25 ng/ml TPO 10 ng/ml IL-3 10 ng/ml IL-6 (0.22 µm sterile filtered)
LTC medium	100 % Myelokult H5100 10 ng/ml FLT3-Ligand 20 ng/ml TPO 1 µM Hydrocortisone 1:250 Ciprofloxacin e 1:100 L-glutamine (0.22 µm sterile filtered)

EL08-1D2 & UG26-1B6 culture medium	400 ml α-MEM, GlutaMAX (Life Tech) 75 ml FCS (heat-inactivated) 25 ml horse serum (heat-inactivated) 5 ml Penicillin-Streptomycin (1:100) 100 µl β-Mercaptoethanol
Annexin/PI buffer	5ml 1 M HEPES (pH 7,4) 28 ml 2.5 M NaCl 0.18 g $CaCl_2$ 467 ml ddH_2O (0.22 µm sterile filtered)
Alizarine Red solution (40 mM)	0.685 g Alizarin Red powder in 50 ml ddH_2O adjust to pH 4,1

4.1.4 Antibodies

Table 6: Antibodies.

Antibody	Clone	Cat. No.	Company	Dilution
Anti-human CD45, PE Cyanine 7	HI30	25-0459-42	eBioscience	2 µl/1e^7 cells
Anti-human CD105(Endoglin)/FITC	SN6	326-040	Ancell	2 µl/1e^7 cells
PE Mouse Anti-Human CD73	AD2	550257	BD	6,8 µl/1e^7 cells
PerCP Cy5.5 Mouse Anti-Human CD90	5E10	561557	BD	2 µl/1e^7 cells
Alexa Fluor 647 Mouse Anti-Human CD271	C40-1457	560326	BD	9,7 µl/1e^7 cells
CD31 (PECAM-1), eFluor 450	WM-59	48-0319-42	eBioscience	1 µl/1e^7 cells
CD235a (Glycophorin A), eFluor 450	HIR2 (GA-R2)	48-9987-42	eBioscience	1 µl/1e^7 cells
FITC Mouse Anti-Human CD34	581	555821	BD	2 µl/1e^6 cells
CD45-FITC	HI30	11-0459-42	eBioscience	1 µl/1e^6 cells
CD90 (Thy-1)-PE	5E10	12-0909-42	eBioscience	2 µl/1e^6 cells
PE Anti-Human CD14 antibody	M5E2	301806	Biolegend	1 µl/1e^6 cells
FITC Mouse Anti-Human HLA-DR	TU36	555560	BD	1 µl/1e^6 cells
Anti-DLK antibody produced in rabbit	polyclonal	ab119386	Abcam	1:1000
Monoclonal Anti-β-Actin antibody produced in mouse	AC-15	A5441	Sigma	1:5000
Amersham ECL Rabbit IgG, HRP-linked whole Ab (from donkey)		NA934	GE Healthcare	1:10000
Amersham ECL Mouse IgG, HRP-linked whole Ab (from sheep)		NA931	GE Healthcare	1:10000
AnnexinV-APC		550474	BD	1:250

4.1.5 Primers

Table 7: Primers.

Primer	Sequence (5' to 3')
DLK1 fw	GACGGGGAGCTCTGTGATAG
DLK1 rev	GGGGCACAGGAGCATTCATA
NOTCH 1 fw	TGAATGGCGGGAAGTGTGAAG
NOTCH 1 rev	CACAGCTGCAGGCATAGTC
NOTCH 3 fw	TTACTACCGAGCCGATCACC
NOTCH 3 rev	CAGAGGAGCTACTGCGTTCC
EIF3 fw	TGTCGGACAGCCAGCTAAAG
EIF3 rev	CCATGATGCTGGACACACTG
JAGGED1 fw	TCGTGCTGCCTTTCAGTTTC
JAGGED1 rev	TACTGTCAGGTTGAACGGTGTC
PPARg fw	GCTGGCCTCCTTGATGAATAA
PPARg rev	ACTCAAACTTGGGCTCCATAAA
LPL fw	TTGGGATACAGCCTTGGAGC
LPL rev	CAGGAGAAAGACGACTCGGG
RUNX2 fw	CAACTTCCTGTGCTCGGTGC
RUNX2 rev	CCCGCCATGACAGTAACCAC
SPP1 fw	GAAGTTTCGCAGACCTGACAT
SPP1 rev	GTATGCACCATTCAACTCCTCG
SFRP1 fw	AATCCAGTCGGCTTGTTCTT
SFRP1 rev	CTAATCTAAATGGCCCTTGCTTTAC
WNT5A fw	CTACGAGAGTGCTCGCATCC
WNT5A rev	CCAGCATGTCTTCAGGCTACA
SOX9 fw	TCGCCACACTCCTCCTCC
SOX9 rev	CTTGCCCGGCTGCACG
AGC1 fw	CCTGGTGTGAGGACGTATGG
AGC1 rev	TGCATAAAAGACCTCACCCTCC
WNT10B fw	AGAGATCACCCACTCCTATGT
WNT10B rev	TCTCTACCACTGTCTCCCATTA
TAGLN fw	CCAGACTGTTGACCTCTTTGA
TAGLN rev	CGGTAGTGCCCATCATTCTT

4.1.6 Primary bone marrow samples

Bone marrow samples were collected from patients newly diagnosed with MDS and AML from diagnostic bone marrow aspiration performed in the hospital ward of the III. Medical Department of Klinikum rechts der Isar, Munich, Germany, after written informed consent. Bone marrow samples of healthy individuals were obtained from remaining femoral heads after hip replacement surgery by courtesy of Dr. Martin Nolde (SANA Klinik, München-Solln, Germany) after written informed consent. Furthermore, bone marrow samples from healthy donors were collected from residuals in BM filter bags after stem cell transplantation, which were kindly provided by Aktion Knochenmarksspende Bayern (Gauting, Germany). The use of all human samples was approved by the TUM Ethics Committee in accordance with the Declaration of Helsinki. Patient characteristics are listed in Table 8.

Table 8: Patient characteristics.

Healthy donor samples									
Sample	Age	Sex	Origin	Karyotype	Somatic mutations				
H 4/15	24	m	healthy donor BM	n/a	n/a				
H 8/15	32	f	healthy donor BM	n/a	n/a				
H 9/15	30	f	healthy donor BM	n/a	n/a				
H 10/15	30	m	healthy donor BM	n/a	n/a				
H 12/15	20	m	healthy donor BM	n/a	n/a				
H 15/15	22	m	healthy donor BM	n/a	n/a				
H 16/15	38	f	healthy donor BM	n/a	n/a				
H 17/15	32	m	healthy donor BM	n/a	n/a				
H 20/15	55	m	femoral head	n/a	n/a				
H 23/15	63	f	healthy donor BM	n/a	n/a				
H 26/15	48	m	healthy donor BM	n/a	n/a				
H 30/15	61	f	femoral head	n/a	n/a				
H32/15	48	m	healthy donor BM	n/a	n/a				
H 34/15	42	m	healthy donor BM	n/a	n/a				
H 37/15	37	m	healthy donor BM	n/a	n/a				
H 38/15	42	m	healthy donor BM	n/a	n/a				
H 39/15	46	f	healthy donor BM	n/a	n/a				
H 42/15	80	m	femoral head	n/a	n/a				
H 43/15	29	m	healthy donor BM	n/a	n/a				
H 45/15	26	m	healthy donor BM	n/a	n/a				
H 48/15	78	m	femoral head	n/a	n/a				
H 68/15	47	m	healthy donor BM	n/a	n/a				
H 67/15	49	f	healthy donor BM	n/a	n/a				
H 68/15	47	m	healthy donor BM	n/a	n/a				
H69/16	59	m	healthy donor BM	n/a	n/a				
H 72/15	39	m	healthy donor BM	n/a	n/a				
H 77/15	49	m	healthy donor BM	n/a	n/a				
H 78/15	56	f	healthy donor BM	n/a	n/a				
H 79/15	50	m	healthy donor BM	n/a	n/a				
H 81/15	48	m	healthy donor BM	n/a	n/a				
H 89/16	45	f	healthy donor BM	n/a	n/a				
H 95/16	55	f	femoral head	n/a	n/a				
H 104/16	66	f	femoral head	n/a	n/a				

	Sample	Age	Sex	Origin	Karyotype	Somatic mutations			
Healthy donor samples	H 110/16	64	m	femoral head	n/a	n/a			
	H 117/16	64	f	femoral head	n/a	n/a			
	H 134/16	54	f	femoral head	n/a	n/a			
	H 135/16	55	m	femoral head	n/a	n/a			
	H 136/16	53	m	femoral head	n/a	n/a			
	H 160/16	54	m	femoral head	n/a	n/a			
	H167/16	65	m	femoral head	n/a	n/a			
	H 172/16	64	m	femoral head	n/a	n/a			
	H 175/16	51	m	femoral head	n/a	n/a			
	H 176/16	67	f	femoral head	n/a	n/a			
	H 177/16	56	f	femoral head	n/a	n/a			
	H 186/16	61	m	femoral head	n/a	n/a			
	H 198/16	54	m	femoral head	n/a	n/a			
	H 200/16	49	m	femoral head	n/a	n/a			
	H 217/16	60	m	femoral head	n/a	n/a			
	H 223/17	64	m	femoral head	n/a	n/a			
	H 224/17	64	f	femoral head	n/a	n/a			
	H 228/17	62	f	femoral head	n/a	n/a			
	H 230/17	70	m	femoral head	n/a	n/a			
	H 241/17	50	f	femoral head	n/a	n/a			
	H 250/17	66	m	femoral head	n/a	n/a			
	H 256/17	57	m	femoral head	n/a	n/a			
	H 259/17	70	f	femoral head	n/a	n/a			
	H 269/17	60	m	femoral head	n/a	n/a			
	H 271/17	69	f	femoral head	n/a	n/a			
	H 272/17	56	f	femoral head	n/a	n/a			
	H 281/17	62	f	femoral head	n/a	n/a			
	H 282/17	88	f	femoral head	n/a	n/a			
	H 296/17	77	f	femoral head	n/a	n/a			
	H 301/17	68	f	femoral head	n/a	n/a			
	H 302/17	62	f	femoral head	n/a	n/a			
	H 311/17	63	m	femoral head	n/a	n/a			
	H 315/17	67	f	femoral head	n/a	n/a			

MDS samples

Sample	Age	Sex	Status at biopsy	Karyotype	Somatic mutations	WHO classification	IPSS	IPSS-R
MDS 135/14	75	m	initial diagnosis	46, XY	SF3B1-, ASXL-mutation	MDS-RS-MLD	low risk (0)	low risk (3)
MDS 157/14	58	f	untreated progress	no metaphases	ETV6-, EZH2-mutation	tMDS EB I-II	unknown	unknown
MDS 164/14	73	m	progressing disease	47, XY, +8	ASXL1-, EZH2-mutation	MDS-MLD	int-I (1)	high risk (5)
MDS165/15	77	m	follow up	46, XY	ASXL1, SF3B1	MDS-RS-MLD	low (0)	low (3)
MDS 169/15	74	m	initial diagnosis	46, XY	TET2	CMML-I	int-I (0.5)	intermediate (3.5)
MDS 172/15	72	m	initial diagnosis	46, XY	RUNX1-mutation	MDS-MLD	low risk (0)	low risk (2)
MDS 173/15	77	f	progressing disease	46, XX	SF3B1	MDS-RS-MLD	int-I (0.5)	intermediate (4)
MDS 175/15	66	f	progressing disease	46, XX	no known mutations	CMML-I	int-I (1)	high risk (5.5)
MDS 177/15	86	m	progressing disease	45, X, -Y	SF3B1-, TET2-mutation	MDS-RS-SLD	low risk (0)	low risk (2)
MDS 179/15	58	m	progressing disease	46, XY, der(10)t(8;10)	ASXL1-mutation	MDS EB I	int-II (1.5)	very high risk (6)
MDS 180/15	70	m	progressing disease	45, XY, -7	Kit-D816V	MDS*	-	-
MDS 182/15	66	f	progressing disease	complex	TP53	MDS*	-	-
MDS 195/15	63	f	progressing disease	46, XX	RUNX1-, TET2-mutation	CMML-I	int-I (0.5)	intermediate risk (3.5)
MDS 196/15	62	f	initial diagnosis	46, XX, del(20q)	no known mutations	MDS EB II	int-II (2)	high risk (5.5)
MDS 208/15	75	m	progressing disease	46, XY	RUNX1, TET2, ASXL1	MDS-MLD	int-I (0.5)	intermediate (4.5)
MDS 210/15	70	m	progressing disease	47, XY, +8	ASXL1, RUNX1	MDS*	-	-
MDS 212/15	74	m	untreated progress	45, X, -Y, del(11)(q14)	no known mutations	MDS EB II	high (2.5)	very high risk (6.5)
MDS 215/15	61	f	progressing disease	47, XX, +13	TET2, SRSF2, ASXL1, RUNX1	MDS/MPN overlap	int-II (2)	high (6)
MDS 216/15	87	m	progressing disease	complex	ASXL1, SF3B1	MDS-MLD	int-I (0.5)	intermediate (4.5)
MDS 222/15	84	m	progressing disease	46, XY	ETV6, ASXL1, EZH2	MDS-MLD	int-I (0.5)	intermediate (4)
MDS 227/15	68	f	progressing disease	46, XX	TET2, SF3B1	MDS-EB1	int-I (0.5)	low (3)
MDS 228/15	74	f	initial diagnosis	46, XX	TET2, SRSF2	CMML-I	int-I (0.5)	low (3)
MDS 241/16	75	f	progressing disease	46, XX	SF3B1	MDS-RS-SLD	low (0)	low risk (2)
MDS245/16	40	m	initial diagnosis	47, XY, +8	ASXL1, KMT2A	MDS*	-	-
MDS 261/16	79	m	progressing disease	46,XY	SF3B1, ASXL1	MDS-RS-MLD	low (0)	low (3.5)
MDS 262/16	73	m	initial diagnosis	46, XY	no known mutations	MDS-MLD	low (0)	low risk (2)
MDS 263/16	81	f	initial diagnosis	46, XX	no known mutations	MDS-MLD	low (0)	low (3)
MDS 285/16	50	m	initial diagnosis	46, XY	SF3B1	MDS-RS-MLD	low (0)	low risk (2)
MDS 295/16	82	f	initial diagnosis	46, XX	no known mutations	MDS-MLD	low (0)	low risk (1.5)
MDS 303/16	70	m	initial diagnosis	46, XY	SF3B1	MDS-MLD	low (0)	low risk (1.5)
MDS 307/16	65	f	progressing disease	46, XX	DNMT3A-mutation	MDS-MLD	int-I (0.5)	intermediate risk (4)
MDS 315/16	75	f	progressing disease	46, XX	unknown	MDS-RS-MLD	low risk (0)	low risk (3)
MDS 378/16	70	m	progressing disease	46, X, -Y	TET2-, CBL-mutation	CMML-I	int-I (0.5)	low risk (2)

* later: progression to sAML

AML samples									
Sample	**Age**	**Sex**	**Status at biopsy**	**Karyotype**	**Somatic mutations**	**CD34 blasts**		
AML (M 245/15)	41	w	initial diagnosis *de novo* AML	47, XX, +8	no known mutations	n/a		
AML 624/14	75	m	initial diagnosis *de novo* AML	46, XY	no known mutations	positive		
AML 647/14	76	m	initial diagnosis *de novo* AML	46, XY	NPM1	n/a		
AML 671/15	59	f	initial diagnosis *de novo* AML	complex	CBFB/MYH11 gene fusion	positive		
AML 673/15	63	m	initial diagnosis *de novo* AML	complex	no known mutations	n/a		
AML 675/15	59	f	initial diagnosis sAML (from MDS)	46, XX	NPM1	positive		
AML 677/15	62	m	initial diagnosis *de novo* AML	47, XY, +8	RUNX1	positive		
AML 681/15	56	m	initial diagnosis *de novo* AML	complex	no known mutations	positive		
AML 685/15	59	f	initial diagnosis *de novo* AML	complex	no known mutations	positive		
AML 688/15	84	f	initial diagnosis *de novo* AML	48, XY, +11, +13	no known mutations	positive		
AML 690/15	63	f	initial diagnosis *de novo* AML	46, XX	no known mutations	positive		
AML 701/15	62	m	initial diagnosis sAML (from MDS)	47, XY, +8	no known mutations	positive		
AML 722/15	59	f	initial diagnosis *de novo* AML	46, XX, inv(16)(p13.1q22)	CBFB/MYH11 gene fusion	n/a		
AML 747/15	21	m	initial diagnosis *de novo* AML	46,XY,t(8;21)(q22;q22)	RUNX1/RUNX1T1 fusion transcript	n/a		
AML 766/15	59	m	initial diagnosis *de novo* AML	46, XY	no known mutations	negative		
AML 772/15	46	m	initial diagnosis *de novo* AML	complex	TP53	positive		
AML 781/15	73	f	initial diagnosis *de novo* AML	complex	no known mutations	positive		
AML 808/15	84	m	initial diagnosis *de novo* AML	46, XY	no known mutations	n/a		
AML 814/16	36	f	initial diagnosis *de novo* AML	46, XX	no known mutations	negative		
AML 820/16	54	f	initial diagnosis *de novo* AML	46, XX	NPM1	n/a		
AML 856/16	53	f	initial diagnosis *de novo* AML	46, XX	RUNX1, SF3B1	positive		
AML 858/16	61	m	initial diagnosis *de novo* AML	47, XY, +11	no known mutations	positive		
AML 860/16	60	m	initial diagnosis *de novo* AML	47, XY, +8	no known mutations	negative		
AML 880/16	52	m	initial diagnosis sAML (from MDS-MPN overlap)	46, XY	ASXL1, CBL, KRAS, U2AF1	negative		
AML 903/16	84	f	initial diagnosis *de novo* AML	46, XX	NPM1	negative		
AML 923/16	59	f	initial diagnosis *de novo* AML	46, XX	NPM1	n/a		
AML 949/16	69	m	initial diagnosis *de novo* AML	46, XY	NPM1	n/a		
AML 971/16	51	m	initial diagnosis *de novo* AML	46, XY	NPM2	n/a		
AML 1005/17	73	m	initial diagnosis *de novo* AML	47, XY, +8, duplication 1q21.1	no known mutations	n/a		
AML 1010/17	40	f	initial diagnosis *de novo* AML	46, XX	NPM1	negative		
AML 1023/17	73	f	initial diagnosis *de novo* AML	46, XX, inv(16)(p13.1q22)	no known mutations	n/a		
AML 1100/17	77	m	initial diagnosis *de novo* AML	46, XX	NPM1	n/a		

4.1.7 Cell lines

The stromal cell lines EL08-1D2 and UG26-1B6 were generated from the fetal liver and urogenital ridge subregions, respectively, of murine embryos (E11) transgenic for the temperature-sensitive form of the SV40 large T antigen (tsA58) immortalizing gene [98]. EL08-1D2 and UG26-1B6 cells were kindly provided by Prof. Dr. Robert Oostendorp (III. Medical Department, Klinikum rechts der Isar, Munich, Germany).

Hep G2 (ATCC® HB8065™) were purchased from American Type Culture Collection (Rockville, MD, USA). Hep G2 is an adherent human hepatoblastoma cell line derived from a 15-year-old Caucasian male with hepatocellular carcinoma [99].

4.1.8 Cytokines & lipoprotein

Table 9: Cytokines & lipoprotein.

Reagent	Company
Recombinant human SCF	R&D Systems, Minnesota, USA
Recombinant human Flt3-ligand	R&D Systems, Minnesota, USA
Recombinant human IL-3	R&D Systems, Minnesota, USA
Recombinant human IL-6	R&D Systems, Minnesota, USA
Recombinant human TPO	R&D Systems, Minnesota, USA
Human LDL	Stem Cell Technologies, Vancouver, Canada

4.2 Methods

4.2.1 Isolation of primary BM-MNCs from patient aspirates and femoral heads

Residual femoral heads obtained by hip replacement surgery of healthy individuals were transported the same day to our laboratory under sterile conditions. BM was harvested by disintegrating and mincing the marrow of the femoral heads using bone-cutting forceps. The BM fragments were collected in tubes with PBS and BM cells were isolated mechanically by shaking the BM suspension. The cell suspension was then filtered with a 70 µm cell strainer and BM-MNCs were isolated by density gradient centrifugation. For this, the cell suspension was carefully layered over Biocoll solution in a 2:1 relation followed by centrifugation at 2100 rpm for 20 min without breaks. The interphase containing the MNCs was transferred to a new vial and cells were washed one time with PBS.

Filter bags containing residual BM of healthy donor aspirates used for stem cell transplantations were transported the same day to our laboratory. BM was harvested by reversely flushing the filter bags with PBS and MNCs were immediately isolated via density gradient centrifugation as described above.

Fresh BM aspirates from patients newly diagnosed with AML or MDS were obtained from the hospital directly after aspiration. BM aspirates were diluted in IMDM and BM-MNCs were immediately isolated via density gradient centrifugation as described above.

For storage, BM-MNCs were resuspended in heat-inactivated FCS supplied with 10 % DMSO and aliquots of max. $1e^8$ cells/vial were cooled down in a freezing container for one day in a -80°C freezer. Cells were then transferred into liquid nitrogen for storage until use.

4.2.2 Isolation of stromal cells from primary bone marrow samples via plastic-adherence

Isolation and culture of stromal cells were performed as previously described [100,101]. BM-MNCs were seeded with a density of ca. 80,000 cells/cm^2 directly into human MSC medium. 10 % (v/v) pooled human platelet lysate (pHPL, prepared as described below) was added freshly to the cell culture. Cells were propagated in a humidified incubator at 37 °C and 5 % CO_2. After three days, a complete medium change was performed. During the following culture period, two-third of the medium was changed twice a week. When cells grew confluent, they were detached with trypsin (0.05 % trypsin in PBS, 3 min, 37°C) and re-seeded with ca. 5000 cells/cm^2. Cells were used for experiments until max. passage 4.

Preparation of pHPL (adopted from [100,102]):

Mix thrombocyte concentrates of at least 12 different healthy donors under sterile conditions, aliquot in 50 ml tubes and freeze at -20°C. Thaw in water bath, centrifuge (1500 rpm, 5 min, RT), transfer the supernatant into a new tube and filter through a 100 µM cell strainer. Do again two freeze-and-thaw cycles and centrifuge to get rid of debris. Store at -20°C. For usage, thaw aliquot, filter through 100 µM cell strainer and then filter sterile through a 0.22 nm filter. Store at 4°C and use within 3 weeks.

4.2.3 FACS analysis

For analysis of surface marker expression of cells by FACS, cells were harvested and resuspended in HF2 buffer. Cells were stained with antibodies listed in 4.1.4 for 30 min at 4°C in the dark. Cells were washed with HF2 buffer, resuspended in HF2 buffer + 1:1000 propidium iodide (1 mg/ml stock) and filtered directly before analysis on a CyAn ADP LxP8 flow cytometer (Beckman Coulter) using the FlowJo software (version 7.6.5, FlowJo LLC.). Single stainings of each fluorochrome (coupled to CD45 antibody) used in the analyzed antibody panel as well as an unstained control were analyzed prior to FACS analysis of the respective samples to adjust the voltage of the flow cytometer's photomultiplier in order to maximize signal-to-background resolution.

4.2.4 FACS-based isolation of MSCs from primary bone marrow samples

For FACS purification of MSC, BM-MNCs were thawed, dead cells were removed by density gradient centrifugation (see 4.2.1), and unspecific binding was blocked by incubation in HF2 buffer. Cells were stained (see 4.2.3) with the following surface marker panel: CD45-PE/Cy7, CD31-eFluor 450, CD235a-eFluor 450, CD271- Alexa Fluor 647, CD73-PE, CD105-FITC, and CD90-PerCP/Cy5.5. After forward/sideward scatter gating, doublet and dead cell exclusion (using propidium iodide staining), living cells were sorted on $CD45^-$, lineage $(CD235a/CD31)^-$,

$CD271^+$, $CD73^+$, and $CD105^+$ surface marker expression for purification of MSCs. Cell sorting was performed on a MoFlo Legacy (Beckmann Coulter).

4.2.5 Viability analysis by Annexin/PI-FACS

$CD34^+$ cells (1000 - 2000 cells/sample) were washed with 2 ml Anexin/PI buffer. Cell pellets were resuspended in 500 µl Annexin/PI staining mix (500 µl Annexin/PI buffer + 2 µl AnnexinV-APC + 1 µl PI solution (0.5 mg/ml stock)). Samples were incubated for 15 min at 4°C in the dark and analyzed within 1 h on a CyAn ADP LxP8 flow cytometer (Beckman Coulter) using the FlowJo software (version 7.6.5, FlowJo LLC.). Single stainings of each fluorochrome (coupled to CD45 antibody) used in the analyzed antibody panel as well as an unstained control were analyzed prior to FACS analysis of the respective samples to adjust the voltage of the flow cytometer's photomultiplier in order to maximize signal-to-background resolution. Cells negative for AnnexinV-APC and PI were counted as viable cells.

4.2.6 Culture of sorted primary MSCs

Sorted MSCs were seeded in human MSC medium (+ 10 % freshly added pHPL). Seeding density was in average 1000 cells/cm^2 for healthy donor samples, or 2500 cells/cm^2 for AML and MDS samples, respectively. Cells were propagated in a humidified incubator at 37 °C and 5 % CO_2. Two-thirds of the medium were changed twice a week. When cells grew confluent, they were detached with trypsin (0.05 % trypsin in PBS, 3 min, 37°C) and seeded with about 500-1000 cells/cm^2. Cells were used for experiments until max. passage 4.

4.2.7 CFU-F Analysis of primary MSC

For CFU-F formation analysis, sorted MSCs were seeded as described in 4.2.6. Colony formation was observed every second day for up to four weeks or until colonies grew confluent. Colonies ≥ 25 cells were counted as CFU-F. CFU-F ability was assessed in sets of two or three samples, comprising always one healthy donor sample to ensure integrity of the sorted cells. CFU-F frequency was calculated by dividing the number of colonies by the number of input cells, followed by normalization of colony number on $1e^4$ input cells.

4.2.8 Short-term and long-term co-culture assays

For co-culture assays of hematopoietic and stromal cells, either primary BM-MSCs or the murine EL08-1D2 cell line were used to form a stromal feeder layer. EL08-1D2 cells were used up to passage 15 and cultured as described [98] in murine stroma medium on 0.1% gelatin-coated cell culture plates until 80 % confluent, followed by sublethal irradiation with 30 gy to prevent further proliferation. Irradiated EL08-1D2 cells were allowed to recover for seven days before co-cultures were set up. Primary BM-MSCs were cultured as described in 4.2.6 until 80 % confluent.

For short-term co-culture, sublethally irradiated EL08-1D2 cells or primary BM-MSCs were washed with PBS before adding the hematopoietic cells. Co-culture was performed for 4 days in serum-free medium supplied with five growth factors (SFM + 5GF) without medium change in a humidified incubator at 37 °C and 5 % CO_2.

For long-term co-culture, hematopoietic cells from short-term co-culture were collected and transferred onto a new layer of sublethally irradiated EL08-1D2 cells. Co-culture was performed for 6 weeks in long-term culture medium (LTC medium) with weekly addition of evaporated medium in a humidified incubator at 37 °C and 5 % CO_2.

4.2.9 Colony-forming Cell (CFC) assay of hematopoietic cells

To analyze the capacity of hematopoietic stem and progenitor cells to proliferate and differentiate in the different myeloid lineages, CFC assays of hematopoietic cells after 4 days co-culture (see 4.2.8) were performed using methylcellulose (StemMACS HSC-CFU complete with Epo, Miltenyi Biotech) according to manufacturer's instructions. After 14 days, colonies were scored using standard criteria for evaluation of the different lineage types (CFU-GEMM, CFU-GM, CFU-G, CFU-M and BFU-E).

For the analysis of the more primitive LTC-ICs, CFC analyses of hematopoietic cells after 6 weeks of long-term co-culture on sublethally irradiated EL08-1D2 (see 4.2.8) were performed.

4.2.10 *In vitro* adipo- and osteogenic differentiation of primary MSC

Sorted MSCs (passage 1 or 2) were expanded until confluent (see 4.2.6) and *in vitro* differentiation was induced by replacing the normal MSC medium with adipogenic or osteogenic induction medium. Cells were cultivated in induction medium for 21 days with complete medium change thrice a week. For each patient sample, an additional cell culture supplied with human MSC medium without differentiation-inducing factors was set up and used as negative control for detection of adipocytes/osteoblasts by staining.

For detection of adipocytes by Oil Red staining, cells were washed with PBS and fixed with formalin solution for 45 min at room temperature. Cells were washed with ddH_2O and covered with Oil Red solution for 3 min at room temperature. Oil red solution was removed, and cells were washed with ddH_2O.

For detection of calcium deposits secreted by osteoblasts via Alizarin Red staining, cells were washed with PBS and fixed with 70% ethanol at -20°C for 1h. Cells were rehydrated with ddH2O and covered with Alizarin Red solution, followed by incubation for 10 min at room temperature with gentle rocking on a laboratory shaker. Alizarin Red solution was removed, and cells were washed carefully with PBS.

Staining was analyzed with a light microscope (Axiovert 25 with an Axiocam ICc1 camera, both Carl Zeiss Microscopy) and digitalized using the AxioVision software (Carl Zeiss Microscopy). For quantification, staining intensity was categorized as follows: 0 = no staining, 1 = weak, 2 = medium, 3 =strong, 4 = intensive.

4.2.11 RNAseq of primary MSC

Total RNA was isolated from +/+ sorted primary MSC from healthy donor, MDS and AML samples using the RNeasy Mini Kit (Qiagen). RNA sequencing (RNAseq) library preparation and data processing was performed according to a modified SCRB-seq (Single-Cell RNA-Barcoding and Sequencing) protocol [103]. Briefly, RNA was reverse transcribed with oligo-dT primers carrying sample barcodes and unique molecular identifiers (UMIs). Next, cDNA of all samples was pooled, unincorporated primers digested by Exonuclease I digest and pre-amplified (12 cycles). After quality control of amplified cDNA, the sequencing library was constructed using the Nextera XT Kit (Illumina) and a custom primer enriching for 3' ends of transcripts. Libraries were paired-end-sequenced on an Illumina HiSeq1500, with the first read to decode sample barcodes and UMIs containing 16 cycles, and the second read into the cDNA fragment containing 50 cycles.

All samples were mapped against human (hg19) genome. Gene annotations were obtained from Ensembl gene models (v75).

R version 3.2.0 was used on a x86_64-pc-linux-gnu (64-bit) platform under Ubuntu 14.04.2 LTS for gene expression analysis and visualization.

To remove genes with low expression, MAST filtering [104] was applied and size factors were estimated using the scran package. Normalization was done by DEseq2 [105], where scran size factors were applied. For gene expression analysis, the fits of the negative binomial with a generalized linear model were analyzed. Coefficients (interpreted as the log2-fold changes) were tested using the Wald test.

Principal component analysis was performed on the 500 most variable genes using variance stabilized data. Sample distances were calculated as Euclidean distances and are represented in a heatmap. Hierarchical clustering and plotting as a heatmap was performed using the pheatmap package. All other graphs were drawn using the ggplot2 package.

4.2.12 Gene expression analysis via qRT-PCR

Gene expression levels of MSCs were measured by quantitative reverse transcription polymerase chain reaction (qRT-PCR). MSCs (passage 1 or 2) were harvested using trypsin and total RNA was extracted using the RNeasy Mini Kit (Qiagen) according to manufacturer's instructions. For qRT-PCR analysis of sorted, uncultivated MSC, total RNA was extracted using the RNeasy Micro Kit (Qiagen) according to manufacturer's instructions. Total RNA concentrations and ratios were determined by spectrophotometry using a NanoDrop (Thermo Scientific) and stored at −80°C. In general, 1 µg RNA was transcribed to cDNA using the Omni Script RT Kit (Qiagen) according to manufacturer's instructions. qRT-PCR was performed with Power SYBR™ Green PCR Master Mix (Thermo Scientific) using the StepOnePlus Real-Time PCR System (Thermo Scientific). Primers are listed in 4.1.5.

Reaction (1x)		Program		
10 µl	Power SYBR Green PCR Master Mix	95°C	10 min	
0,5 µl	0,01 mM Primer forward	95°C	15 sec	44 cycles
0,5 µl	0,01 mM Primer reverse	60°C	1 min	
1 µl	cDNA			
8 µl	ddH_2O			

For each patient sample, technical triplicates were analyzed. Relative mRNA expression was calculated by ΔΔCt method and StepOnePlus Software (version 2.3).

4.2.13 Analysis of RNA integrity and yield

RNA integrity and yield from samples after different pre-processing procedures were analyzed on a 2100Bioanalyzer (Agilent Technologies). For that, we incubated thawed healthy donor BM-MSC overnight in HF2 buffer at 4°C, followed by density gradient purification (see 4.2.1) and FACS isolation of MSC (see 4.2.4) on the next day. Additionally, aliquots of the same healthy sample were thawed on the second day, one was purified by density gradient centrifugation before cell sorting, and one was sorted immediately without density gradient purification. Furthermore, BM-MNCs were isolated from a fresh healthy femoral head that was transported to the laboratory the same day, purified by density gradient centrifugation, and immediately sorted. For every sample, 500 +/+ MSC were sorted. This approach was done for three sample sets, with the exception of one set that lacked the sample without density gradient purification. Samples were kept on dry ice directly after sorting of each sample, and total RNA was extracted immediately using the RNeasy Micro Kit (Qiagen) according to manufacturer's instructions. RNA was stored immediately at -80 °C until analysis. All extracted RNA samples were simultaneously analyzed on one chip using the RNA 6000 Pico Kit (Agilent Technologies) on the bioanalyzer. Analysis of results, calculation of RNA concentration and RIN numbers, and visualization of electropherograms was done by Eukaryote Total RNA Pico assay using the 2100Bioanalyzer software (version 2.6).

4.2.14 Protein expression analysis via western blot

For analysis of DLK1 protein expression in MSCs by western blotting, BM-MNCs were sorted on $CD45^-$/lin(CD31/CD235a)$^-$/$CD271^+$ expression, seeded and expanded as described in 4.2.6. Cells were harvested, washed and shock frozen in liquid nitrogen. Cell pellets were thawed on ice, resuspended in lysis buffer and incubated on ice for 20 min. After that, lysates were sonicated (10 sec, 4 cycles, 30 % power). Lysates were centrifuged for 15 minutes at 4°C and 13000 rpm and supernatants were collected. Protein concentration was determined using the DC Protein Assay Kit II (Bio-Rad) following the manufacturer's instructions. Protein absorption was measured at 750 nm using the ELx800 Universal Microplate Reader (BioTek Instruments Inc.) and the Bio Tek Gen5 data analysis software (version 5.2), and protein concentrations were calculated.

40 µg total protein per sample were mixed with 5x loading dye, incubated at 95°C for 10 min and loaded onto a 4 - 15 % Mini-PROTEAN TGX Stain-Free Protein Gel (Bio-Rad) and proteins were separated by SDS-PAGE in an electrophoresis chamber (30 min at 60 V, then 40 min at 120V) in 1x running buffer. Proteins were blotted onto a 0.45 µm PVDF membrane (previously rinsed with methanol) in 1x transfer buffer in a wet-transfer device (Bio-Rad) with 1000 mA for 1h at 4°C. Unspecific binding of antibodies was prevented by blocking the membrane in 5 % BSA in TBS-T for 30 min.

For detection of DLK1, the membrane was incubated overnight at 4°C with anti-DLK primary antibody (1:1000 in 5% BSA in TBS-T). The membrane was washed 3x for 10 min with TBS-T and incubated with anti-rabbit IgG ECL HRP-linked secondary antibody (1:10000 in 5 % BSA in TBS-T) for 30 min. After washing 2x with TBS-T and 1x with TBS, antibody binding was visualized on light-sensitive screens (Kodak) using the SuperSignal West chemiluminescent substrate (Thermo Scientific). Signal intensity was analyzed using the ImageJ software (version 1.6.0).

Antibodies were stripped off the membranes by incubation in strip buffer for 3 min. For protein quantification, ß-ACTIN was detected as housekeeping control using anti-ß-actin primary antibody (1:5000 in 5 % skim milk powder in TBS-T) and anti-mouse IgG ECL HRP-linked secondary antibody (1:10000 in 5% skim milk powder in TBS-T).

4.2.15 Analysis of effects of DLK1-conditioned EL08-1D2 stroma cells on viability and CFU-capacity of hematopoietic cells

For the culture of hematopoietic cells in conditioned medium only (no co-culture on EL08-1D2), sublethally irradiated (30 gy) EL08-1D2 stroma cells were cultured for four days in serum-free medium (SFM, supplemented only with LDL and without the five cytokines) with or without added murine recombinant DLK1 (2,5 µg/ml final concentration). For the third condition (DLK1 extra), SFM conditioned on EL08-1D2 without DLK1 treatment was supplied with murine recombinant DLK1 (2.5 µg/ml final concentration) just before $CD34^+$ culture. Conditioned SFM was collected, supplemented with the five cytokines and sterile filtered. $CD34^+$ hematopoietic cells from healthy donors, MDS, and AML patient samples (n = 3 each) were isolated from thawed whole BM samples by using the human CD34 MicroBead Kit (Miltenyi) according to manufacturer's instructions. $CD34^+$ cells (4000 cells/condition) were cultured in conditioned SFM for four days in a humidified incubator at 37 °C and 5 % CO_2. After four days in the conditioned SFM, $CD34^+$ cells were harvested and Annexin V/PI-FACS analysis (see 4.2.5) and CFC assays (see 4.2.9) were performed.

For cocultures of EL08-1D2 and $CD34^+$ from healthy, MDS, and AML samples, sublethally (30 gy) irradiated EL08-1D2 were used as feeder layer (24-well-plates). To guarantee comparability, the same $CD34^+$ samples were used as in the experiment without EL08-1D2 coculture (see above), with exception of one MDS sample due to limited sample size. $CD34^+$ cells (30000 cells/condition) were resuspended in SFM (including the five cytokines) with or without murine recombinant DLK1 (2.5 µg/ml final concentration) and added onto the EL08-1D2 cell layer. Cocultures were propagated for 4 days in a humidified incubator at 37 °C and

5 % CO_2. After that, $CD34^+$ cells were harvested and Annexin V/PI-FACS analysis (see 4.2.5) and CFC assays (see 4.2.9) were performed.

4.2.16 Statistics

Statistical analyses were performed by Mann-Whitney test, Wilcoxon signed rank test, Log-rank (Mantel-Cox) test, Gehan-Breslow-Wilcoxon test, and linear regression analysis using GraphPad Prism software (version 5.01, GraphPad Inc, La Jolla, CA). *P* values are presented in the figures where a statistically significant difference was found: *, $P < 0.05$; **, $P < 0.01$; ***, $P < 0.001$.

5 Results

5.1 Patient samples and healthy bone marrow sources

A total of 131 human primary bone marrow (BM) samples was analyzed in this study, comprising 66 healthy donor samples, 33 MDS patient samples, and 32 AML patient samples (patient characteristics are listed in Table 8). Healthy donor samples were isolated from iliac crest aspirates as well as from femoral heads after hip replacement surgery.

5.2 Isolation of putative MSC from primary bone marrow samples

Isolation of mesenchymal stem cells (MSC) is often done by using their ability to adhere to plastic surfaces including cell culture dishes [52,53,106]. This method for isolation is not ideal, as it results in a heterogeneous mixture of different kinds of adhesive stroma cells (such as macrophages or endothelial cells), and has no clearly defined starting population [107–112]. Furthermore, there is risk of unpredictable influences by hematopoietic cells that are co-cultured for the first days before removal of non-adherent cells [107,113]. To circumvent these limitations, MSC are frequently isolated from primary BM by their surface marker expression profile using fluorescence-activated cell sorting (FACS) [61,93,114,115].

For a standardized isolation of prospective MSC from all three disease types (AML, MDS, and healthy donor controls), we established a sorting scheme using FACS of bone marrow-mononuclear cells (BM-MNC) from untreated, newly diagnosed AML and MDS patient samples and age-matched healthy donors. Different sets of previously described markers were analyzed, before we came up with our final panel. In the beginning, we were using plastic-adherence selected stroma cells instead of fresh BM-MNC to narrow down on the prospective MSC population (see Figure 3A-C).

At first, we tested a surface marker panel adopted from Pinho et al., where the MSC population was identified by negative expression of the hematopoietic marker CD45 and positive expression of CD146, CD51, and platelet derived growth factor receptor α (PDGFRa) [116]. Our FACS analysis showed only a very small $PDGFRa^+$ population, and an even smaller $CD146^+$ population (see Figure 3A). When expanding the panel with CD31 for exclusion of endothelial cells, the $CD31^-/CD45^-/CD51^+$ population did not show a clear split-up into CD146 positive and negative cells, and no $PDGFRa^+$ cells could be found (see Figure 3B).

Next, we created a surface marker panel modified from Kaltz et al., who showed in a microarray-based approach that the CFU-F forming potential, a key criterion for MSC, is enriched in cells double-positive for CD146 and integrin subunit alpha 11 (ITGA11) expression. Additionally, the microarray data showed the lack of leptin receptor (LepR) expression in the

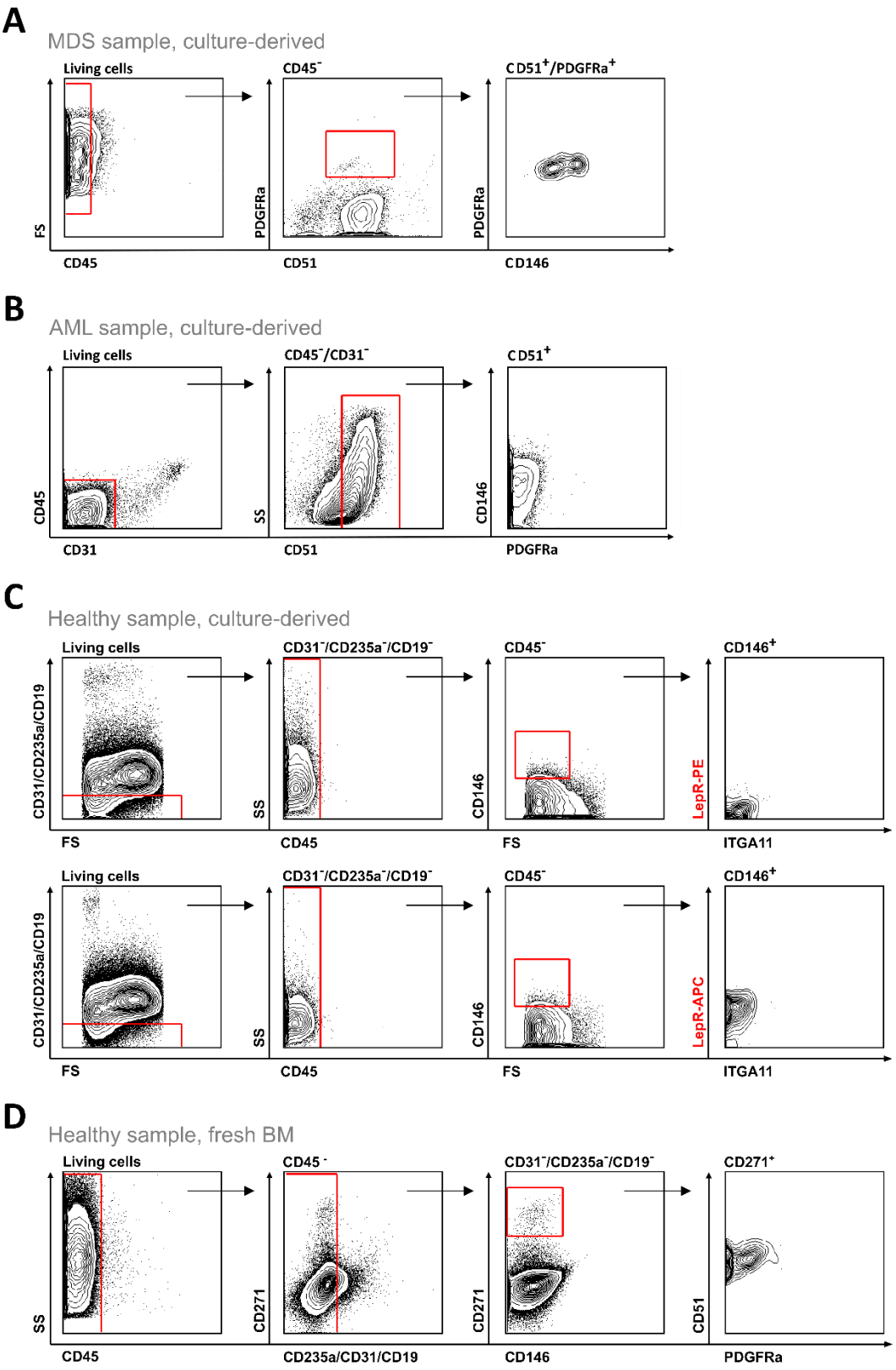

Figure 3: Establishment of a sorting scheme for purification of prospective MSC from primary BM-MNCs by FACS.

Surface marker expression of culture-derived stroma cells (harvested after passage 2) or uncultivated BM-MNC was analyzed by FACS. **(A)** Stroma cells were gated on negative expression of CD45 and positive expression of PDGFRa, CD51, followed by analysis of CD146 surface marker expression. Representative plot of FACS analysis

of culture-derived stroma cells from an MDS sample. **(B)** Stroma cells were gated on negative expression of CD45 and CD31, and positive expression of CD51, followed by analysis of PDGFRa and CD146 expression. Representative plot of FACS analysis of culture-derived stroma cells from an AML sample. **(C)** In this surface marker panel, two antibodies for LepR coupled to different fluorochromes (top row: LepR-PE, bottom row: LepR-APC), were compared. Stroma cells were gated on negative expression of the lineage markers CD19, CD235a and CD31, followed by exclusion of CD45 expressing cells. Cells most positive for CD146 were analyzed on expression of ITGA11 expression and LepR. Representative FACS plots of culture-derived stroma cells from a healthy donor sample are shown. **(D)** BM-MNC were gated on negative expression of CD45, CD31, CD235a and CD19, followed by analysis of CD146 and CD271 expression. CD271 positive cells were further analyzed on expression of CD51 and PDGFRa. Representative FACS plots of fresh, uncultivated BM-MSC from a healthy donor sample.

analyzed BM-MSC [117]. In our FACS analysis, we compared two antibodies for LepR, coupled to different fluorochromes (PE and APC, see top row and bottom row of Figure 3C). Cells were gated on negative expression of the lineage markers CD19 (B-cells), CD235a (erythrocyte progenitors), and CD31 (endothelial cells), followed by exclusion of CD45 expressing cells. When next looking at CD146 expression, most of the cells were $CD146^-$ and it was not possible to detect a clearly defined $CD146^+$ population. Checking the cells most positive for CD146 on ITGA11 expression showed no $ITGA11^+$ cells, and LepR expression was completely contrary for the two different antibodies used (negative for LepR-PE and positive for LepR-APC, see Figure 3C).

Since CD146 in our case seemed to be a poor marker for defining the MSC population, we decided to add CD271 as a well described MSC marker in our FACS panel [114,115,118–120]. FACS analysis of fresh, uncultivated BM-MNC showed a clearly defined, highly CD271-positive population within the $CD45^-$ fraction, that was also negative for the lineage markers CD235a, CD31 and CD19 (see Figure 3D). Examining the $CD45^-/lin^-$ population on CD146 expression showed again no $CD146^+$ cells. Furthermore, the $CD45^-/lin^-/CD271^+$ cell population was completely positive for CD51 expression, but most of them were negative for PDGFRa.

Due to these results, we created a new marker panel using CD31 and CD235a for endothelial and erythroid lineage exclusion, CD45 for exclusion of hematopoietic cells, and CD271 as MSC marker. Furthermore, we included CD73, CD105 and CD90, which are part of the minimal MSC surface marker criteria postulated by the International Society for Cellular Therapy (ISCT), to further narrowing down on the MSC population [61]. FACS analysis of fresh, uncultivated BM-MSC from a healthy donor showed again a clear $CD271^+$ subpopulation within the $CD45^-/lin^-$ cell fraction (see Figure 4A). When further refining the $CD45^-/lin^-/CD271^+$ population by looking at CD73 and CD105 expression, a clear split up into a $CD73^+/CD105^+$ double-positive and a $CD73^-/CD105^-$ double-negative subpopulation was observed. Interestingly, the $CD73^+/CD105^+$ double-positive (hence called +/+) population additionally was positive for CD90 expression, whereas the $CD73^-/CD105^-$ double-negative (hence called -/-) population did not express CD90, pointing at the +/+ subpopulation to most likely comprise the prospective MSC population. When analyzing uncultivated BM-MSC from healthy femoral heads (Figure 4B), MDS (Figure 4C), and AML (Figure 4D) patient samples with this surface marker panel, we found all subpopulations clearly defined in all the different kinds of samples, which brought us to use this gating strategy for isolation of the prospective MSC subpopulation from uncultivated BM-MSC.

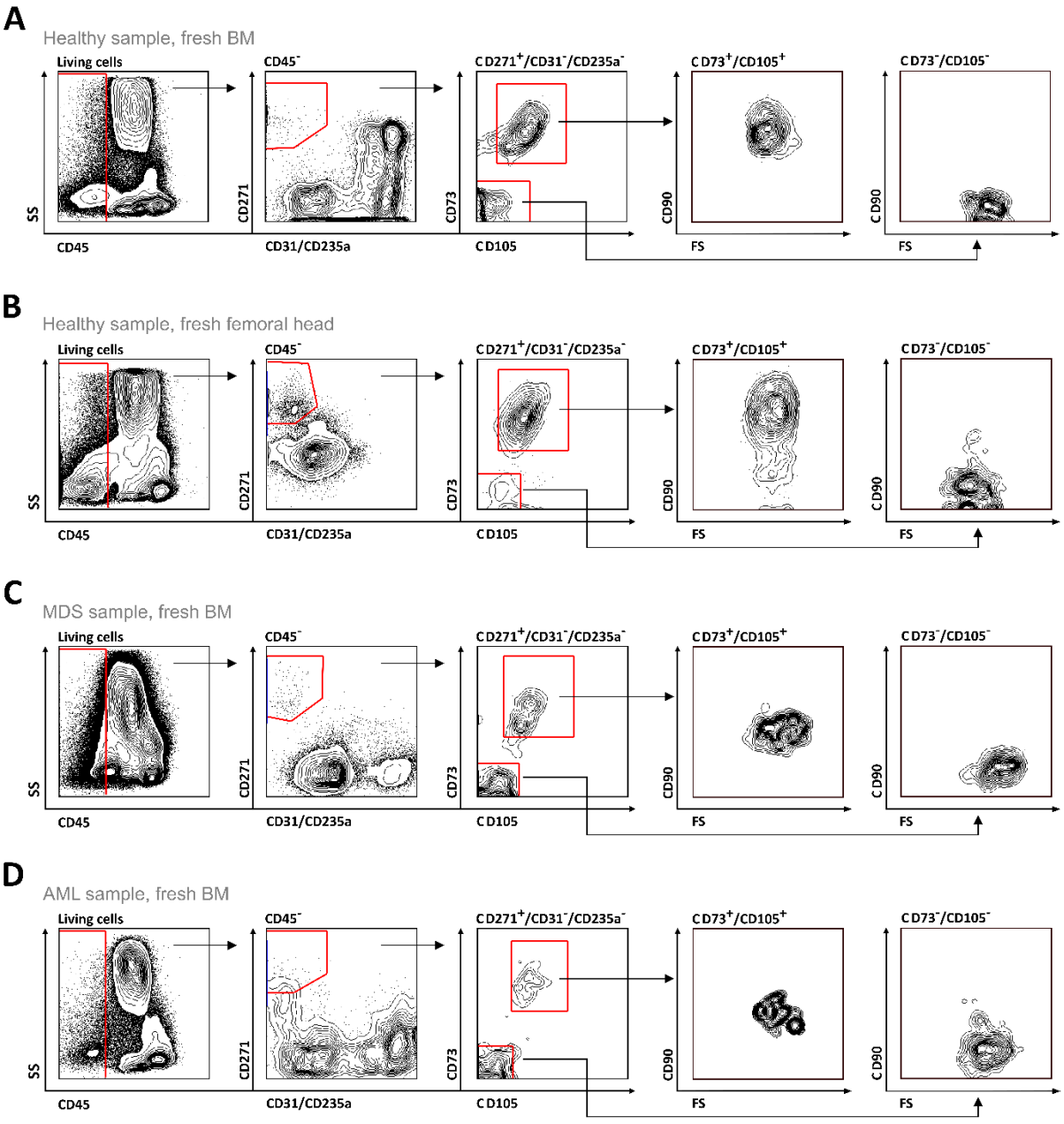

Figure 4: Surface marker panel for the isolation of prospective MSC from primary BM-MSC by FACS.

BM-MNC were gated on negative expression of CD45, CD31 and CD235a, and positive expression of CD271, followed by analysis of CD73 and CD105 expression. $CD73^+/CD105^+$ and $CD73^-/CD105^-$ subpopulations were further analyzed on CD90 expression. Representative FACS plots are shown for analysis of uncultivated BM-MNC from healthy donor aspirate **(A)**, healthy femoral head **(B)**, MDS **(C)**, and AML **(D)** samples.

5.3 Characterization of FACS-isolated putative MSC subpopulations

5.3.1 Statistical frequencies of the sorted subpopulations and age-relation

For characterization of the prospective MSC subpopulations, we analyzed several BM-MNC samples from healthy donors, MDS and AML patients via FACS, and calculated the frequencies of the different subpopulations from their cell counts (see Figure 5A).

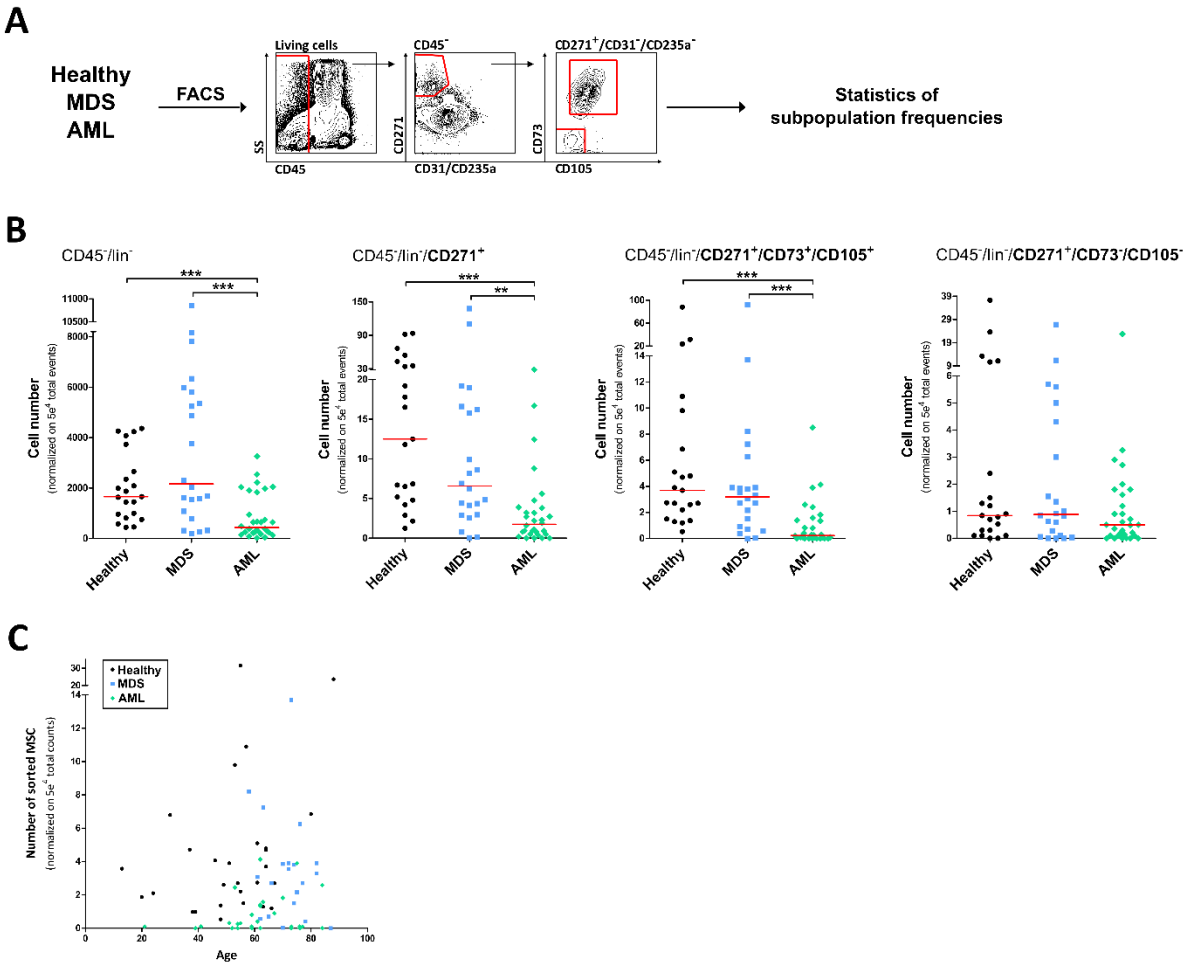

Figure 5: Subpopulation frequencies of prospective MSC and relation to patient age.

(A) Experimental design. Uncultivated BM-MNC from healthy donors, MDS and AML samples were analyzed on $CD45^-/CD31^-/CD235a^-/CD271^+/CD73^+/CD105^+$ and $CD45^-/CD31^-/CD235a^-/CD271^+/CD73^-/CD105^-$subpopulations by FACS, and statistical frequencies of the subpopulations as well as the parental and grand-parental populations were calculated. **(B)** Event counts of the subpopulations were normalized on $5e^4$ total event counts per sample. Statistical frequencies of cell numbers within the $CD45^-$ population, its $CD45^-/CD31^-/CD235a^-/CD271^+$ daughter population ($CD45^-/lin^-/CD271^+$), and the $CD45^-/CD31^-/CD235a^-/CD271^+/CD73^+/CD105^+$ ($CD73^+/CD105^+$) and $CD45^-/CD31^-/CD235a^-/CD271^+/CD73^-/CD105^-$ ($CD73^-/CD105^-$) subpopulations from healthy donors (n = 29), MDS (n = 22) and AML (n = 30) samples are shown from left to right. Medians are indicated in red. **(C)** Event counts of the $CD45^-/CD31^-/CD235a^-/CD271^+/CD73^+/CD105^+$ prospective MSC subpopulation from healthy donors (n = 29), MDS (n = 22) and AML (n = 30) samples (normalized on $5e^4$ total event counts per sample) were plotted against the age (years) of the respective patient sample to test for a possible correlation of patient age and MSC number by linear regression analysis.

Comparison of the subpopulation frequencies from healthy to malignant samples showed a significant reduction of the +/+ subpopulation and its parental populations in AML samples compared to healthy as well as MDS samples (see Figure 5B). Frequencies of the -/- subpopulation did not differ between the different sample types. Since MDS and AML are diseases of the elderly [17,23–25], we plotted the age of the respective patient/donor against the number of sorted +/+ cells to check for a possible correlation (see Figure 5C). Linear regression analysis showed no correlation of age and MSC cell number (healthy donor samples: $r^2 = 0.1$, $P = 0.99$, MDS samples: $r^2 = 0.04$, $P = 0.41$, AML samples: $r^2 = 0.05$, $P = 0.23$).

5.3.2 CFU-F formation ability of the prospective MSC subpopulations

CFU-F formation is a key criterion for MSC [52,58,106]. To verify MSC identity, both $CD271^+$ subpopulations, +/+ and -/-, were simultaneously sorted and seeded separately to assess their CFU-F formation potential, followed by re-analysis of their surface marker expression profile after two passages by FACS (see Fig. 6A).

CFU-F formation was found exclusively in the +/+ population of healthy donors, MDS and AML samples, indicating that this subpopulation contains the actual MSC (see Fig. 6B). When comparing the CFU-F frequency of sorted +/+ cells from healthy donors, MDS and AML samples, the CFU-F formation potential was significantly reduced in the malignant samples (see Fig. 6C).

Survival analysis of sorted +/+ CFU-F derived cells over a period of two passages showed a drastically reduced survival rate for AML samples compared to healthy donor samples, and a diminished survival rate for MDS samples (see Figure 6D).

Furthermore, we could observe morphological changes in cells expanded from +/+ CFU-F colonies in MDS and AML, that often appeared to be wider in diameter and flatter compared to healthy donor cells that were sorted and seeded at the same time and conditions (see Figure 6E).

Cells expanded from +/+ CFU-F colonies were re-analyzed by FACS to check if the *in vitro* culture conditions led to changes on their surface marker expression profile. We found the +/+ sorted cells, also after two passaging steps, to be positive for expression of CD271, CD90, CD73, CD105 and CD146, and negative for CD45, HLA-DR, CD34 and CD14 expression, consistent with key MSC criteria [61] (see Fig. 6F).

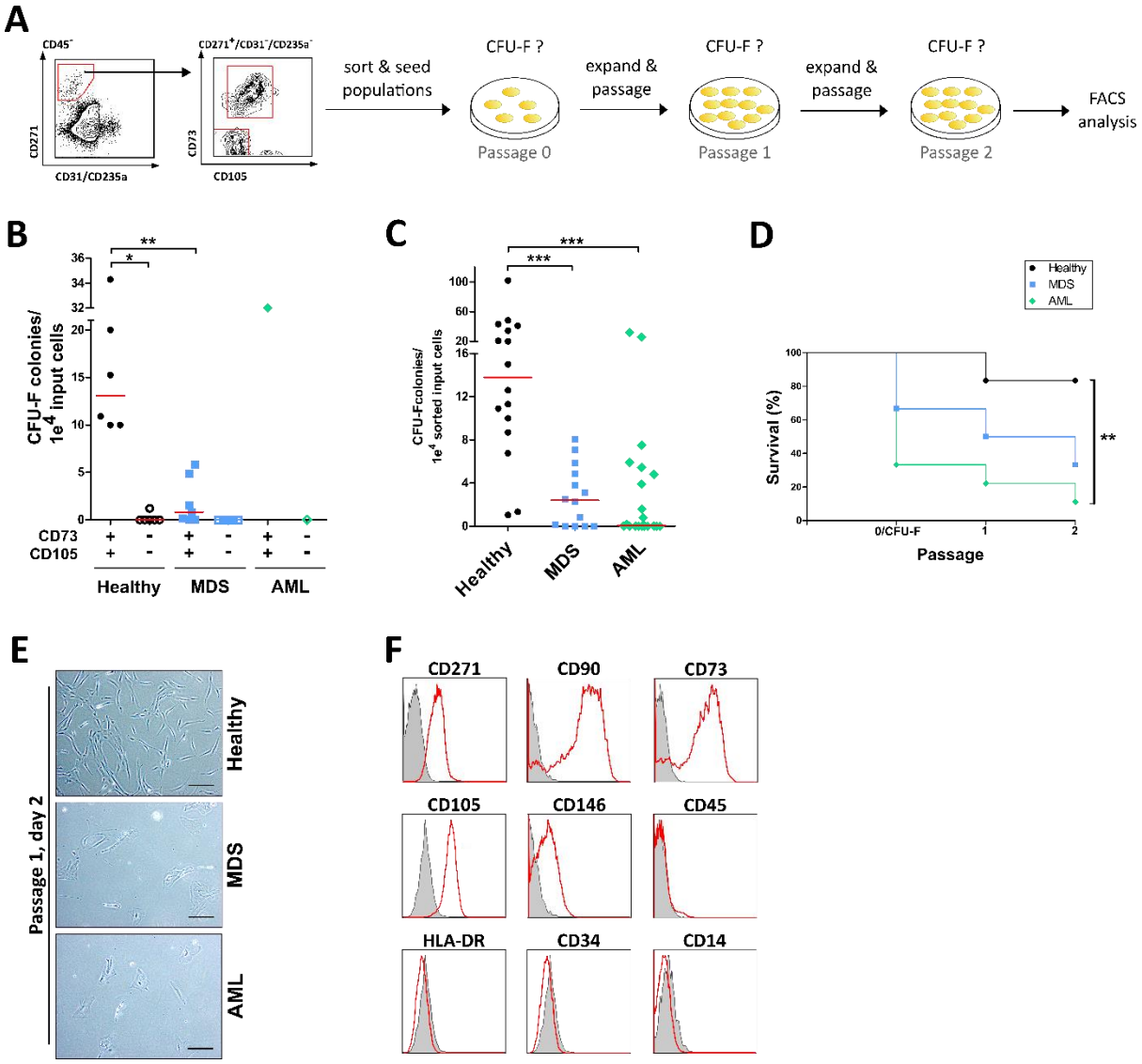

Figure 6: CFU-F formation ability, survival and FACS characteristics of the prospective MSC subpopulations.

(A) Experimental design. The CD45$^-$/CD31$^-$/CD235a$^-$/CD271$^+$/CD73$^+$/CD105$^+$ (+/+) and CD45$^-$/CD31$^-$/CD235a$^-$/CD271$^+$/CD73$^-$/CD105$^-$ (-/-) subpopulations were simultaneously sorted from BM-MNC from healthy donors, MDS, and AML sample by FACS. Sorted subpopulations were seeded separately to assess their CFU-F formation potential, followed by re-analysis of their surface marker expression profile after two passages by FACS. **(B)** Number of counted CFU-F colonies (normalized on 1e^4 input cells) in the +/+ and -/- subpopulations of healthy donors (n = 6), MDS (n = 7), and AML (n = 1) samples. Medians are indicated in red. **(C)** Number of counted CFU-F colonies (normalized on 1e^4 input cells) in the +/+ subpopulation of healthy donors (n = 16), MDS (n = 14), and AML (n = 20) samples. Medians are indicated in red. **(D)** Kaplan-Meier curve for survival (%) of +/+ sorted samples after initial seeding (0/CFU-F), passage 1, and passage 2. Healthy donors, n = 6; MDS, n = 6; AML, n = 9. **(E)** Representative light microscopy pictures showing the morphology of +/+ sorted cells from healthy donor, MDS and AML samples at day 2 after passage 1. Cells were sorted, seeded and expanded at the same time and conditions. Scale bars = 100 µm. **(F)** Re-analysis of surface marker expression of +/+ sorted cells by FACS after passage 2. Representative histograms are shown for a healthy donor sample. Grey filled lines indicate IgG controls, red lines the respective antibodies.

5.3.3 Coculture of sorted primary MSC and primary CD34+ cells

Used as a feeder layer, MSC have the ability to support CD34$^+$ hematopoietic cells in coculture [115]. To check if coculture of CD34$^+$ cells on healthy MSC compared to coculture on MDS and AML MSC alters short-term as well as long-term proliferation potential of the CD34$^+$ cells, we set up 4-day-coculture assays with several combinations of MSC and CD34$^+$ cells (see Figure 7A). For that, MSC from healthy donors, MDS, and AML patient samples were sorted and expanded to form a confluent feeder layer. CD34$^+$ cells from healthy donors, MDS, and AML BM-MNC samples were added to the MSC layers, resulting in a total of seven different coculture combinations: Healthy CD34$^+$ on healthy, MDS, and AML MSC; MDS CD34$^+$ on healthy and MDS MSC; and AML CD34$^+$ on healthy and AML MSC, respectively.

Compared to coculture of the respective CD34$^+$ cells on healthy MSC, frequencies of short-term colony-forming units (CFU) as well as long-term culture initiating cells (LTC-IC) were not altered in cocultures of healthy CD34$^+$ on MDS MSC and slightly reduced in cocultures on AML MSC (see Figure 7B+C). A slightly reduced CFU frequency and a pronounced reduction in LTC-ICs was observed in MDS CD34$^+$ cells cocultured on MDS MSC compared to coculture on healthy MSC. Also, AML CD34$^+$ cocultured on AML MSC showed the tendency of reduced short-term and long-term proliferation potential compared to coculture on healthy MSC.

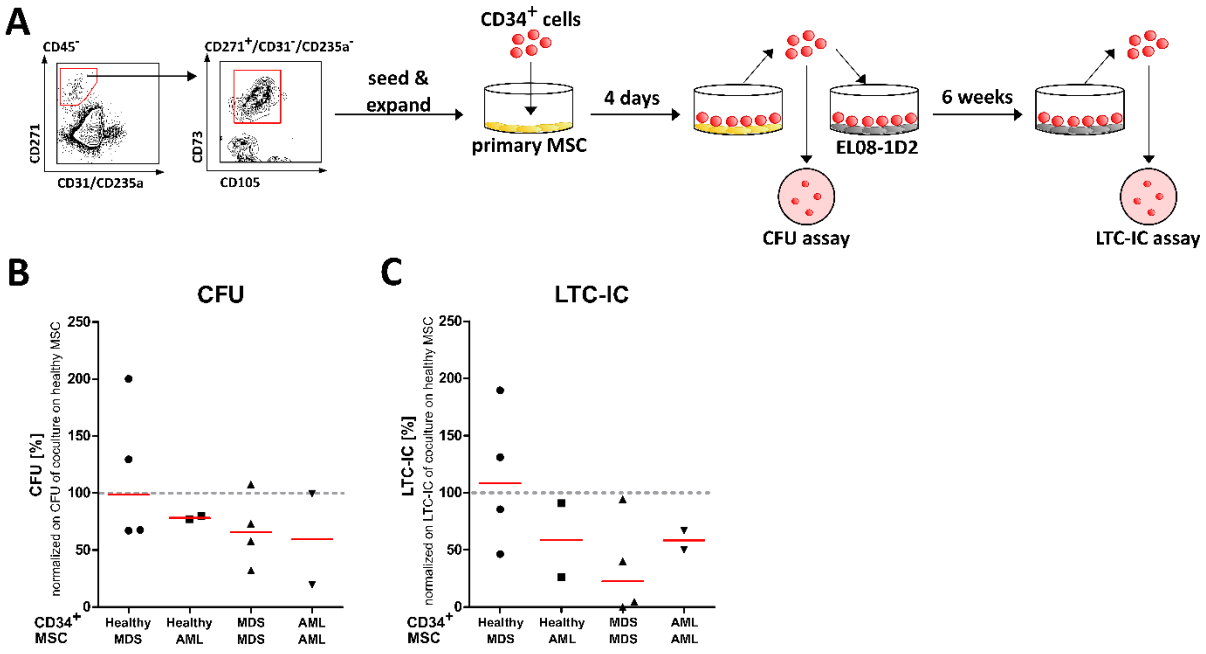

Figure 7: Short-term and long-term proliferation potential of CD34$^+$ cells cocultured on primary MSC.

(A) Experimental design. CD45$^-$/CD31$^-$/CD235a$^-$/CD271$^+$/CD73$^+$/CD105$^+$ (+/+) sorted MSC from healthy donors, MDS, and AML patient samples were sorted and expanded to form a confluent feeder layer. CD34$^+$ cells from healthy donors, MDS, and AML BM-MNC samples were added to the MSC layers, resulting in a total of seven different coculture combinations: Healthy CD34$^+$ on healthy, MDS, and AML MSC; MDS CD34$^+$ on healthy and MDS MSC; and AML CD34$^+$ on healthy and AML MSC, respectively. Cells were cocultured for 4 days and CD34$^+$ cells were harvested. Short-term proliferation potential was assessed by colony-forming unit (CFU) assay in methylcellulose. Long-term culture initiating cell (LTC-IC) capacity of the CD34$^+$ cells was assessed after 6 weeks of coculture on sublethally irradiated (30 Gy) EL08-1D2 stroma cells by plating in methylcellulose. **(B)** CFU colonies were scored after 14 days in methylcellulose according to standard criteria. Results are shown as CFU

frequencies [%] of CD34⁺ cells cocultured on the indicated malignant MSC layer in relation to CFU frequencies [%] of the respective CD34⁺ cells cocultured on healthy MSC. Medians are indicated in red. **(C)** LTC-IC colonies were scored after 14 days in methylcellulose according to standard criteria. Results are shown as LTC-IC frequencies [%] of CD34⁺ cells cocultured on the indicated malignant MSC layer in relation to LTC-IC frequencies [%] of the respective CD34⁺ cells cocultured on healthy MSC. Medians are indicated in red.

5.3.4 *In vitro* adipo- and osteogenic differentiation potential of sorted MSC

Another key feature of MSC is their ability to differentiate into adipocytes and osteoblasts [49,56,59,60]. Since there are previous findings, that the adipo-/osteogenic balance of the niche is important for regulation of hematopoiesis and that this balance is disturbed in course of malignant transformation [48,71,72,121,122], we analyzed the *in vitro* adipogenic and osteogenic differentiation potential of the sorted MSC population of malignant and healthy samples.

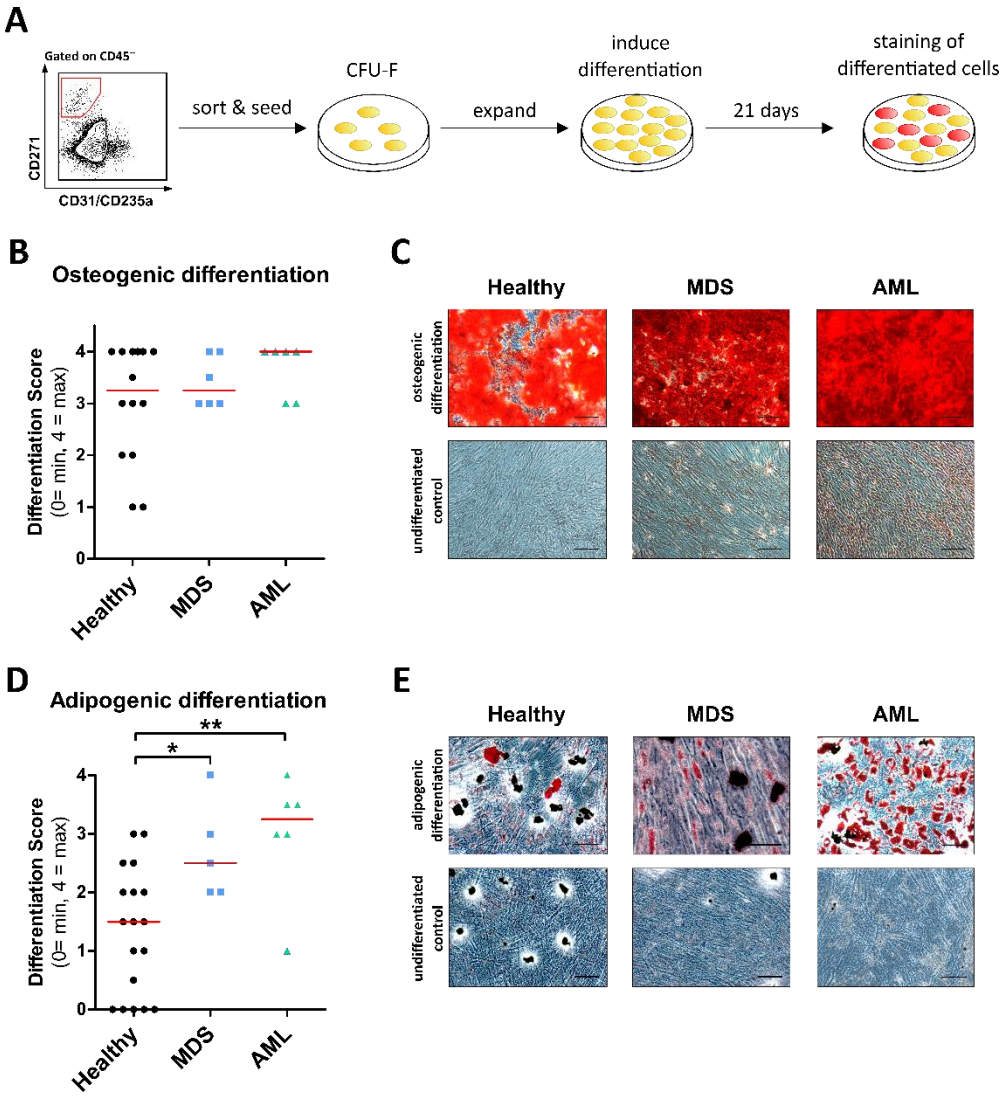

Figure 8: *In vitro* adipogenic and osteogenic differentiation potential of sorted MSCs.

(A) Experimental setup. CD45⁻/CD31⁻/CD235a⁻/CD271⁺ sorted MSC from healthy donors, MDS, and AML samples were seeded and CFU-F forming cells were expanded until confluent. Osteogenic and adipogenic differentiation

were induced *in vitro* for 21 days. Osteoblasts were detected by Alizarin Red staining of calcium deposits. Adipocytes were detected by Oil Red staining of fatty vacuoles. Stained samples were categorized according to a staining intensity score as follows: 0 = no staining, 1 = weak, 2 = medium, 3 = strong, 4 = intensive. **(B)** Quantification of *in vitro* osteogenic differentiation potential of sorted MSCs from healthy donors (n = 14), MDS (n = 6), and AML (n = 6) patient samples. Medians are indicated in red. **(C)** Representative images of Alizarin Red staining of osteogenic differentiated healthy donor, MDS, and AML samples (top row) and their respective undifferentiated controls (bottom row). Scale bars = 100 µm. **(D)** Quantification of *in vitro* adipogenic differentiation potential of sorted MSCs from healthy donors (n = 18), MDS (n = 5), and AML (n = 6) patient samples. Medians are indicated in red. **(E)** Representative images of Oil Red staining of adipogenic differentiated healthy donor, MDS, and AML samples (top row) and their respective undifferentiated controls (bottom row). Scale bars = 100 µm.

CFU-F forming colonies from $CD45^-$/lin(CD31/CD235a)$^-$/$CD271^+$ sorted MSC from healthy donors, AML and MDS samples were expanded and *in vitro* adipogenic and osteogenic differentiation was induced for 21 days (see Figure 8A). Calcium-deposits produced by osteoblasts were stained with Alizarin Red (see Figure 8C) and adipocytes were detected by Oil Red staining of their fatty vacuoles (see Figure 8E). Adipogenic and osteogenic differentiation potential was quantified using a staining intensity score (0 = no staining, 4 = intensive staining). A high osteogenic differentiation capacity was detected in MSC from all sample types, but no significant differences in intensity levels were observed (see Figure 8B). Interestingly, a significantly increased adipogenic potential was found in MSC from AML and MDS samples compared to healthy MSC (see Fig. 8D).

5.4 Gene expression analyses of sorted healthy, MDS and AML MSC subpopulations

5.4.1 Transcriptome analysis by RNAseq

To further characterize the sorted MSC subpopulations, we performed transcriptome analysis via RNAseq to look for differences between the +/+ and -/- subpopulations and detect differentially regulated pathways or alterations in expression of functionally related gene groups in MDS and AML patient samples compared to healthy ones, in order to get more clues about MSC remodeling in course of the diseases and their possible impact on the hematopoietic compartment.

For that, about 500 cells of the +/+ and -/- subpopulations were sorted simultaneously from five healthy donors, MDS, and AML samples each, followed by total RNA extraction and analysis of the gene expression profiles by RNAseq (see Figure 9A). Exploratory data analysis showed that the collected data could not be used for a proper and precise transcriptome analysis due to several reasons. First, after pre-processing and mapping to the human genome only $6.3e^6$ unique molecular identifier (UMI) reads were detected in total, which is very little for a number of 30 samples. Second, the average number of expressed genes with at least one UMI count is 12704 (median: 12771), which is very little (see Figure 9B). Furthermore, the library size, depicting the number of UMI reads per sample (exonic mapped), is very small with a median of $1.6e^5$ UMI/sample and has a large variation (min: 37510 UMI/sample, max: 666000 UMI/sample; see Figure 9C). Since the large variation in library size, high dropout rate, and low average gene expression in our data set resemble more the properties of single cell

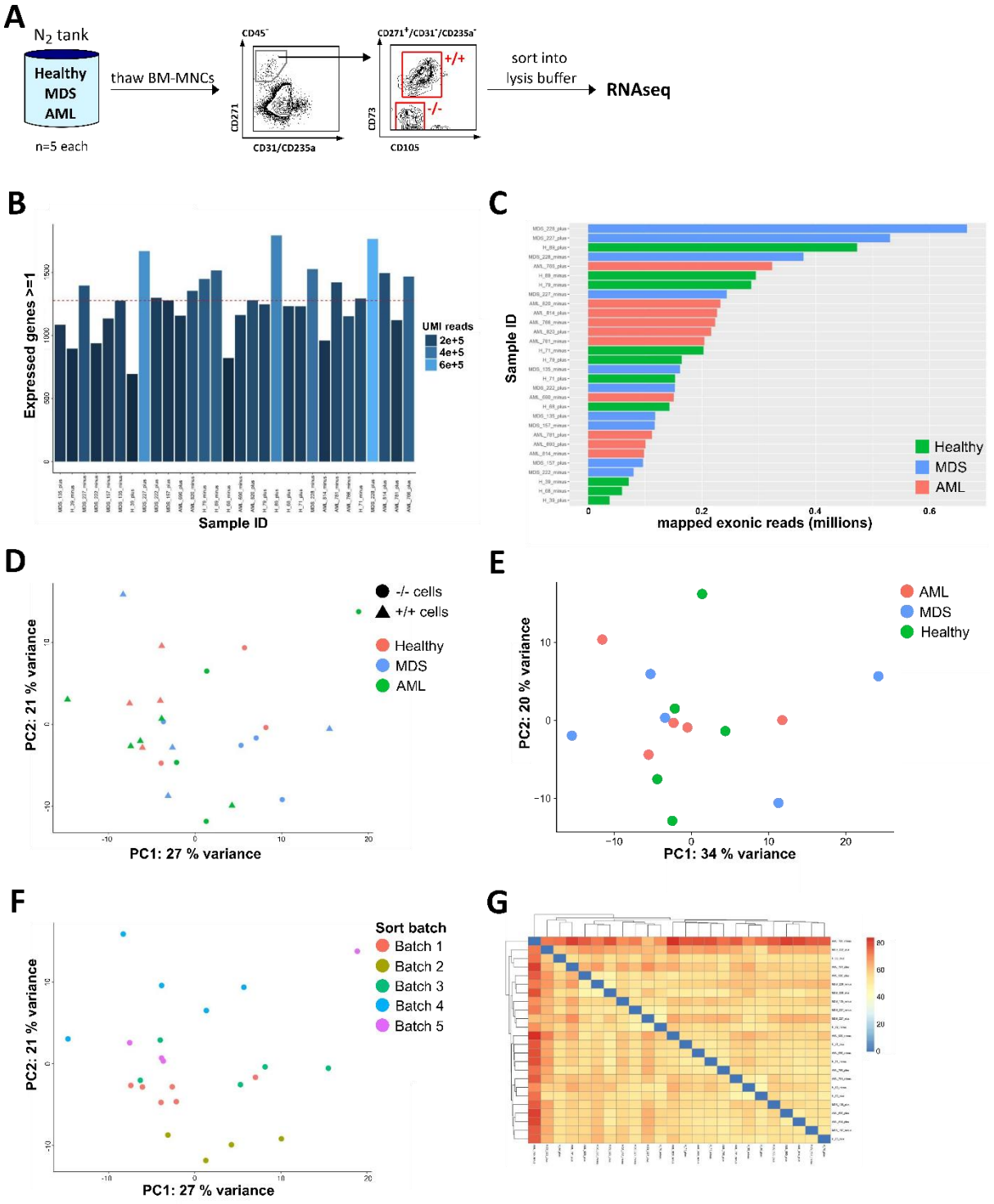

Figure 9: Transcriptome analysis of sorted MSC subpopulations by RNAseq.

(A) Experimental setup. 500 cells of the +/+ and -/- MSC subpopulations were sorted simultaneously from healthy donors, MDS, and AML BM-MNC (n = 5 each), followed by total RNA extraction and transcriptome analysis by RNAseq. **(B)** Plot showing the number of expressed genes with at least one UMI count in the sorted samples. Median (12771 genes) is indicated as a dashed red line. **(C)** Library size, indicated as number of exonic mapped UMI reads per sample. Green bars: healthy donor samples, blue bars: MDS samples, light red bars: AML samples. **(D)** Principle component analysis of sorted +/+ and -/- populations from healthy donors, MDS, and AML samples. Triangles: +/+ cells, circles: -/- cells. Healthy donor samples are indicated in light red, MDS samples in

blue, and AML samples in green. **(E)** Principle component analysis of sorted +/+ cells only. Healthy donor samples are indicated in green, MDS samples in blue, and AML samples in light red. **(F)** Principal component analysis of sorted samples according to their sort date batches. In one sort batch, one healthy donor, one MDS, and one AML sample were processed. **(G)** Heatmap visualizing hierarchical clustering of sample distances (Euclidean distances) of sorted +/+ and -/- populations from healthy donors, MDS, and AML samples. Differences in Euclidean distances are plotted in blue and red colors.

RNAseq assays rather than bulk-sorted cells, normalization methods developed for single cell-data were applied. Principal component analysis (PCA) of the normalized data set showed no clustering of the individual samples between healthy donors, MDS, and AML samples (see Figure 9D), also not when only considering the +/+ samples that contain the proper MSC subpopulation (see Figure 9E). Clusters could only be observed, when comparing the samples according to their sorting day batches, where always a set of one healthy donor, one MDS, and one AML patient sample had been sorted in one experiment per day (see Figure 9F). Furthermore, no differenced occurred when performing hierarchical clustering (see Figure 9G). Overall, these data hint at a loss or degradation of RNA already during cell sorting or sample processing.

5.4.2 Gene expression analysis of sorted, uncultivated MSC

To check the expression of a selected set of genes, including *LPL, RUNX2, SPP1, SFRP1*, and *DLK1*, in uncultivated MSC, RNA was immediately extracted from freshly sorted, uncultivated +/+ MSC and analyzed by qRT-PCR (see Figure 10A+B).

Establishing this method, we first analyzed expression of these genes using cDNA transcribed from 50 ng RNA extracted from 500 +/+ sorted healthy donor MSC, as well as cDNA created from 50 ng and 1000 ng universal human RNA (see Figure 10C). Evaluation of target gene expression normalized on *EIF3* mRNA expression showed that 50 ng universal human RNA were sufficient for the detection of the five target genes (see Figure 10C, light grey bars). Expression of *LPL*, *RUNX2* and *SPP1* could also be detected in cDNA from 50 ng +/+ sorted human healthy MSC RNA, however, expression of *SFRP1* and *DLK1* were below detection limit (see Figure 10C, blue bars).

The main experiment focused on the detection of the selected gene set in 500 +/+ sorted MSC from healthy donor, MDS, and AML patient samples (n=6, each). Due to low sort outcomes in MDS and AML patient samples, the number of +/+ sorted MSC samples used for RNA extraction were reduced to four MDS and five AML samples. For the qRT-PCR analysis, we decided to use 100 ng total RNA for transcription to cDNA, since this was the highest RNA amount we could extract from most of the sorted MSC samples, with the exception of one MDS and two AML MSC RNA samples that contained slightly less RNA (indicated with grey squares in Fig. 10D). Evaluation of target gene expression normalized on *EIF3* mRNA expression showed no differences of *LPL, RUNX2, SPP1, SFRP1*, and *DLK1* mRNA levels between healthy donor, MDS and AML MSC samples (see Figure 10D). Gene expression levels were in general very low to non-detectable in AML MSC samples. *DLK1* expression was not detectable in any of the samples except for one MDS MSC sample. Overall, the results indicate

that the used amount and/or the quality of the extracted RNA was not sufficient for a precise and proper gene expression analysis.

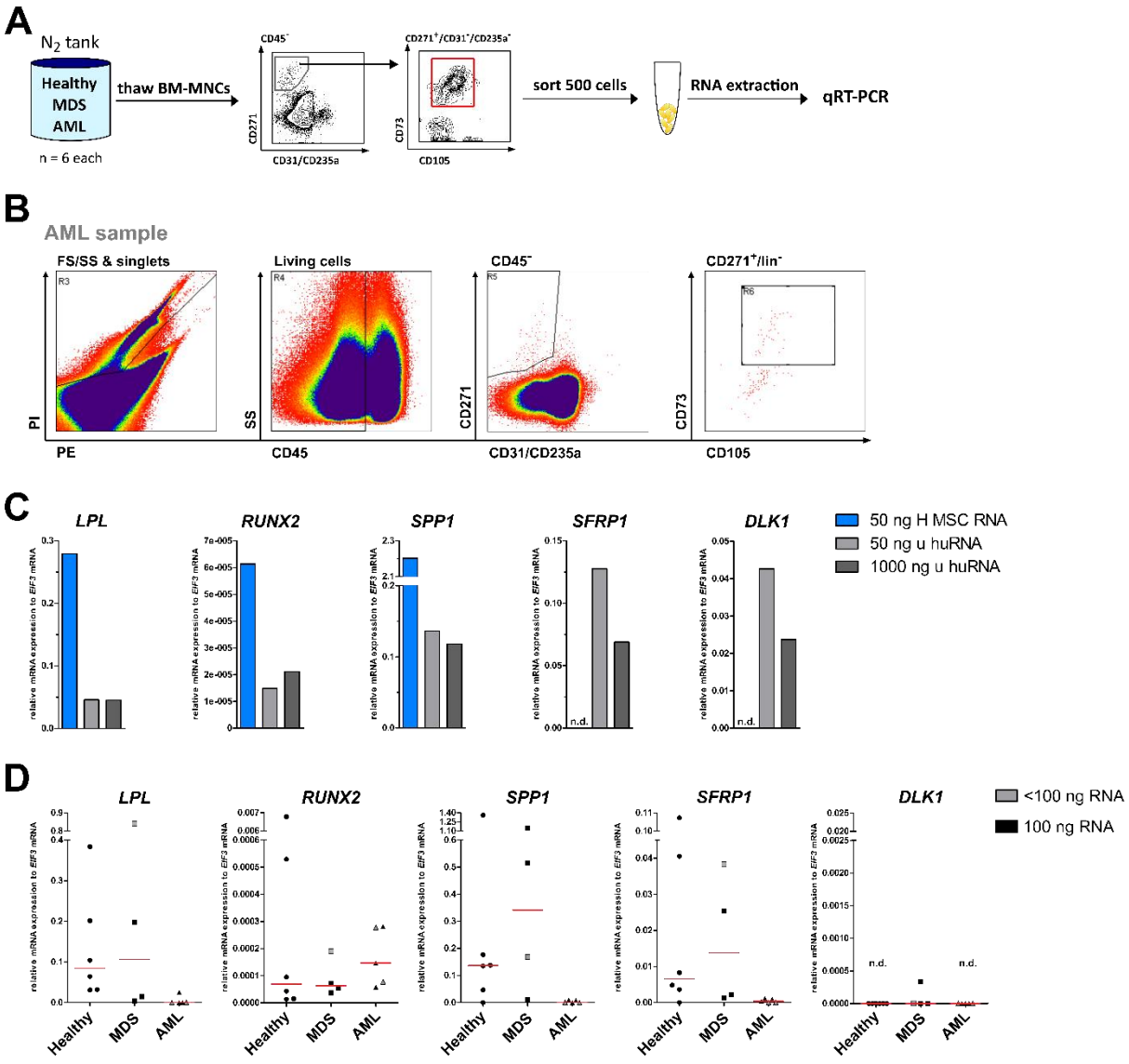

Figure 10: Gene expression analysis from freshly sorted, uncultivated MSC.

(A) Experimental design. 500 +/+ MSC were sorted from healthy donor, MDS, and AML BM-MNC samples (n = 6 each). Total RNA was immediately extracted from freshly sorted MSC, transcribed to cDNA, and used for the detection of *LPL*, *RUNX2*, *SPP1*, *SFRP1,* and *DLK1* gene expression via qRT-PCR. **(B)** Representative FACS plot of an AML sample, showing the gating for isolation of the living (PI^-), $CD45^-/CD31^-/CD235a^-/CD271^+/CD73^+/CD105^+$ MSC subpopulation. **(C)** Test experiment for analysis of target gene expression, using cDNA transcribed from 50 ng RNA extracted from +/+ sorted healthy donor MSC (50 ng H MSC RNA, blue bars), as well as cDNA created from 50 ng and 1000 ng universal human RNA (50 ng u huRNA, light grey bars; 1000 ng u huRNA, dark grey bars). Results are shown with target gene expression normalized on *EIF3* mRNA expression. n.d. = not detectable. **(D)** Target gene expression (normalized on *EIF3* mRNA expression) in sorted healthy donor (n = 6), MDS (n = 4), and AML (n = 5) MSC samples. Samples with 100 ng RNA for cDNA transcription are indicated in black. Samples, where less than 100 ng RNA (two MDS samples: 70 ng RNA each, one AML sample: 55 ng) was available for cDNA transcription are indicated in light grey. Medians are indicated in red. n. d. = not detectable.

5.4.3 Troubleshooting of sample processing for cell sorting

The results of the RNAseq experiments and gene expression analysis of uncultivated MSC sorted from thawed BM-MNC suggest that RNA yield and quality from frozen BM samples were impaired. Matching that observation, there are publications showing that cryopreservation of stem cells hampers their post-thaw viability [123,124]. Due to these findings, we wanted to investigate if the sort yield of MSC is altered when sorted from cryopreserved or fresh BM-MNCs, respectively. For that, we compared three aliquots of the same healthy BM-MSC sample undergoing different processing conditions: one was analyzed by FACS immediately after harvesting of the BM-MNCs, the other two were cryopreserved using FCS + 10 % DMSO (our standard freezing medium) or Bambanker™ as freezing medium,

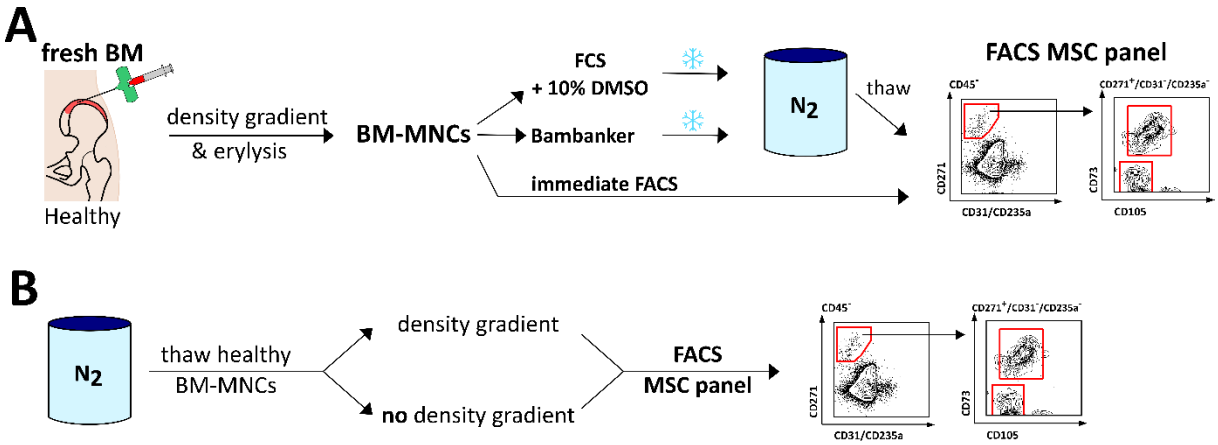

Figure 11: Test of different sample processing approaches for cell sorting.

(A) Experimental design. BM-MNCs were isolated from fresh healthy donor BM aspirate by density gradient centrifugation. The BM-MNC ample was split into three, and one part was FACS analyzed immediately on the +/+ MSC subpopulation. The other two were cryopreserved using FCS + 10 % DMSO or Bambanker™ as freezing medium. After storage in N_2 for three days, samples were thawed and FACS analyzed on the +/+ MSC subpopulation. **(B)** Experimental design. BM-MNC from a healthy donor sample were thawed and split into two. One part was analyzed immediately on the +/+ MSC subpopulation by FACS, the other was purified by an additional density gradient centrifugation step before FACS analysis.

and FACS-analyzed after three days of storage in N_2 (see Figure 11A). Bambanker™ is a commercial freezing medium that is recommended for the cryopreservation of sensitive cells like induced pluripotent stem cells [125].

Gated cells were normalized to $2e^7$ total counts. Compared to the cryopreserved samples, the immediately sorted sample showed a more than 10-fold higher number of the $CD73^+/CD105^+$ MSC subpopulation within the immediately sorted, unfrozen aliquot compared to the cryopreserved ones (see Table 10). The +/+ subpopulation was only slightly higher in the Bambanker™ aliquot than in the aliquot cryopreserved in FCS + 10 % DMSO, which is most likely a technical artefact due to handling and sorting.

Table 10: Subpopulation counts of MSC sorted from differentially processed sample aliquots.

A fresh sample of BM-MNCs from a healthy donor was split into three parts and one was immediately analyzed by FACS (fresh MSC) according to our surface marker panel for isolation of +/+ MSC. The other two were cryopreserved using FCS + 10 % DMSO or Bambanker™ as freezing medium and FACS-analyzed after three days of storage in N_2. Subpopulation counts were normalized on $2e^7$ total counts.

	Subpopulations		
Sample	**$CD45^-$**	**$CD271^+/lin^-$**	**$CD73^+/CD105^+$**
Fresh MSC	6033109	178062	143845
Bambanker	336408	12326	10056
FCS + 10 % DMSO	220173	10150	9027

We hypothesized that viability-enriched BM-MNC samples are less prone to post-thaw apoptosis, which could help improving the RNA yield from the MSC subpopulation. To prove this, dead cells were excluded by an additional density gradient centrifugation step after thawing of the BM-MNC sample and compared to an untreated thawed sample: For that, a healthy donor BM-MNC sample was split after thawing. One half was FACS-analyzed immediately, and the other half was density gradient-purified before FACS (see Figure 11B). Gated cells were normalized to $2e^7$ total counts. Although the density gradient purification reduced the total sample size about 3 - 4 times, the number of cell counts in the +/+ subpopulation was found to be 2.7-times increased in the density gradient-purified sample compared to the untreated sample (see Table 11). This finding suggests a more efficient MSC isolation in the viability-enriched sample.

Table 11: Subpopulation counts of MSC sorted from BM-MNC with or without density gradient centrifugation step after thawing.

A healthy donor BM-MSC sample was split after thawing, and in one half, dead cells were removed by density gradient centrifugation (density gradient) before FACS analysis, and one half was immediately analyzed by FACS (no density gradient) according to our surface marker panel for isolation of MSC. Subpopulation counts were normalized on $2e^7$ total ungated counts.

	Subpopulations		
Sample	**$CD45^-$**	**$CD271^+/lin^-$**	**$CD73^+/CD105^+$**
Density gradient	261898	13172	11911
No density gradient	335832	5484	4411

5.4.4 Quality control of RNA from differentially processed sample sources

The experiments concerning sample processing so far suggest, that density gradient centrifugation of BM-MNCs after thawing could help to improve the yield of viable MSC by FACS isolation. To investigate if this also has an impact on RNA yield and quality, we compared integrity and amount of RNA extracted from differentially processed samples on a bioanalyzer, where RNA gets separated by size in an on-chip gel electrophoresis. The resulting data are used to calculate RNA concentration and the RNA integrity number (RIN), which is a variable describing RNA integrity in a range from 0 to 10.

Since early-apoptotic cells are not detected with propidium iodide (PI) staining in FACS, we tested if post-thaw stressed, early apoptotic BM-MNC could be excluded from the analysis by letting the thawed sample rest overnight, giving the opportunity for these cells to complete apoptosis. For that, we incubated thawed healthy donor BM-MSC overnight in HF2 buffer at 4°C, followed by density gradient purification and FACS isolation of MSC on the next day (see Figure 12A). Additionally, aliquots of the same healthy sample were thawed on the second day, one was purified by density gradient centrifugation before cell sorting, and one was sorted immediately without density gradient purification. Furthermore, BM-MNCs were isolated from a fresh healthy femoral head that was transported to the laboratory the same day, purified by erylysis and density gradient centrifugation, and immediately sorted. For every sample, 500 +/+ MSC were sorted and RNA was extracted immediately. All extracted RNA samples were loaded on one chip and RNA integrity and concentration was assessed with a bioanalyzer.

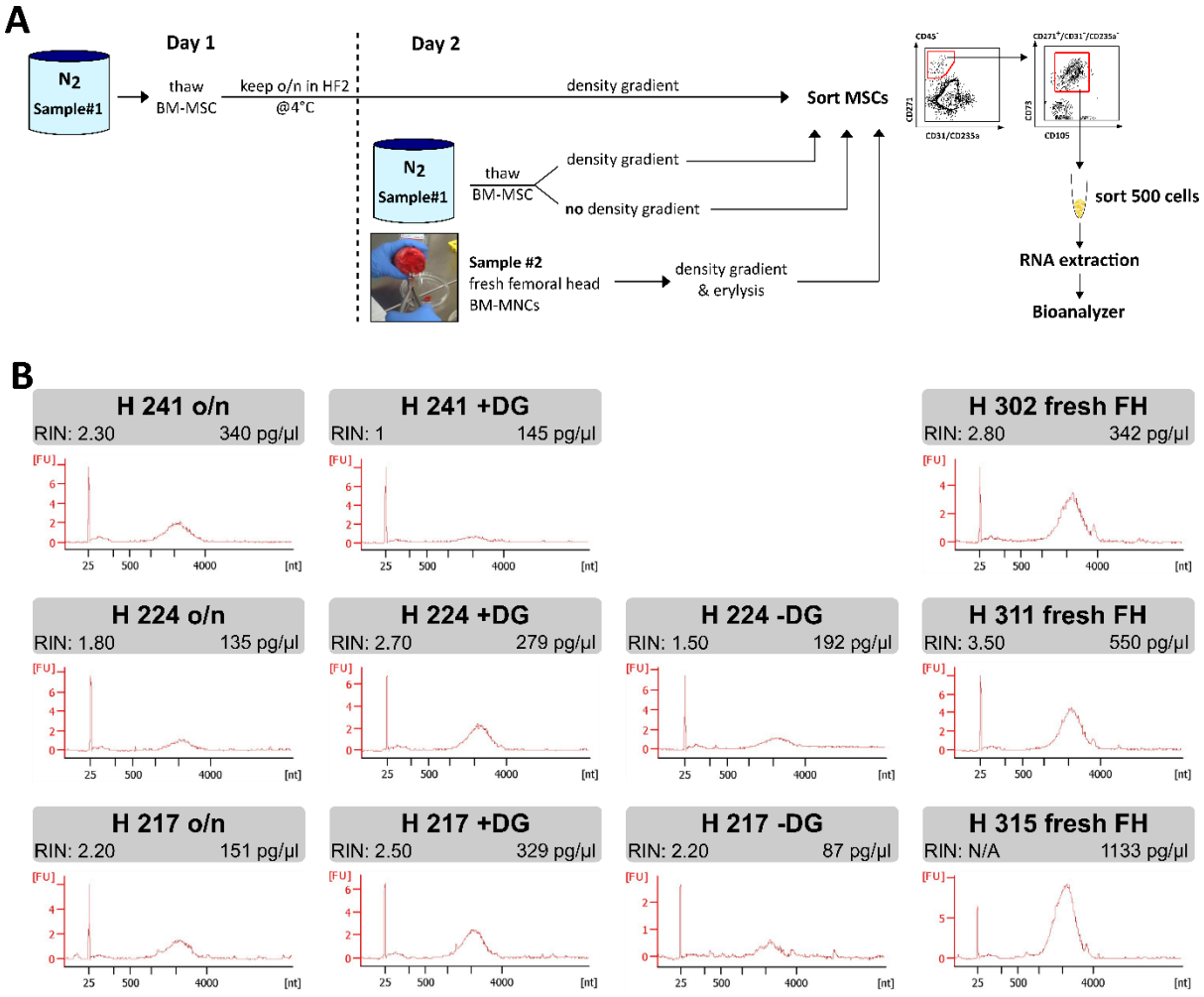

Figure 12: Impact of different sample processing approaches on quality and quantity of RNA from sorted MSC.

(A) Experimental design. Healthy donor BM-MNC were thawed and incubated overnight in HF2 buffer at 4°C, followed by density gradient purification and FACS isolation of +/+ MSC on the next day. Additionally, aliquots of the same healthy sample were thawed on the second day, one was purified by density gradient centrifugation before cell sorting, and one was sorted immediately without density gradient purification. Furthermore, BM-

MNCs were isolated from a fresh healthy femoral head that was transported to the laboratory the same day, purified by erylysis and density gradient centrifugation, and +/+ MSC were sorted immediately. For every sample, 500 +/+ MSC were sorted and total RNA was extracted immediately. This approach was done for three sample sets, with exception of one set that lacked the sample without density gradient purification. All extracted RNA samples were loaded onto one chip and analyzed with a bioanalyzer. **(B)** Electropherograms depict RNA size [nt] versus fluorescence intensity [fluorescence units = FU]. The first peak at 25 nt is an internal control, followed by a broader peak at about 2000 nt – 4000 nt that indicates the ribosomal RNA (rRNA), which is used for calculation of RNA integrity number (RIN), a variable describing RNA integrity with a range from 0 (lowest) to 10 (highest). RNA concentration [pg/µl] of each sample was calculated from electrophoresis data. H = healthy donor sample, o/n = samples incubated overnight in HF2 buffer, + DG = samples with density gradient step before FACS, - DG = samples without density gradient purification before FACS, FH = femoral head sample, N/A = not available.

Electropherograms depict RNA size [nt] versus fluorescence intensity [fluorescence units = FU]. The first peak at 25 nt is an internal control, followed by a broader peak at about 2000 nt – 4000 nt that indicates the ribosomal RNA (rRNA), which is used for RIN calculation (see Figure 12B). Overall, RIN numbers are relatively low. As expected, the rRNA peaks are highest in the RNA samples from fresh femoral heads, which is also mirrored in their RNA concentrations and RIN numbers. For two of the differentially processed samples (H224 and H217), highest RIN and RNA concentration was found in the samples purified by density gradient after thawing. On the contrary, overnight-resting of the samples and waiving of density gradient centrifugation resulted in the lowest values for RIN number and RNA concentration.

5.4.5 Gene expression analysis of sorted MSC expanded from CFU-F colonies

Since RNAseq and qRT-PCR from small numbers of sorted, uncultivated MSC did not give reliable results, we decided to perform gene expression analyses of selected target genes from sorted and subsequently expanded MSC. Our FACS analysis results of sorted MSC after passage 2 already showed, that the sorted MSC kept their key surface marker expression profile also after expansion in *in vitro* culture (see Figure 6F). Due to the fact, that only +/+ sorted MSC were able to form CFU-F colonies (see Figure 6B), we sorted healthy donor, MDS and AML BM-MSC on the $CD45^-/CD271^+/lin^-$ mother population, culture-expanded the CFU-F forming cells and harvested them for RNA extraction and subsequent gene expression analysis by qRT-PCR (see Figure 13 A). Gene expression was analyzed for specific marker genes: *LPL* and *PPARG* (adipogenic differentiation), *RUNX2* and *SPP1* (osteogenic differentiation), *TAGLN* (smooth muscle differentiation), *SFRP1* (Wnt pathway inhibitor), *WNT10B* and *WNT5A* (activating ligands of the canonical and non-canonical Wnt pathway, respectively), *SOX9* and *AGC1* (chondrogenic differentiation), *DLK1* (orphan Notch pathway ligand, inhibitor of adipogenic differentiation), *NOTCH1* and *NOTCH3* (Notch pathway receptors), and *JAGGED1* (activating Notch pathway ligand).

Gene expression levels of adipogenic, osteogenic and chondrogenic differentiation markers, as well as from Wnt pathway ligands were not significantly altered (see Figure 13B, first and second row). Significant differences in gene expression between healthy, MDS and AML MSC were only observed for *DLK1* and *JAGGED1* expression (see Figure 13B, bottom row). *DLK1*

expression was significantly reduced in MDS and AML MSC compared to healthy MSC, with the expression level of MDS MSC being an intermediate between healthy and AML MSC expression levels. Expression of *JAGGED 1* was significantly increased in AML MSC compared to healthy MSC. Overall, MDS MSC did not show increased *JAGGED1* expression, except for a subset of four MDS MSC samples that displayed a high *JAGGED1* expression. In contrast, gene expression levels of the Notch pathway receptors *NOTCH1* and *NOTCH3* were not altered.

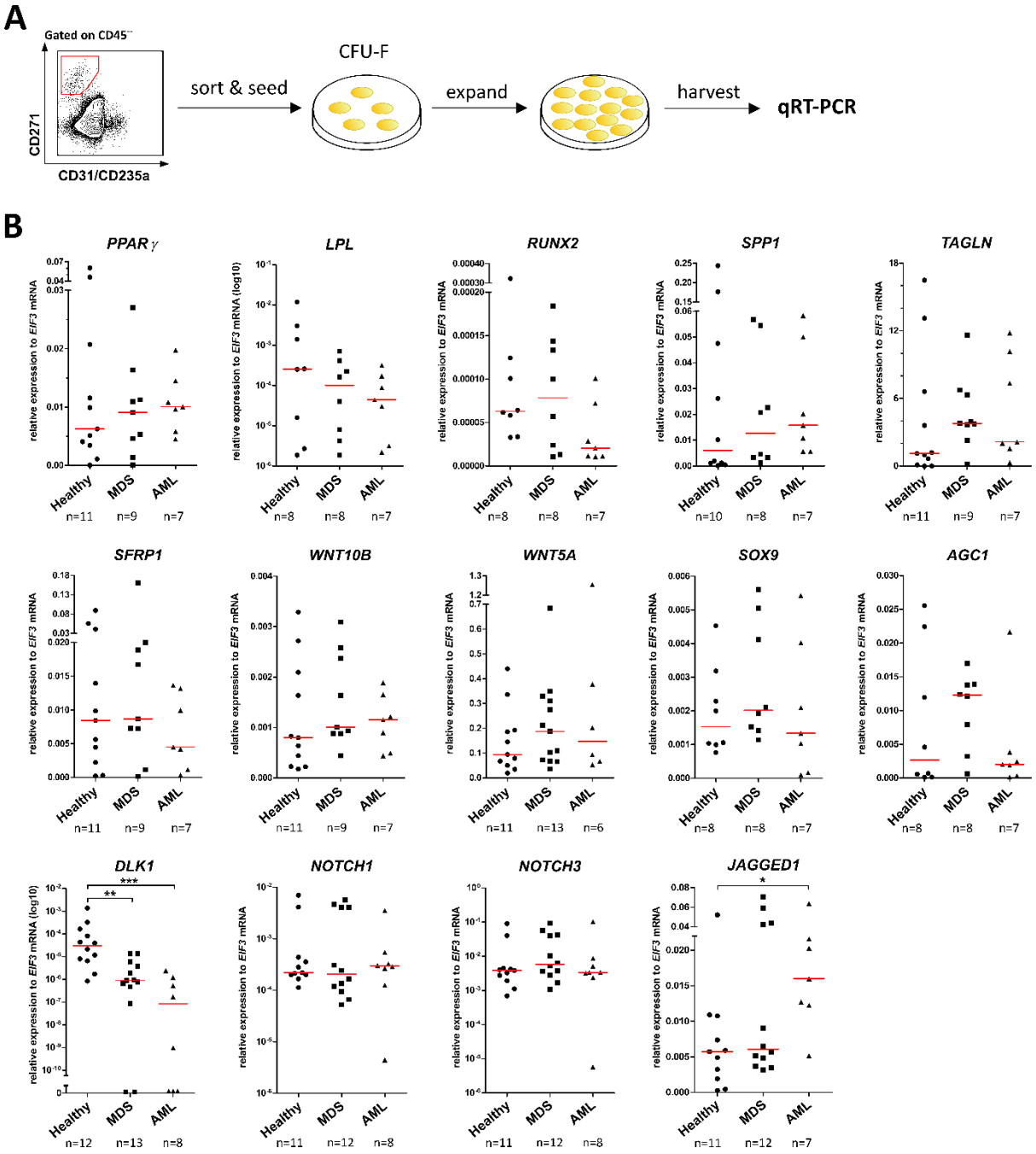

Figure 13: Gene expression analysis of sorted, expanded MSC.

(A) Experimental design. BM-MNC from healthy donor, MDS, and AML samples were thawed and sorted on $CD45^-/CD31^-/CD235a^-/CD271^+$ MSC subpopulation, cells were seeded, and CFU-F colonies were expanded. Cells were harvested after passage 1 or 2, total RNA was extracted, and expression of target genes was analyzed by

qRT-PCR. **(B)** Results show the relative gene expression of *LPL*, *PPARγ*, *RUNX2*, *SPP1*, *TAGLN*, *SFRP1*, *WNT10B*, *WNT5A*, *SOX9*, *AGC1, DLK1*, *NOTCH1*, *NOTCH3*, and *JAGGED1* of each patient sample, all normalized on *EIF3* gene expression. Medians are indicated in red. Sample numbers are indicated on the bottom of each graph.

5.5 Analysis of DLK1 expression in MSC and its possible impacts on the hematopoietic compartment

5.5.1 DLK1 protein expression in sorted MSC

Our previous result showed that *in vitro* adipogenic differentiation potential is significantly increased in MDS and AML MSC (see Figure 8D), whereas simultaneously the gene expression levels of the adipogenic inhibitor *DLK1* are significantly reduced in the malignant samples (see Figure 13B). This raised our interest in further analyzing the DLK1 molecule and its possible impacts on BM structure and potential consequences on the hematopoietic compartment in context of MDS and AML.

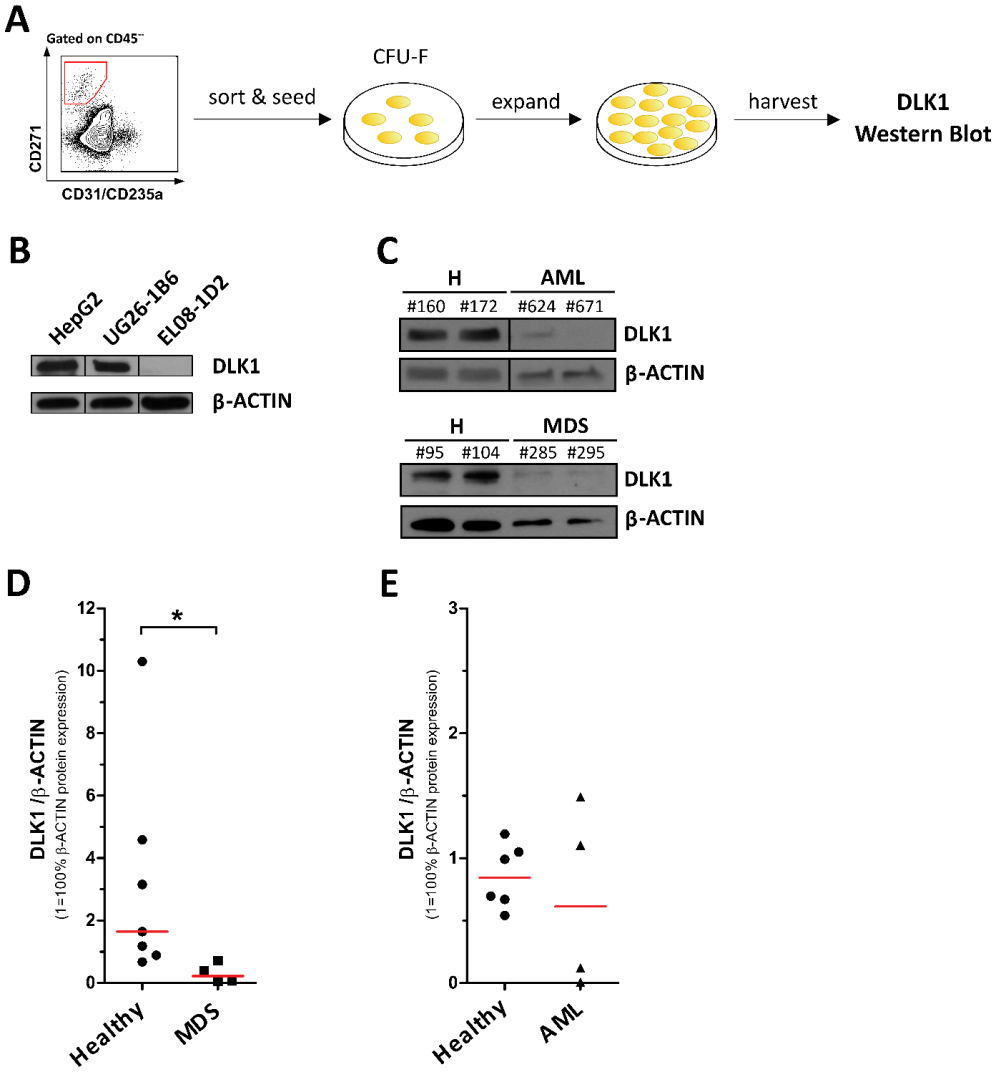

Figure 14: Detection of DLK1 protein expression in sorted MSC.

(A) Experimental design. $CD45^-$/lin(CD31/CD235a)$^-$/$CD271^+$ sorted MSC from healthy donors, MDS, and AML samples were seeded and CFU-F forming cells were expanded and harvested for DLK1 protein expression analysis by western blot. **(B)** Representative immunoblot for detection of DLK1 in HepG2 and UG26-1B6 cell lines

(positive controls), and EL08-1D2 cell line (negative control). β-ACTIN protein expression was detected as housekeeping control. **(C)** Representative immunoblots for detection of DLK1 with β-ACTIN as housekeeping control in sorted MSC from healthy donors, MDS, and AML samples. Numbers indicate individual patient samples. H = healthy donors. **(D) & (E)** Quantification of immunoblotting is shown as relative protein expression of DLK1 normalized on β-ACTIN expression with 1 = 100 % β-ACTIN expression. Medians are indicated in red. **(D)** Healthy donors n = 7, MDS n = 4. **(E)** Healthy donors n = 6, AML n = 4.

For that, we performed western blot analysis for detection of DLK1 on protein level in sorted and subsequently expanded MSC from healthy donors, MDS, and AML patients (see Figure 14A), to check if the differential gene expression is also displayed on protein level.

The primary antibody used for DLK1 detection was first tested with lysates from the human cell line HepG2, and murine UG26-1B6 and EL08-1D2 cell lines. HepG2 was used as a positive control by the antibody supplier, whereas the murine cell lines were used as positive (UG26-1B6) and negative (EL08-1D2) control since the antibody was also predicted to have cross-species reactivity for murine DLK1. Signals were detected at the expected height of ca. 50 kDa in HepG2 and UG26-1B6 lysates but not in EL08-1D2 lysate (see Figure 14B), indicating that the antibody was suitable for DLK1 detection in human and murine samples.

Mirroring the results on RNA level, immunoblotting with lysates from sorted primary MSC showed significantly reduced DLK1 protein levels in MDS MSC compared to healthy MSC (see Figure 14 C+D). Furthermore, DLK1 expression was strongly reduced in two of four AML MSC samples (see Figure 14 C+E).

5.5.2 Treatment of EL08-1D2 stroma cells with DLK1 and possible impact on hematopoietic cells

We wanted to investigate if DLK1 treatment of stroma cells leads to changes in their cellular pathways that subsequently result in altered signaling cues towards the hematopoietic compartment.

For that, sublethally irradiated EL08-1D2 stroma cells, which lack DLK1 expression (see Figure 14 B and [126]), were cultured for four days in serum-free medium (SFM) with or without added murine recombinant DLK1 (2.5 µg/ml). The conditioned SFM was used for culture of $CD34^+$ hematopoietic cells from healthy donors, MDS, and AML patient samples (n = 3 each, see Figure 15A). After four days in the conditioned SFM, $CD34^+$ cells were harvested and Annexin V/PI-FACS analysis and CFU assays were performed to check for a stroma-mediated effect on viability and short-term proliferation potential of the hematopoietic cells. To check for the possibility of a direct effect of murine DLK1 on the human $CD34^+$ cells, in a third approach, SFM conditioned by EL08-1D2 without DLK1 treatment was supplied with DLK1 just before $CD34^+$ culture.

Compared to healthy controls, viability was reduced independently of DLK1 treatment by about 40 % and 25 % in MDS and AML $CD34^+$ cells, respectively (see Figure 15C).

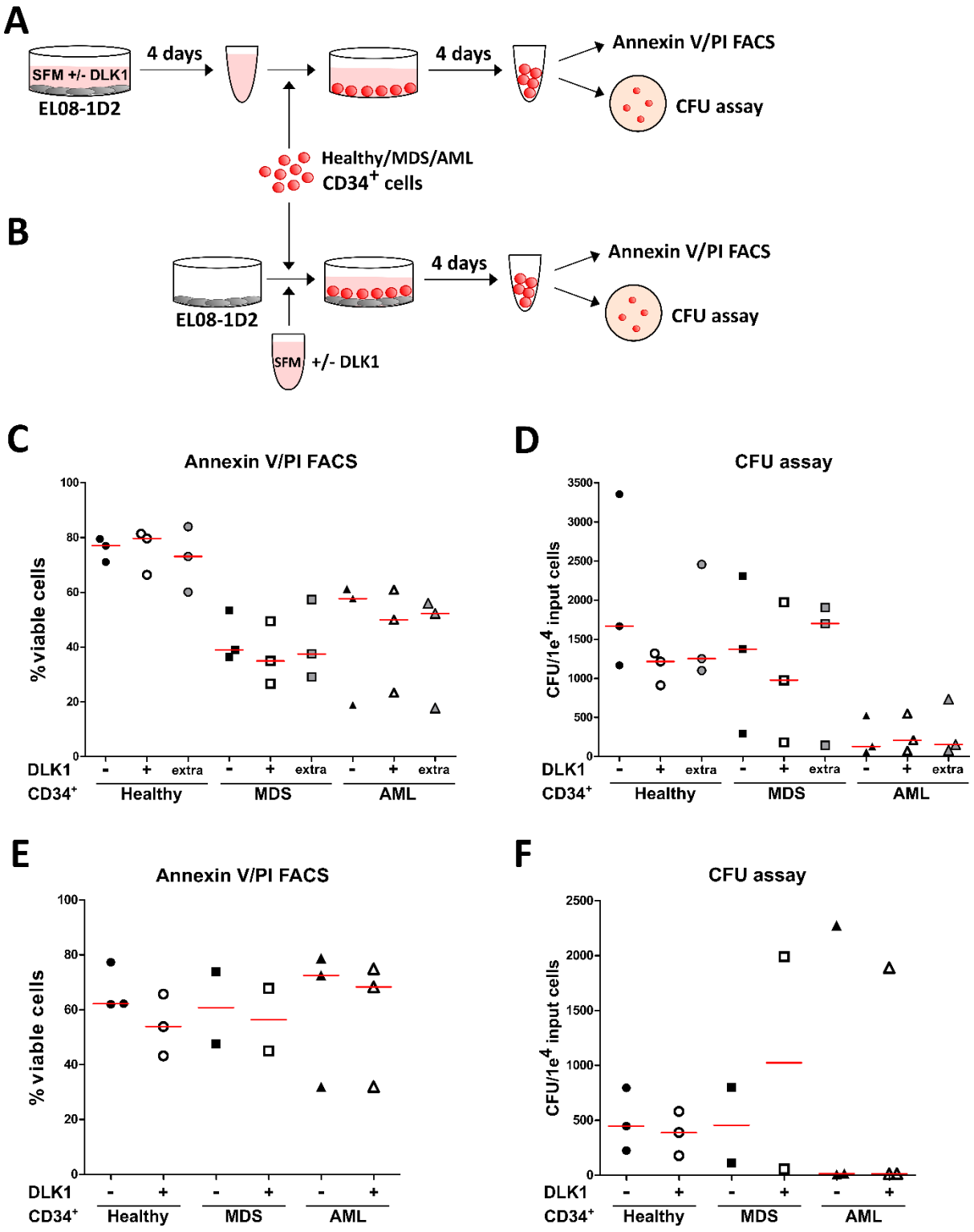

Figure 15: Effect of DLK1-treated EL08-1D2-conditioned medium on viability and short-term proliferation capacity of CD34⁺ cells.

(A) & (B) Experimental design. **(A)** Serum-free medium (SFM) was conditioned for four days on sublethally irradiated (30 Gy) murine EL08-1D2 stroma cells with or without treatment with recombinant murine DLK1. SFM was harvested and used for 4-day-culture of CD34⁺ cells from primary healthy donor, MDS, or AML BM-MNC samples (n = 3 each). Additionally, as a third medium condition, conditioned SFM from EL08 without DLK1 treatment was supplemented with DLK1 just before 4-day-culture of CD34⁺ cells, as a control for a possible direct effect of murine recombinant DLK1 protein on CD34⁺ cells. CD34⁺ cells were harvested after 4-day-culture in the

three different medium conditions and viability and short-term proliferation capacity were analyzed by Annexin V/PI-FACS and CFU assay in methylcellulose, respectively. **(B)** Cocultures of sublethally irradiated (30 Gy) EL08-1D2 stroma cells and $CD34^+$ cells from healthy (n = 3), MDS (n = 2), and AML (n = 3) samples for four days in SFM with or without added recombinant murine DLK1, followed by Annexin V/PI-FACS analysis and CFU assays of the $CD34^+$ cells. The same $CD34^+$ samples were used as in the experiment described in (A). **(C)** Annexin V/PI-FACS analysis of $CD34^+$ cells after 4-day-culture in EL08-conditioned SFM as described in (A). Results are shown as percentage of viable (Annexin V^-/PI^-) cells, with medians indicated in red. + DLK1 = EL08-conditioned SFM with DLK1 treatment, - DLK1 = EL08-conditioned SFM without DLK1 treatment, extra = EL08-contitioned SFM without DLK1 treatment, where DLK1 was added just before $CD34^+$ culture. **(D)** Short-term proliferation capacity of $CD34^+$ cells after 4-day-culture in EL08-conditioned SFM as described in (A). Results are shown as number of total CFU colonies (normalized on $1e^4$ input cells), with medians indicated in red. + DLK1 = EL08-conditioned SFM with DLK1 treatment, - DLK1 = EL08-conditioned SFM without DLK1 treatment, extra = EL08-contitioned SFM without DLK1 treatment, where DLK1 was added just before $CD34^+$ culture. **(E)** Annexin V/PI-FACS analysis of $CD34^+$ cells after 4-day-co-culture on EL08-1D2 stroma cells as described in (B). Results are shown as percentage of viable (Annexin V^-/PI^-) cells, with medians indicated in red. + DLK1 = co-culture on EL08-1D2 with DLK1 treatment, - DLK1 = co-culture on EL08-1D2 without DLK1 treatment. **(F)** Short-term proliferation capacity of $CD34^+$ cells after 4-day-co-culture on EL08-1D2 stroma cells as described in (B). Results are shown as number of total CFU colonies (normalized on $1e^4$ input cells), with medians indicated in red. + DLK1 = co-culture on EL08-1D2 with DLK1 treatment, - DLK1 = co-culture on EL08-1D2 without DLK1 treatment.

However, no differences in viability were observed between the different SFM conditions in presence or absence of DLK1 or for DLK1 extra added just before $CD34^+$ culture, neither within one disease type nor across all samples. Short-term proliferation capacity was in general strongly reduced in AML $CD34^+$ samples compared to healthy and MDS $CD34^+$ samples (see Figure 15D). CFU number was slightly reduced in healthy and MDS $CD34^+$ cells cultured in SFM conditioned with DLK1 compared to culture in SFM conditioned without DLK1, whereas culture in conditioned SFM with subsequently added DLK1 lead to reduced CFU numbers in healthy $CD34^+$ but increased CFU numbers in MDS $CD34^+$ cells.

Since signaling towards the hematopoietic compartment is not only transmitted by soluble factors, but also by direct cell-cell contacts, we parallelly set up cocultures of EL08-1D2 and $CD34^+$ from healthy, MDS, and AML samples for four days in SFM with or without added DLK1, followed by Annexin V/PI-FACS analysis and CFU assays of the $CD34^+$ cells (see Figure 15B). To guarantee comparability, the same $CD34^+$ samples were used as in the experiment without EL08-1D2 coculture, with exception of one MDS sample due to limited sample size.

Viability analysis of $CD34^+$ cells cocultured with EL08 in SFM with or without DLK1 showed a small tendency for a slight reduction of viability in cocultures with DLK1 for all health conditions (see Figure 15E). We could not observe the overall reduction in viability for MDS and AML $CD34^+$ as in the cultures without EL08, which is expected since EL08 are known to support malignant hematopoietic cells in culture [98,127–129]. Short-term proliferation potential was reduced in two of three AML $CD34^+$ samples, however the third sample had the highest CFU numbers, independently of DLK1 treatment (see Figure 15F). CFU number was also highly increased in one of two MDS $CD34^+$ samples when cocultured on EL08 with DLK1. Proliferation capacity was not changed in healthy $CD34^+$ when cocultured on EL08 with or without DLK1.

Overall, the data showed no consistent tendency or pattern of alterations in viability or short-term proliferation potential of $CD34^+$ cells for the different medium conditions.

6 Discussion

The knowledge of the involvement of the bone marrow microenvironment in development and progress of hematologic malignancies has expanded in the last decades, yet, there are many gaps concerning pathways and signaling cues involved in malignant remodeling of the niche and its consequences on hematopoiesis [40,68,69,130–134].

6.1 Prospective, precise isolation of MSC from non-cultured MDS and AML patient BM samples

Since currently there is no single surface marker that precisely defines MSC, different marker combinations were published for isolation of MSC from primary BM [61,93,114,115]. However, a fully defined profile of these cells remains elusive yet, and it is of great importance to identify robust marker combinations to define the *in vivo* identity of these rare cells for a better understanding of their role in course of BM/hematopoietic diseases [107]. After testing different surface marker combinations, we finally decided for the panel used throughout this study, which enabled us to frequently isolate primary MSC from non-cultured healthy donors, MDS, as well as AML BM samples. Being able to prospectively isolate the same precisely defined niche population from different kinds of related diseases such as MDS and AML offers the possibility to perform comparative studies of common features and differences of the microenvironment in both disease types, which can help gathering more insights in disease progression and leukemic transition from MDS to AML.

The surface markers of the panel used in this study are all part of the MSC minimal criteria for MSC isolation postulated by the ISCT [61]. The fact that only the $CD45^-/CD31^-/CD235a^-/CD271^+/CD73^+/CD105^+$ (+/+) cells possess CFU-F formation ability and are able to differentiate into adipocytes and osteoblasts *in vitro* further supports the assumption that this cell population indeed comprises the rare MSC subpopulation.

We found strongly reduced CFU-F frequencies, diminished survival upon passaging, as well as morphological changes in +/+ sorted MSC from MDS and AML samples compared to healthy donors, which is in line with previous reports of plastic-adherence- as well as FACS-isolated MSC [93–95,135]. These features are indicating increased cellular stress, which could be caused by an increased inflammatory niche signature in course of malignant transformation, as reported by Zambetti and colleagues in transcriptome analyses of fresh FACS-isolated, uncultivated MDS MSC [136].

Similar to Le et al., who reported reduced expression levels of the MSC marker CD146 in plastic-adherence-derived, cultured AML stroma cells [122], we found the frequency of the $CD45^-/CD31^-/ CD235a^-/CD271^+$ MSC population to be significantly reduced in uncultivated primary AML BM samples. Since $CD271^+$ cells were shown to secrete hematopoietic supportive factors and are able to create niche structures containing bone, fat, and invading hematopoietic cells in ectopic mouse xenografts, the decrease of this cell population can suggest a decreased hematopoietic supportive ability in AML [107,120,137].

It has been shown that cultured MSC have a changed surface marker expression profile compared to freshly isolated, uncultivated cells [113,120,138]. CD271 was shown to be downregulated during *in vitro* culture of MSC [137–140]. In contrast to most other studies, we did not use FCS as a source for growth factors in the MSC culture medium, since the molecular composition is batch-dependent, and bears the risk of transmitting bovine pathogens and inducing xenoimmunization against bovine proteins [141–145]. Instead, we used pooled human platelet lysate (pHPL) according to the protocol developed by Schallmoser and colleagues, that has lot-to-lot constant composition in crucial growth factors, promotes MSC proliferation, CFU-F formation, and chromosomal stability better than culture-medium containing FCS, and bears no risk of xenogeneic immune responses [100–102,141,146–148]. In our study, re-analysis of FACS-isolated +/+ MSC at passage 2 after expansion of CFU-F forming colonies showed that these cells still robustly expressed CD271, CD73, CD105, and CD90, and lacked expression of other negative MSC markers. This suggests that our prospectively isolated MSC still kept their surface marker profile after *in vitro* culture conditions and are therefore more likely to depict the properties of proper *in vivo* MSC in experiments that need a larger number of cells, such as differentiation analyses.

6.2 Cryo-preservation-linked limitations on MSC yield and properties

For clinical use as well as research, there is on the one hand the need of fresh, unbiased MSCs that are most likely to depict the *in vivo* situation but on the other the necessity to store freshly isolated MSCs for use at a later time point for logistic reasons.
Cryopreservation is currently the gold-standard for long-term storage of viable cells. Usually, serum-containing medium or fetal calf serum (FCS) in combination with a cryoprotective agent (CPA) for prevention of intracellular ice crystal formation, in most cases dimethyl sulfoxide (DMSO), is used [149–152]. This procedure is already well established for HSCs used in therapeutic applications as well as research assays [153]. However, there is no common consensus about the ideal conditions for cryopreservation of non-hematopoietic cells. Most of the published protocols have adapted the conditions used for preservation of HSCs [154–156]. Due to logistic reasons, we had to store the freshly aspirated BM patient samples by cryopreservation until use in experiments.

It has been shown that cryopreservation can alter MSC properties such as surface marker expression, response to inflammatory stimuli, or epigenetic changes [157–164]. Furthermore, cryopreservation-caused effects are suggested to cause cardiac or respiratory complications in BM/MSC-transfused patients, mainly due to the cell-toxic effects of DMSO and post-thaw loss of cell viability, as well as reduced homing efficacy [157,165–168]. As these clinical data show impaired functionality of cryopreserved MSC *in vivo*, they are most likely also hampered *in vitro*. The CFU-F frequencies of sorted MSC observed in this study were lower compared to other published data with fresh, unfrozen FACS-isolated MSC [93,115,119,120]. This is consistent with a comparative study with porcine MSC, where the CFU-F frequency of thawed, cryopreserved MSC was significantly lower than in fresh, non-frozen samples [169]. Additionally, our results on RNA integrity after different sample processing procedures showed highest RINs and RNA yield in non-frozen MNC samples from freshly prepped femoral heads,

compared to cryopreserved femoral head-MNC samples. This further indicates that cryopreservation has a negative impact on RNA quality.

Next to the toxic effects of DMSO, mechanical and osmotic stress during the freeze-thaw cycle can lead to membrane and cytoskeleton damage, as well as matrix decoupling [124,165,168,170]. This is strongly disadvantageous for anchorage-dependent cells such as MSC, since it leads to reduction or loss of cell adhesion, thereby inducing apoptosis [123]. Supporting the importance of cell adhesion for survival, studies with genetically engineered MSC overexpressing adhesion molecules like integrin α-4 or transaminase have shown enhanced survival and homing rates *in vivo* [171]. Since the BM-MNC cannot adhere during the process of isolation, freeze/thaw, staining, and FACS isolation of MSC, this could enhance the non-adhesion-mediated apoptosis. Supporting this, our experiments on RNA integrity showed lower RINs and RNA yield in thawed BM-MNC samples, that were kept overnight in a buffer-containing tube at 4 °C, compared to their counterparts that were thawed, density-gradient-purified and FACS isolated in one go on the next day.

Furthermore, it was shown that physical stress during the process of FACS isolation can lead to cell damage and significant reduction of RNA integrity in the sorted cells [172–174]. Additionally, Cui and co-workers observed an increased rate of cell clumping in samples from thawed, cryopreserved cells [175]. Although we tried to prevent clumping of thawed cells by treatment with DNaseI, it is possible that remaining smaller cell clumps lead to reduced cell yield by FACS isolation, since clumps of two cells and more were excluded by pulse width gating on singlet cells. In addition, it was shown that cryo-storage of RNA at low concentrations, as it was the case for the RNA extracted from sorted MSC in our study, has a negative effect on RNA integrity [176].

As other groups were successful in extracting intact RNA from fresh, non-frozen, FACS-isolated MSC [93,136], the problem of poor RNA quality and low yields in our study is most likely caused by combined effects of cryopreservation- and FACS isolation-mediated stress or cell damage.

Current research trends towards the study of transcriptome and proteome from fresh, unmanipulated, non-cultured primary MSC concerning their role in development and progress of hematologic malignancies. However, cryopreservation is often a logistically necessary step prior to analysis. Our results show the urgent need of further research on effects and impairments by cryopreservation, and the development of new cryo-storage protocols, alternative CPAs to DMSO, and improved methods for RNA extraction from small numbers of primary cell samples.

6.3 Possible involvement of *DLK1* in adipogenic remodeling of the niche in course of MDS and AML

The adipo-/osteogenic balance of the BM niche plays an important role in the regulation of hematopoiesis [71]. There are several studies showing an inhibitory effect of adipocytes on healthy hematopoietic cells [48,70,72–74,177]. However, conflicting results were published about

the adipo-/osteogenic differentiation potential in MSC from MDS and AML patients suggesting mostly normal, but also elevated [178], or reduced [179] adipogenic potential of malignant MSC (also reviewed in [40]).

Our analyses showed a high osteogenic differentiation potential with unchanged gene expression of the osteogenic markers *RUNX2* and *SPP1* for prospectively isolated MSC in both healthy and malignant samples. Thus, our findings do not confirm decreased osteogenic potential observed in plastic-adherence selected malignant MSC [94,95,180]. In line with our findings, Chen *et al.* observed expression of osteolineage markers in both prospectively isolated healthy and MDS MSC using a nearly identical sorting strategy ($CD45^-/7AAD^-/CD235a^-/CD31^-/CD271^+/CD105^+$) [93]. This observation and our findings suggest that prospective isolation of non-hematopoietic and non-endothelial $CD271^+/CD105^+/CD73^+$ cells may select for a primary MSC population that differs in its adipo-osteogenic potential compared to plastic-adherence-selected MSC, which likely comprise a more heterogeneous cell population.

To our knowledge, we are the first to show a significantly increased *in vitro* adipogenic differentiation potential in primary FACS-isolated MSC from MDS and AML patients compared to healthy controls. Supporting our findings, Le et al. recently also reported increased adipogenic and delayed osteogenic potential in plastic-adherence-selected MSC from AML patients [122].

Matching the pronounced adipogenic bias in malignant MSC is our observation of the strong reduction of the adipogenic inhibitor DLK1 in MDS and AML MSC samples on both gene and protein expression level. The inhibitory function on adipogenic differentiation of BM MSC by DLK1 and its importance in regulation of the adipo-/osteogenic balance is well reported [86,89,92,181,182]. Emphasizing the significance of DLK1 in regulation of human adipogenesis, a single nucleotide polymorphism in the *DLK1* locus was found to be associated with childhood and adolescence obesity in humans [183].

In accordance with these facts, our findings support the hypothesis that an increased pool of adipogenic primed niche cells in MDS and AML patient BM, caused by decreased inhibition of adipogenesis, which is mediated at least in part by decreased DLK1 levels, could have a negative impact on healthy hematopoiesis, thereby creating a microenvironment that gives advantage to the malignant clone to proliferate and overtake the BM. This hypothesis is further supported by the findings, that obese humans are more prone to develop leukemia, and have worse outcomes in therapy compared to normal-weight patients [184–187].

Fatty acids are stored as triglycerides in the vacuoles of adipocytes [188]. Enhanced biogenesis of fatty acids is frequently observed in hematologic malignancies and necessary for accelerated cell growth and proliferation [189–191]. It was recently shown that oxidation of fatty acids is significantly increased in leukemic blasts, which is crucial for their proliferation and is also linked to protection from apoptosis and chemotherapeutics [75,192–195]. Shafat and colleagues recently showed that AML cells reprogram BM adipocytes to create a pro-tumoral environment, which also involves increased lipolysis and transfer from FA from adipocytes to AML blasts [75]. In this context, it would make sense that an increased need of FA by the

leukemic stem cells is reflected in a shift of MSC differentiation potential towards the adipogenic lineage, giving rise to an increased pool of adipocytes that are able to store lipids in their vacuoles and releasing them when needed.

Next to its function as adipocytic inhibitor, DLK1 was recently found to be an inflammatory inhibitor that is able to negatively regulate pro-inflammatory macrophage activation [196]. Transcriptome analyses of FACS-isolated, uncultivated MDS MSC showed an increased inflammatory signaling in these cells [93,136]. Furthermore, a recent study observed that adipocytes induce a proinflammatory phenotype in residing AML blasts by secretion of molecules like TNFa and IL-1b, leading to lipolysis and release of FA, and that this inflammatory process is most likely reinforced by a FA-mediated positive feedback mechanism [195]. In context with these findings, the downregulation of DLK1 mRNA and protein expression in MDS and AML MSC observed in our study could contribute to promote the pro-tumoral inflammatory niche state.

Although we found the *in vitro* adipogenic differentiation potential significantly increased and mRNA expression of *DLK1* significantly decreased in MDS and AML MSC, we did not observe a parallel upregulation in mRNA expression of *PPARγ* or *LPL*, which are commonly used marker genes for adipogenic differentiation. A reason for that could be that *PPARγ* and *LPL,* in contrast to *DLK1,* are not expressed in preadipocytes but in later stages of adipocyte differentiation, when the cell gets remodeled, expands, and incorporates lipids into its vacuoles [80,197,198]. In our study, we used different experimental systems, with chemically induced MSC for assessment of *in vitro* differentiation potential, versus MSC kept in their undifferentiated stage in MSC medium until harvest for qRT-PCR analysis. The fact, that the MSC used for gene expression analysis were not actively differentiating could on the one hand explain why we found no increased levels of *PPARγ* and *LPL* in these cells, and on the other hand does not exclude an increased adipogenic potential in these cells.

Next to the significant decrease of *DLK1* mRNA levels in MDS and AML MSC, we found the gene expression of the activating, canonical Notch pathway ligand *JAGGED1* significantly upregulated in AML MSC, as well as in several MDS MSC samples.
The Notch-mediated inhibitory effect of DLK1 on adipocyte differentiation is not fully elucidated, yet. It was already shown in yeast and mammalian two-hybrid systems that DLK1 specifically interacts with NOTCH1, and that DLK1-mediated Notch pathway inhibition results in reduced levels of the Notch-downstream component Hes-1 in 3T3-L1 preadipocytes [88,91]. Dlk1, as a non-canonical Notch1 receptor ligand, was shown to interact with the same binding site of Notch1 as Jagged1, and Notch 1 binding competition of the two ligands modulates Notch pathway signaling [88,90,91,199]. Interestingly, Urs and colleagues reported, that Jagged1 enhances adipogenesis in allografts of 3T3-L1 preadipocyte cells, and supports growth and proliferation of endothelial cells, thereby most likely supporting angiogenesis and neovascularization, which is closely associated to adipogenesis [200]. Additionally, Jagged1 was found to be upregulated in tumor-associated blood vessels in brain and ovarian cancer [201], underlining the involvement of Jagged1 in cancer evolution/development. Further supporting our results, Kode and co-workers found upregulated Jagged1 levels in murine osteoblasts with constitutively active β-catenin expression, leading to enhanced Notch

signaling in HSC, which induces their leukemic transformation and *de novo* development of AML [64]. Since osteoblasts are the progeny of MSC, these findings support our observation of upregulated *JAGGED1* expression in malignant MSC, which can act also in this cell type as a leukemogenesis-promoting factor/event. Verifying increased JAGGED1 expression in primary MDS and AML MSC on protein level and checking for β-catenin expression in MSC and downstream Notch-targets in hematopoietic cells from primary MDS and AML samples could help to re-assess and transfer these findings into the human system.
Furthermore, increased Notch signaling possibly has a negative feedback impact on DLK1 expression [202]. A decrease in DLK1 expression in the malignant MSC could therefore lead to enhanced binding of JAGGED1 to NOTCH1, resulting in increased Notch signaling, which in turn further supports downregulation of DLK1 levels, thereby supporting adipogenesis via reduced DLK1-mediated inhibition and enhanced JAGGED1-mediated activation.
The fact that we observed increased *JAGGED1* expression in several MDS MSC samples at similar levels to that in AML MSC, could hint at an advanced state in niche remodeling towards adipogenesis in these MDS patients, possibly marking an increased risk of transition towards an acute leukemia.

DLK1 is an imprinted gene with paternal expression only. It is already known, that DLK1 is overexpressed in $CD34^+$ hematopoietic cells from MDS and AML patients [203,204]. Recently, it was shown, that DLK1 is biallelic expressed in a greater part of the $DLK1^{hi}$ $CD34^+$ cells and that this process is regulated methylation-dependently by an upstream insulator element [203]. Release of biallelic expression by changes in methylation patterns can be dependent on cell identity and the surrounding microenvironment, as well as on other clinical factors such as age or co-morbidities. Since in our study, elevated DLK1 protein levels were only found in noticeably young AML patients (20 and 39 years), this could be an indicative factor for a good outcome in these patients, as the higher DLK1 levels could prevent or attenuate adipogenic remodeling and inflammatory signature. More samples are needed to assess if DLK1 expression correlates with a specific risk subgroup in AML patients.

Membrane-tethered DLK1 can be cleaved at the extracellular domain by the TACE protease to release a soluble ligand [76,80,81]. There are contrary data about the function and activity of soluble versus membrane-tethered DLK1. For example, Mei *et al.* showed, that only the soluble form of Dlk1 mediates adipogenic inhibition, whereas Mortensen and colleagues reported, that only membrane-bound Dlk1 inhibits adipocyte differentiation [82,83]. However, a tightly regulated dosage control of cleaved and membrane-bound DLK1 seems to be necessary for proper coordination of functions, and also small changes in DLK1 expression can have influence on cell properties and developmental programs [83,205–208]. The fact, that we used only soluble, but not membrane-tethered DLK1, could be the reason why we did not observe any differences in viability and short-term proliferation potential of healthy, MDS, and AML $CD34^+$ cells after culture in medium conditioned by EL08-1D2 stroma cells in presence or absence of DLK1. Repetition of the experiment with stroma cells overexpressing or lacking DLK1 could give more insight into this issue. Since the immunoblotting antibody used in this study targeted the extracellular domain of DLK1, and both human *DLK1* mRNA isoforms contain the sequences for intracellular-, transmembrane-, cleavage-, and cytoplasmic domain, we could not discriminate possible differences between levels of soluble

versus membrane-tethered *DLK1* by qRT-PCR or western blot. This could be interesting for future studies, as well as possible differences in expression or activity of the TACE protease.

Overall, our findings indicate a changed functionality in prospectively isolated, primary MSC from MDS and AML patient BM samples, showing significantly reduced CFU-F frequencies and increased *in vitro* adipogenic differentiation potential. Reduced expression of the adipogenic inhibitor *DLK1* on gene and protein level within the malignant samples supports these findings and points to a changed adipo-/osteogenic balance within the stem cell niche during malignant transformation, which could be a contributing factor for disease progression. Together with the findings of other groups, our results underline the need of further research on the complex role of the *DLK1* molecule in BM niche remodeling and disease progression in context of hematologic malignancies.

7 References

1. Becker, A. J., McCulloch, E. A. & Till, J. E. Cytological demonstration of the clonal nature of spleen colonies derived from transplanted mouse marrow cells. *Nature* **197**, 452–4 (1963).

2. McCulloch, E. A. & Till, J. E. The radiation sensitivity of normal mouse bone marrow cells, determined by quantitative marrow transplantation into irradiated mice. *Radiat. Res.* **13**, 115–25 (1960).

3. Till, J. E. & McCulloch, E. A. A Direct Measurement of the Radiation Sensitivity of Normal Mouse Bone Marrow Cells. *Radiat. Res.* **14**, 213 (1961).

4. Seita, J. & Weissman, I. L. Hematopoietic stem cell: self-renewal versus differentiation. *Wiley Interdiscip. Rev. Syst. Biol. Med.* **2**, 640–53 (2010).

5. Ogawa, M. Differentiation and proliferation of hematopoietic stem cells. *Blood* **81**, 2844–53 (1993).

6. Passegué, E., Wagers, A. J., Giuriato, S., Anderson, W. C. & Weissman, I. L. Global analysis of proliferation and cell cycle gene expression in the regulation of hematopoietic stem and progenitor cell fates. *J. Exp. Med.* **202**, 1599–611 (2005).

7. Walter, D. *et al.* Exit from dormancy provokes DNA-damage-induced attrition in haematopoietic stem cells. *Nature* **520**, 549–52 (2015).

8. Yamaguchi, M. *et al.* Different adhesive characteristics and VLA-4 expression of CD34(+) progenitors in G0/G1 versus S+G2/M phases of the cell cycle. *Blood* **92**, 842–8 (1998).

9. Geiger, H., de Haan, G. & Florian, M. C. The ageing haematopoietic stem cell compartment. *Nat. Rev. Immunol.* **13**, 376–89 (2013).

10. Pang, W. W. *et al.* Human bone marrow hematopoietic stem cells are increased in frequency and myeloid-biased with age. *Proc. Natl. Acad. Sci. U. S. A.* **108**, 20012–7 (2011).

11. Pang, W. W., Schrier, S. L. & Weissman, I. L. Age-associated changes in human hematopoietic stem cells. *Semin. Hematol.* **54**, 39–42 (2017).

12. Rossi, D. J. *et al.* Deficiencies in DNA damage repair limit the function of haematopoietic stem cells with age. *Nature* **447**, 725–9 (2007).

13. Rossi, D. J. *et al.* Hematopoietic stem cell quiescence attenuates DNA damage response and permits DNA damage accumulation during aging. *Cell Cycle* **6**, 2371–6 (2007).

14. Rundberg Nilsson, A., Soneji, S., Adolfsson, S., Bryder, D. & Pronk, C. J. Human and Murine Hematopoietic Stem Cell Aging Is Associated with Functional Impairments and Intrinsic Megakaryocytic/Erythroid Bias. *PLoS One* **11**, e0158369 (2016).

15. Corces-Zimmerman, M. R. & Majeti, R. Pre-leukemic evolution of hematopoietic stem cells: the importance of early mutations in leukemogenesis. *Leukemia* **28**, 2276–2282 (2014).

16. Genovese, G. *et al.* Clonal hematopoiesis and blood-cancer risk inferred from blood

DNA sequence. *N. Engl. J. Med.* **371**, 2477–87 (2014).

17. Montalban-Bravo, G. & Garcia-Manero, G. Myelodysplastic syndromes: 2018 update on diagnosis, risk-stratification and management. *Am. J. Hematol.* **93**, 129–147 (2018).

18. Arber, D. A. *et al.* The 2016 revision to the World Health Organization classification of myeloid neoplasms and acute leukemia. *Blood* **127**, 2391–2405 (2016).

19. Greenberg, P. L. *et al.* Myelodysplastic syndromes, version 2.2015. *J. Natl. Compr. Canc. Netw.* **13**, 261–72 (2015).

20. Greenberg, P. L. *et al.* Myelodysplastic Syndromes, Version 2.2017, NCCN Clinical Practice Guidelines in Oncology. *J. Natl. Compr. Cancer Netw.* **15**, 60–87 (2017).

21. Greenberg, P. *et al.* International scoring system for evaluating prognosis in myelodysplastic syndromes. *Blood* **89**, 2079–88 (1997).

22. Döhner, H., Weisdorf, D. J. & Bloomfield, C. D. Acute Myeloid Leukemia. *N. Engl. J. Med.* **373**, 1136–1152 (2015).

23. De Kouchkovsky, I. & Abdul-Hay, M. 'Acute myeloid leukemia: a comprehensive review and 2016 update'. *Blood Cancer J.* **6**, e441–e441 (2016).

24. Shah, A., Andersson, T. M.-L., Rachet, B., Björkholm, M. & Lambert, P. C. Survival and cure of acute myeloid leukaemia in England, 1971-2006: a population-based study. *Br. J. Haematol.* **162**, 509–516 (2013).

25. Siegel, R. L., Miller, K. D. & Jemal, A. Cancer statistics, 2017. *CA. Cancer J. Clin.* **67**, 7–30 (2017).

26. Noone, A. *et al.* SEER Cancer Statistics Review, 1975-2015, National Cancer Institute. Bethesda, MD. *based on November 2017 SEER data submission, posted to the SEER web site, April 2018* based on November 2017 SEER data submission, poste (2018). Available at: https://seer.cancer.gov/csr/1975_2015/. (Accessed: 29th September 2018)

27. Döhner, H. *et al.* Diagnosis and management of acute myeloid leukemia in adults: recommendations from an international expert panel, on behalf of the European LeukemiaNet. *Blood* **115**, 453–474 (2010).

28. Döhner, H. *et al.* Diagnosis and management of AML in adults: 2017 ELN recommendations from an international expert panel. *Blood* **129**, 424–447 (2017).

29. Verma, D. *et al.* Late relapses in acute myeloid leukemia: analysis of characteristics and outcome. *Leuk. Lymphoma* **51**, 778–782 (2010).

30. Dick, J. E. Stem cell concepts renew cancer research. *Blood* **112**, 4793–807 (2008).

31. Hope, K. J., Jin, L. & Dick, J. E. Acute myeloid leukemia originates from a hierarchy of leukemic stem cell classes that differ in self-renewal capacity. *Nat. Immunol.* **5**, 738–743 (2004).

32. Kreso, A. & Dick, J. E. Evolution of the Cancer Stem Cell Model. *Cell Stem Cell* **14**, 275–291 (2014).

33. Mossner, M. *et al.* Mutational hierarchies in myelodysplastic syndromes dynamically

adapt and evolve upon therapy response and failure. *Blood* **128**, 1246–1259 (2016).

34. Li, S., Mason, C. E. & Melnick, A. Genetic and epigenetic heterogeneity in acute myeloid leukemia. *Curr. Opin. Genet. Dev.* **36**, 100–106 (2016).

35. Medinger, M., Lengerke, C. & Passweg, J. Novel Prognostic and Therapeutic Mutations in Acute Myeloid Leukemia. *Cancer Genomics Proteomics* **13**, 317–29 (2016).

36. Ganguly, B. B. & Kadam, N. N. Mutations of myelodysplastic syndromes (MDS): An update. *Mutat. Res. Rev. Mutat. Res.* **769**, 47–62 (2016).

37. Papaemmanuil, E. *et al.* Clinical and biological implications of driver mutations in myelodysplastic syndromes. *Blood* **122**, 3616–3627 (2013).

38. Haferlach, T. *et al.* Landscape of genetic lesions in 944 patients with myelodysplastic syndromes. *Leukemia* **28**, 241–247 (2014).

39. Cancer Genome Atlas Research Network *et al.* Genomic and epigenomic landscapes of adult de novo acute myeloid leukemia. *N. Engl. J. Med.* **368**, 2059–74 (2013).

40. Goulard, M., Dosquet, C. & Bonnet, D. Role of the microenvironment in myeloid malignancies. *Cell. Mol. Life Sci.* **75**, 1377–1391 (2018).

41. Ribatti, D., Mangialardi, G. & Vacca, A. Stephen Paget and the 'seed and soil' theory of metastatic dissemination. *Clin. Exp. Med.* **6**, 145–149 (2006).

42. Asada, N., Takeishi, S. & Frenette, P. S. Complexity of bone marrow hematopoietic stem cell niche. *Int. J. Hematol.* **106**, 45–54 (2017).

43. Birbrair, A. & Frenette, P. S. Niche heterogeneity in the bone marrow. *Ann. N. Y. Acad. Sci.* **1370**, 82–96 (2016).

44. Cordeiro-Spinetti, E., Taichman, R. S. & Balduino, A. The Bone Marrow Endosteal Niche: How Far from the Surface? *J. Cell. Biochem.* **116**, 6–11 (2015).

45. Pleyer, L., Valent, P. & Greil, R. Mesenchymal Stem and Progenitor Cells in Normal and Dysplastic Hematopoiesis-Masters of Survival and Clonality? *Int. J. Mol. Sci.* **17**, 1009 (2016).

46. Schofield, R. The relationship between the spleen colony-forming cell and the haemopoietic stem cell. *Blood Cells* **4**, 7–25 (1978).

47. Ehninger, A. & Trumpp, A. The bone marrow stem cell niche grows up: mesenchymal stem cells and macrophages move in. *J. Exp. Med.* **208**, 421–8 (2011).

48. Naveiras, O. *et al.* Bone-marrow adipocytes as negative regulators of the haematopoietic microenvironment. *Nature* **460**, 259–263 (2009).

49. Friedenstein, A. J. Precursor cells of mechanocytes. *Int. Rev. Cytol.* **47**, 327–59 (1976).

50. Friedenstein, A. J. Stromal mechanisms of bone marrow: cloning in vitro and retransplantation in vivo. *Haematol. Blood Transfus.* **25**, 19–29 (1980).

51. Friedenstein, A. J., Piatetzky-Shapiro, I. I. & Petrakova, K. V. Osteogenesis in transplants of bone marrow cells. *J. Embryol. Exp. Morphol.* **16**, 381–90 (1966).

52. Friedenstein, A. J., Chailakhjan, R. K. & Lalykina, K. S. The development of fibroblast colonies in monolayer cultures of guinea-pig bone marrow and spleen cells. *Cell Tissue Kinet.* **3**, 393–403 (1970).

53. Friedenstein, A. J., Chailakhyan, R. K., Latsinik, N. V., Panasyvk, A. F. & Keiliss-Borok, I. V. Stromal cells responsible for transferring the microenvironment of the hemopoietic tissues. Cloning in vitro and retransplantation in vivo. *Transplantation* **17**, 331–340 (1974).

54. Friedenstein, A. J. *et al.* Precursors for fibroblasts in different populations of hematopoietic cells as detected by the in vitro colony assay method. *Exp. Hematol.* **2**, 83–92 (1974).

55. Latsinik, N. V, Luria, E. A., Friedenstein, A. J., Samoylina, N. L. & Chertkov, I. L. Colony-forming cells in organ cultures of embryonal liver. *J. Cell. Physiol.* **75**, 163–5 (1970).

56. Pittenger, M. F. *et al.* Multilineage potential of adult human mesenchymal stem cells. *Science* **284**, 143–7 (1999).

57. Bianco, P., Robey, P. G. & Simmons, P. J. Mesenchymal Stem Cells: Revisiting History, Concepts, and Assays. *Cell Stem Cell* **2**, 313–319 (2008).

58. Friedenstein, A. J., Chailakhyan, R. K. & Gerasimov, U. V. Bone marrow osteogenic stem cells: in vitro cultivation and transplantation in diffusion chambers. *Cell Tissue Kinet.* **20**, 263–272 (1987).

59. Owen, M. & Friedenstein, A. J. Stromal stem cells: marrow-derived osteogenic precursors. *Ciba Found. Symp.* **136**, 42–60 (1988).

60. Caplan, A. I. Mesenchymal stem cells. *J. Orthop. Res.* **9**, 641–650 (1991).

61. Dominici, M. *et al.* Minimal criteria for defining multipotent mesenchymal stromal cells. The International Society for Cellular Therapy position statement. *Cytotherapy* **8**, 315–317 (2006).

62. Sacchetti, B. *et al.* Self-renewing osteoprogenitors in bone marrow sinusoids can organize a hematopoietic microenvironment. *Cell* **131**, 324–36 (2007).

63. Raaijmakers, M. H. G. P. *et al.* Bone progenitor dysfunction induces myelodysplasia and secondary leukaemia. *Nature* **464**, 852–7 (2010).

64. Kode, A. *et al.* Leukaemogenesis induced by an activating β-catenin mutation in osteoblasts. *Nature* **506**, 240–244 (2014).

65. Kode, A. *et al.* FoxO1-dependent induction of acute myeloid leukemia by osteoblasts in mice. *Leukemia* **30**, 1–13 (2016).

66. Medyouf, H. The microenvironment in human myeloid malignancies: emerging concepts and therapeutic implications. *Blood* **129**, 1617–1626 (2017).

67. Wiseman, D. H. Donor cell leukemia: a review. *Biol. Blood Marrow Transplant.* **17**, 771–89 (2011).

68. Schepers, K., Campbell, T. B. & Passegué, E. Normal and Leukemic Stem Cell Niches:

Insights and Therapeutic Opportunities. *Cell Stem Cell* **16**, 254–267 (2015).

69. Schroeder, T., Geyh, S., Germing, U. & Haas, R. Mesenchymal stromal cells in myeloid malignancies. *Blood Res.* **51**, 225–232 (2016).

70. Chitteti, B. R. *et al.* Impact of interactions of cellular components of the bone marrow microenvironment on hematopoietic stem and progenitor cell function. *Blood* **115**, 3239–3248 (2010).

71. Sugimura, R. & Li, L. Shifting in Balance Between Osteogenesis and Adipogenesis Substantially Influences Hematopoiesis. *J. Mol. Cell Biol.* **2**, 61–62 (2010).

72. Ambrosi, T. H. *et al.* Adipocyte Accumulation in the Bone Marrow during Obesity and Aging Impairs Stem Cell-Based Hematopoietic and Bone Regeneration. *Cell Stem Cell* **20**, 1–14 (2017).

73. Bethel, M., Chitteti, B. R., Srour, E. F. & Kacena, M. A. The Changing Balance Between Osteoblastogenesis and Adipogenesis in Aging and its Impact on Hematopoiesis. *Curr. Osteoporos. Rep.* **11**, 99–106 (2013).

74. Zhu, R.-J., Wu, M.-Q., Li, Z.-J., Zhang, Y. & Liu, K.-Y. Hematopoietic recovery following chemotherapy is improved by BADGE-induced inhibition of adipogenesis. *Int. J. Hematol.* **97**, 58–72 (2013).

75. Shafat, M. S. *et al.* Leukemic blasts program bone marrow adipocytes to generate a protumoral microenvironment. *Blood* **129**, 1320–1332 (2017).

76. Wang, Y., Kim, K.-A., Kim, J.-H. & Sul, H. S. Pref-1, a preadipocyte secreted factor that inhibits adipogenesis. *J. Nutr.* **136**, 2953–6 (2006).

77. Lee, Y. L., Helman, L., Hoffman, T. & Laborda, J. dlk, pG2 and Pref-1 mRNAs encode similar proteins belonging to the EGF-like superfamily. Identification of polymorphic variants of this RNA. *Biochim. Biophys. Acta - Gene Struct. Expr.* **1261**, 223–232 (1995).

78. Smas, C. M. & Sul, H. S. Pref-1, a protein containing EGF-like repeats, inhibits adipocyte differentiation. *Cell* **73**, 725–34 (1993).

79. Smas, C. M., Green, D. & Sul, H. S. Structural characterization and alternate splicing of the gene encoding the preadipocyte EGF-like protein Pref-1. *Biochemistry* **33**, 9257–9265 (1994).

80. Smas, C. M., Chen, L. & Sul, H. S. Cleavage of membrane-associated pref-1 generates a soluble inhibitor of adipocyte differentiation. *Mol. Cell. Biol.* **17**, 977–88 (1997).

81. Wang, Y. & Sul, H. S. Ectodomain Shedding of Preadipocyte Factor 1 (Pref-1) by Tumor Necrosis Factor Alpha Converting Enzyme (TACE) and Inhibition of Adipocyte Differentiation. *Mol. Cell. Biol.* **26**, 5421–5435 (2006).

82. Mei, B., Zhao, L., Chen, L. & Sul, H. S. Only the large soluble form of preadipocyte factor-1 (Pref-1), but not the small soluble and membrane forms, inhibits adipocyte differentiation: role of alternative splicing. *Biochem. J.* **364**, 137–44 (2002).

83. Mortensen, S. B. *et al.* Membrane-Tethered Delta-Like 1 Homolog (DLK1) Restricts Adipose Tissue Size by Inhibiting Preadipocyte Proliferation. *Diabetes* **61**, 2814–2822

(2012).

84. Laborda, J. The role of the epidermal growth factor-like protein dlk in cell differentiation. *Histol. Histopathol.* **15**, 119–129 (2000).

85. Tax, F. E., Yeargers, J. J. & Thomas, J. H. Sequence of C. elegans lag-2 reveals a cell-signalling domain shared with Delta and Serrate of Drosophila. *Nature* **368**, 150 (1994).

86. Wang, Y. & Sul, H. S. Pref-1 Regulates Mesenchymal Cell Commitment and Differentiation through Sox9. *Cell Metab.* **9**, 287–302 (2009).

87. Wang, Y., Zhao, L., Smas, C. & Sul, H. S. Pref-1 Interacts with Fibronectin To Inhibit Adipocyte Differentiation. *Mol. Cell. Biol.* **30**, 3480–3492 (2010).

88. Baladrón, V. *et al.* dlk acts as a negative regulator of Notch1 activation through interactions with specific EGF-like repeats. *Exp. Cell Res.* **303**, 343–59 (2005).

89. Nueda, M.-L., Baladrón, V., Sánchez-Solana, B., Ballesteros, M.-Á. & Laborda, J. The EGF-like Protein dlk1 Inhibits Notch Signaling and Potentiates Adipogenesis of Mesenchymal Cells. *J. Mol. Biol.* **367**, 1281–1293 (2007).

90. Sánchez-Solana, B. *et al.* The EGF-like proteins DLK1 and DLK2 function as inhibitory non-canonical ligands of NOTCH1 receptor that modulate each other's activities. *Biochim. Biophys. Acta* **1813**, 1153–64 (2011).

91. Traustadóttir, G. Á. *et al.* Evidence of non-canonical NOTCH signaling: Delta-like 1 homolog (DLK1) directly interacts with the NOTCH1 receptor in mammals. *Cell. Signal.* **28**, 246–54 (2016).

92. Nueda, M.-L., García-Ramírez, J. J., Laborda, J. & Baladrón, V. dlk1 Specifically Interacts with Insulin-Like Growth Factor Binding Protein 1 to Modulate Adipogenesis of 3T3-L1 Cells. *J. Mol. Biol.* **379**, 428–442 (2008).

93. Chen, S. *et al.* Massive parallel RNA sequencing of highly purified mesenchymal elements in low-risk MDS reveals tissue-context-dependent activation of inflammatory programs. *Leukemia* **30**, 1938–1942 (2016).

94. Geyh, S. *et al.* Insufficient stromal support in MDS results from molecular and functional deficits of mesenchymal stromal cells. *Leukemia* **27**, 1841–51 (2013).

95. Geyh, S. *et al.* Functional inhibition of mesenchymal stromal cells in acute myeloid leukemia. *Leukemia* **30**, 683–691 (2015).

96. Kim, J.-A. *et al.* Microenvironmental Remodeling as a Parameter and Prognostic Factor of Heterogeneous Leukemogenesis in Acute Myelogenous Leukemia. *Cancer Res.* **75**, 2222–2231 (2015).

97. Medyouf, H. *et al.* Myelodysplastic cells in patients reprogram mesenchymal stromal cells to establish a transplantable stem cell niche disease unit. *Cell Stem Cell* **14**, 824–837 (2014).

98. Oostendorp, R. A. J. *et al.* Embryonal subregion-derived stromal cell lines from novel temperature-sensitive SV40 T antigen transgenic mice support hematopoiesis. *J. Cell Sci.* **115**, 2099–108 (2002).

99. Knowles, B. B., Howe, C. C. & Aden, D. P. Human hepatocellular carcinoma cell lines secrete the major plasma proteins and hepatitis B surface antigen. *Science* **209**, 497–9 (1980).

100. Schallmoser, K. & Strunk, D. Preparation of pooled human platelet lysate (pHPL) as an efficient supplement for animal serum-free human stem cell cultures. *J. Vis. Exp.* 20–23 (2009). doi:10.3791/1523

101. Schallmoser, K. *et al.* Rapid large-scale expansion of functional mesenchymal stem cells from unmanipulated bone marrow without animal serum. *Tissue Eng. Part C. Methods* **14**, 185–96 (2008).

102. Burnouf, T., Strunk, D., Koh, M. B. C. & Schallmoser, K. Human platelet lysate: Replacing fetal bovine serum as a gold standard for human cell propagation? *Biomaterials* **76**, 371–87 (2016).

103. Soumillon, M., Cacchiarelli, D., Semrau, S., van Oudenaarden, A. & Mikkelsen, T. S. Characterization of directed differentiation by high-throughput single-cell RNA-Seq. *bioRxiv* (2014). doi:10.1101/003236

104. Finak, G. *et al.* MAST: a flexible statistical framework for assessing transcriptional changes and characterizing heterogeneity in single-cell RNA sequencing data. *Genome Biol.* **16**, 278 (2015).

105. Love, M. I., Huber, W. & Anders, S. Moderated estimation of fold change and dispersion for RNA-seq data with DESeq2. *Genome Biol.* **15**, 550 (2014).

106. Bianco, P., Riminucci, M., Gronthos, S. & Robey, P. G. Bone Marrow Stromal Stem Cells: Nature, Biology, and Potential Applications. *Stem Cells* **19**, 180–192 (2001).

107. Li, H., Ghazanfari, R., Zacharaki, D., Lim, H. C. & Scheding, S. Isolation and characterization of primary bone marrow mesenchymal stromal cells. *Ann. N. Y. Acad. Sci.* **1370**, 109–118 (2016).

108. Pevsner-Fischer, M., Levin, S. & Zipori, D. The Origins of Mesenchymal Stromal Cell Heterogeneity. *Stem Cell Rev. Reports* **7**, 560–568 (2011).

109. Simmons, P. J. & Torok-Storb, B. Identification of stromal cell precursors in human bone marrow by a novel monoclonal antibody, STRO-1. *Blood* **78**, 55–62 (1991).

110. Sivasubramaniyan, K. *et al.* Phenotypic and functional heterogeneity of human bone marrow- and amnion-derived MSC subsets. *Ann. N. Y. Acad. Sci.* **1266**, 94–106 (2012).

111. Tormin, A. *et al.* Characterization of bone marrow-derived mesenchymal stromal cells (MSC) based on gene expression profiling of functionally defined MSC subsets. *Cytotherapy* **11**, 114–128 (2009).

112. Vogel, W. *et al.* Heterogeneity among human bone marrow-derived mesenchymal stem cells and neural progenitor cells. *Haematologica* **88**, 126–33 (2003).

113. Battula, V. L. *et al.* Isolation of functionally distinct mesenchymal stem cell subsets using antibodies against CD56, CD271, and mesenchymal stem cell antigen-1. *Haematologica* **94**, 173–184 (2009).

114. Bühring, H.-J. *et al.* Novel markers for the prospective isolation of human MSC. *Ann. N. Y. Acad. Sci.* **1106**, 262–71 (2007).

115. Li, H. *et al.* Low/negative expression of PDGFR-alpha identifies the candidate primary mesenchymal stromal cells in adult human bone marrow, Supplementary information. *Stem Cell Reports* **3**, 965–974 (2014).

116. Pinho, S. *et al.* PDGFRα and CD51 mark human Nestin $^{+}$ sphere-forming mesenchymal stem cells capable of hematopoietic progenitor cell expansion. *J. Exp. Med.* **210**, 1351–1367 (2013).

117. Kaltz, N. *et al.* Novel markers of mesenchymal stem cells defined by genome-wide gene expression analysis of stromal cells from different sources. *Exp. Cell Res.* **316**, 2609–17 (2010).

118. Ghazanfari, R., Li, H., Zacharaki, D., Lim, H. C. & Scheding, S. Human Non-Hematopoietic CD271 pos /CD140a low/neg Bone Marrow Stroma Cells Fulfill Stringent Stem Cell Criteria in Serial Transplantations. *Stem Cells Dev.* **25**, 1652–1658 (2016).

119. Mabuchi, Y. *et al.* LNGFR+THY-1+VCAM-1hi+ Cells Reveal Functionally Distinct Subpopulations in Mesenchymal Stem Cells. *Stem Cell Reports* **1**, 152–165 (2013).

120. Tormin, A. *et al.* CD146 expression on primary nonhematopoietic bone marrow stem cells is correlated with in situ localization. *Blood* **117**, 5067–5077 (2011).

121. Congdon, K. L. *et al.* Activation of Wnt Signaling in Hematopoietic Regeneration. *Stem Cells* **26**, 1202–1210 (2008).

122. Le, Y. *et al.* Adipogenic Mesenchymal Stromal Cells from Bone Marrow and Their Hematopoietic Supportive Role: Towards Understanding the Permissive Marrow Microenvironment in Acute Myeloid Leukemia. *Stem Cell Rev. Reports* **12**, 235–244 (2016).

123. Galipeau, J. Concerns arising from MSC retrieval from cryostorage and effect on immune suppressive function and pharmaceutical usage in clinical trials. *ISBT Sci. Ser.* **8**, 100–101 (2013).

124. Ragoonanan, V., Hubel, A. & Aksan, A. Response of the cell membrane-cytoskeleton complex to osmotic and freeze/thaw stresses. *Cryobiology* **61**, 335–44 (2010).

125. Takata, Y. *et al.* Generation of iPS cells using a BacMam multigene expression system. *Cell Struct. Funct.* **36**, 209–22 (2011).

126. Ledran, M. H. *et al.* Efficient hematopoietic differentiation of human embryonic stem cells on stromal cells derived from hematopoietic niches. *Cell Stem Cell* **3**, 85–98 (2008).

127. Garz, A.-K. *et al.* Azacitidine combined with the selective FLT3 kinase inhibitor crenolanib disrupts stromal protection and inhibits expansion of residual leukemia-initiating cells in FLT3-ITD AML with concurrent epigenetic mutations. *Oncotarget* **8**, 108738–108759 (2017).

128. Oostendorp, R. A. J. *et al.* Stromal cell lines from mouse aorta-gonads-mesonephros subregions are potent supporters of hematopoietic stem cell activity. *Blood* **99**, 1183–

9 (2002).

129. Parmar, A. *et al.* Stromal niche cells protect early leukemic FLT3-ITD+ progenitor cells against first-generation FLT3 tyrosine kinase inhibitors. *Cancer Res.* **71**, 4696–706 (2011).

130. Anthony, B. A. & Link, D. C. Regulation of hematopoietic stem cells by bone marrow stromal cells. *Trends Immunol.* **35**, 32–37 (2014).

131. Boulais, P. E. & Frenette, P. S. Making sense of hematopoietic stem cell niches. *Blood* **125**, 2621–9 (2015).

132. Calvi, L. M. & Link, D. C. The hematopoietic stem cell niche in homeostasis and disease. *Blood* **126**, 2443–51 (2015).

133. Duarte, D., Hawkins, E. D. & Lo Celso, C. The interplay of leukemia cells and the bone marrow microenvironment. *Blood* **131**, 1507–1511 (2018).

134. Frenette, P. S., Pinho, S., Lucas, D. & Scheiermann, C. Mesenchymal Stem Cell: Keystone of the Hematopoietic Stem Cell Niche and a Stepping-Stone for Regenerative Medicine. *Annu. Rev. Immunol.* **31**, 285–316 (2013).

135. Chandran, P. *et al.* Mesenchymal stromal cells from patients with acute myeloid leukemia have altered capacity to expand differentiated hematopoietic progenitors. *Leuk. Res.* **39**, 486–493 (2015).

136. Zambetti, N. A. *et al.* Mesenchymal Inflammation Drives Genotoxic Stress in Hematopoietic Stem Cells and Predicts Disease Evolution in Human Pre-leukemia. *Cell Stem Cell* **19**, 613–627 (2016).

137. Churchman, S. M. *et al.* Transcriptional profile of native CD271+ multipotential stromal cells: evidence for multiple fates, with prominent osteogenic and Wnt pathway signaling activity. *Arthritis Rheum.* **64**, 2632–43 (2012).

138. Qian, H., Le Blanc, K. & Sigvardsson, M. Primary Mesenchymal Stem and Progenitor Cells from Bone Marrow Lack Expression of CD44 Protein. *J. Biol. Chem.* **287**, 25795–25807 (2012).

139. Jones, E. A. *et al.* Isolation and characterization of bone marrow multipotential mesenchymal progenitor cells. *Arthritis Rheum.* **46**, 3349–60 (2002).

140. Quirici, N. *et al.* Isolation of bone marrow mesenchymal stem cells by anti-nerve growth factor receptor antibodies. *Exp. Hematol.* **30**, 783–91 (2002).

141. Bieback, K. Platelet lysate as replacement for fetal bovine serum in mesenchymal stromal cell cultures. *Transfus. Med. Hemother.* **40**, 326–35 (2013).

142. Gregory, C. A., Reyes, E., Whitney, M. J. & Spees, J. L. Enhanced engraftment of mesenchymal stem cells in a cutaneous wound model by culture in allogenic species-specific serum and administration in fibrin constructs. *Stem Cells* **24**, 2232–43 (2006).

143. Mackensen, A., Drager, R., Schlesier, M., Mertelsmann, R. & Lindemann, A. Presence of IgE antibodies to bovine serum albumin in a patient developing anaphylaxis after vaccination with human peptide-pulsed dendritic cells. *Cancer Immunol. Immunother.*

49, 152–156 (2000).

144. Selvaggi, T. A., Walker, R. E. & Fleisher, T. A. Development of antibodies to fetal calf serum with arthus-like reactions in human immunodeficiency virus-infected patients given syngeneic lymphocyte infusions. *Blood* **89**, 776–9 (1997).

145. Tuschong, L., Soenen, S. L., Blaese, R. M., Candotti, F. & Muul, L. M. Immune Response to Fetal Calf Serum by Two Adenosine Deaminase-Deficient Patients After T Cell Gene Therapy. *Hum. Gene Ther.* **13**, 1605–1610 (2002).

146. Crespo-Diaz, R. *et al.* Platelet lysate consisting of a natural repair proteome supports human mesenchymal stem cell proliferation and chromosomal stability. *Cell Transplant.* **20**, 797–811 (2011).

147. Schallmoser, K. *et al.* Human platelet lysate can replace fetal bovine serum for clinical-scale expansion of functional mesenchymal stromal cells. *Transfusion* **47**, 1436–46 (2007).

148. Shahdadfar, A., Frønsdal, K., Haug, T., Reinholt, F. P. & Brinchmann, J. E. In vitro expansion of human mesenchymal stem cells: choice of serum is a determinant of cell proliferation, differentiation, gene expression, and transcriptome stability. *Stem Cells* **23**, 1357–66 (2005).

149. Hirose, M. *et al.* Osteogenic potential of cryopreserved human bone marrow-derived mesenchymal cells after thawing in culture. *Mater. Sci. Eng. C* **24**, 355–359 (2004).

150. Xiang, Y. *et al.* Ex vivo expansion, adipogenesis and neurogenesis of cryopreserved human bone marrow mesenchymal stem cells. *Cell Biol. Int.* **31**, 444–450 (2007).

151. Liu, G., Shu, C., Cui, L., Liu, W. & Cao, Y. Tissue-engineered bone formation with cryopreserved human bone marrow mesenchymal stem cells. *Cryobiology* **56**, 209–215 (2008).

152. Liu, Y. *et al.* Cryopreservation of human bone marrow-derived mesenchymal stem cells with reduced dimethylsulfoxide and well-defined freezing solutions. *Biotechnol. Prog.* **26**, 1635–1643 (2010).

153. Berz, D., McCormack, E. M., Winer, E. S., Colvin, G. A. & Quesenberry, P. J. Cryopreservation of hematopoietic stem cells. *Am. J. Hematol.* **82**, 463–472 (2007).

154. Berz, D. & Colvin, G. Cryopreservation of Hematopoietic and Non-Hematopoietic Stem Cells – A Review for the Clinician. in *New Advances in Stem Cell Transplantation* (ed. Demirer, T.) 231–266 (InTech, 2012). doi:10.5772/1322

155. Liu, G. *et al.* Evaluation of the viability and osteogenic differentiation of cryopreserved human adipose-derived stem cells. *Cryobiology* **57**, 18–24 (2008).

156. Thirumala, S., Goebel, W. S. & Woods, E. J. Clinical grade adult stem cell banking. *Organogenesis* **5**, 143–154 (2009).

157. Pollock, K., Sumstad, D., Kadidlo, D., McKenna, D. H. & Hubel, A. Clinical mesenchymal stromal cell products undergo functional changes in response to freezing. *Cytotherapy* **17**, 38–45 (2015).

158. Pollock, K. *et al.* Improved Post-Thaw Function and Epigenetic Changes in Mesenchymal Stromal Cells Cryopreserved Using Multicomponent Osmolyte Solutions. *Stem Cells Dev.* **26**, 828–842 (2017).

159. Moll, G. *et al.* Do Cryopreserved Mesenchymal Stromal Cells Display Impaired Immunomodulatory and Therapeutic Properties? *Stem Cells* **32**, 2430–2442 (2014).

160. François, M. *et al.* Cryopreserved mesenchymal stromal cells display impaired immunosuppressive properties as a result of heat-shock response and impaired interferon-γ licensing. *Cytotherapy* **14**, 147–152 (2012).

161. Al-Saqi, S. H. *et al.* Defined serum- and xeno-free cryopreservation of mesenchymal stem cells. *Cell Tissue Bank.* **16**, 181–193 (2015).

162. Iwatani, M. *et al.* Dimethyl Sulfoxide Has an Impact on Epigenetic Profile in Mouse Embryoid Body. *Stem Cells* **24**, 2549–2556 (2006).

163. Thaler, R., Spitzer, S., Karlic, H., Klaushofer, K. & Varga, F. DMSO is a strong inducer of DNA hydroxymethylation in pre-osteoblastic MC3T3-E1 cells. *Epigenetics* **7**, 635–651 (2012).

164. Chinnadurai, R. *et al.* Cryopreserved Mesenchymal Stromal Cells Are Susceptible to T-Cell Mediated Apoptosis Which Is Partly Rescued by IFNγ Licensing. *Stem Cells* **34**, 2429–2442 (2016).

165. Chinnadurai, R. *et al.* Actin cytoskeletal disruption following cryopreservation alters the biodistribution of human mesenchymal stromal cells in vivo. *Stem cell reports* **3**, 60–72 (2014).

166. Júnior, A. M. *et al.* Neurotoxicity associated with dimethylsulfoxide-preserved hematopoietic progenitor cell infusion. *Bone Marrow Transplant.* **41**, 95–6 (2008).

167. Pal, R., Hanwate, M. & Totey, S. M. Effect of holding time, temperature and different parenteral solutions on viability and functionality of adult bone marrow-derived mesenchymal stem cells before transplantation. *J. Tissue Eng. Regen. Med.* **2**, 436–444 (2008).

168. Ragoonanan, V., Less, R. & Aksan, A. Response of the cell membrane–cytoskeleton complex to osmotic and freeze/thaw stresses. Part 2: The link between the state of the membrane–cytoskeleton complex and the cellular damage. *Cryobiology* **66**, 96–104 (2013).

169. Ock, S.-A. & Rho, G.-J. Effect of dimethyl sulfoxide (DMSO) on cryopreservation of porcine mesenchymal stem cells (pMSCs). *Cell Transplant.* **20**, 1231–9 (2011).

170. Xu, X., Liu, Y., Cui, Z., Wei, Y. & Zhang, L. Effects of osmotic and cold shock on adherent human mesenchymal stem cells during cryopreservation. *J. Biotechnol.* **162**, 224–31 (2012).

171. Copland, I. B. & Galipeau, J. Death and inflammation following somatic cell transplantation. *Semin. Immunopathol.* **33**, 535–50 (2011).

172. Liu, L. *et al.* Maintaining RNA Integrity for Transcriptomic Profiling of Ex Vivo Cultured

Limbal Epithelial Stem Cells after Fluorescence-Activated Cell Sorting (FACS). *Biol. Proced. Online* **19**, 15 (2017).

173. Mollet, M., Godoy-Silva, R., Berdugo, C. & Chalmers, J. J. Acute hydrodynamic forces and apoptosis: a complex question. *Biotechnol. Bioeng.* **98**, 772–788 (2007).

174. Suh, T. K., Schenk, J. L. & Seidel, G. E. J. High pressure flow cytometric sorting damages sperm. *Theriogenology* **64**, 1035–1048 (2005).

175. Cui, L.-L., Kinnunen, T., Boltze, J., Nystedt, J. & Jolkkonen, J. Clumping and Viability of Bone Marrow Derived Mesenchymal Stromal Cells under Different Preparation Procedures: A Flow Cytometry-Based In Vitro Study. *Stem Cells Int.* **2016**, 1764938 (2016).

176. Olivieri, E. H. R. *et al.* Biobanking Practice: RNA Storage at Low Concentration Affects Integrity. *Biopreserv. Biobank.* **12**, 46–52 (2014).

177. Poncin, G. *et al.* Characterization of spontaneous bone marrow recovery after sublethal total body irradiation: importance of the osteoblastic/adipocytic balance. *PLoS One* **7**, e30818 (2012).

178. Wu, Y. *et al.* Impaired Expression of Focal Adhesion Kinase in Mesenchymal Stromal Cells from Low-Risk Myelodysplastic Syndrome Patients. *Front. Oncol.* **7**, 164 (2017).

179. Varga, G. *et al.* Inappropriate notch activity and limited mesenchymal stem cell plasticity in the bone marrow of patients with myelodysplastic syndromes. *Pathol. Oncol. Res.* **13**, 311–319 (2007).

180. Wenk, C. *et al.* Direct modulation of the bone marrow mesenchymal stromal cell compartment by azacitidine enhances healthy hematopoiesis. *Blood Adv.* **2**, 3447–3461 (2018).

181. Hudak, C. S. *et al.* Pref-1 Marks Very Early Mesenchymal Precursors Required for Adipose Tissue Development and Expansion. *Cell Rep.* **8**, 678–687 (2014).

182. Moon, Y. S. *et al.* Mice lacking paternally expressed Pref-1/Dlk1 display growth retardation and accelerated adiposity. *Mol. Cell. Biol.* **22**, 5585–92 (2002).

183. Wermter, A.-K. *et al.* Preferential reciprocal transfer of paternal/maternal DLK1 alleles to obese children: first evidence of polar overdominance in humans. *Eur. J. Hum. Genet.* **16**, 1126–34 (2008).

184. Gelelete, C. B. *et al.* Overweight as a prognostic factor in children with acute lymphoblastic leukemia. *Obesity (Silver Spring).* **19**, 1908–11 (2011).

185. Lichtman, M. A. Obesity and the Risk for a Hematological Malignancy: Leukemia, Lymphoma, or Myeloma. *Oncologist* **15**, 1083–1101 (2010).

186. Meloni, G. *et al.* Obesity and autologous stem cell transplantation in acute myeloid leukemia. *Bone Marrow Transplant.* **28**, 365–7 (2001).

187. Poynter, J. N. *et al.* Obesity over the life course and risk of acute myeloid leukemia and myelodysplastic syndromes. *Cancer Epidemiol.* **40**, 134–140 (2016).

188. Ahmadian, M., E Duncan, R., Jaworski, K., Sarkadi-Nagy, E. & Sul, H. S. Triacylglycerol metabolism in adipose tissue. *Future Lipidol.* **2**, 229–237 (2007).

189. Mason, P. *et al.* SCD1 inhibition causes cancer cell death by depleting mono-unsaturated fatty acids. *PLoS One* **7**, e33823 (2012).

190. Menendez, J. A. & Lupu, R. Fatty acid synthase and the lipogenic phenotype in cancer pathogenesis. *Nat. Rev. Cancer* **7**, 763–77 (2007).

191. Southam, A. D. *et al.* Drug Redeployment to Kill Leukemia and Lymphoma Cells by Disrupting SCD1-Mediated Synthesis of Monounsaturated Fatty Acids. *Cancer Res.* **75**, 2530–40 (2015).

192. Behan, J. W. *et al.* Adipocytes impair leukemia treatment in mice. *Cancer Res.* **69**, 7867–74 (2009).

193. Samudio, I. *et al.* Pharmacologic inhibition of fatty acid oxidation sensitizes human leukemia cells to apoptosis induction. *J. Clin. Invest.* **120**, 142–56 (2010).

194. Tabe, Y. *et al.* Bone Marrow Adipocytes Facilitate Fatty Acid Oxidation Activating AMPK and a Transcriptional Network Supporting Survival of Acute Monocytic Leukemia Cells. *Cancer Res.* **77**, 1453–1464 (2017).

195. Ye, H. *et al.* Leukemic Stem Cells Evade Chemotherapy by Metabolic Adaptation to an Adipose Tissue Niche. *Cell Stem Cell* **19**, 23–37 (2016).

196. González, M. J. *et al.* DLK1 is a novel inflammatory inhibitor which interferes with NOTCH1 signaling in TLR-activated murine macrophages. *Eur. J. Immunol.* **45**, 2615–2627 (2015).

197. Moseti, D., Regassa, A. & Kim, W.-K. Molecular Regulation of Adipogenesis and Potential Anti-Adipogenic Bioactive Molecules. *Int. J. Mol. Sci.* **17**, 1–24 (2016).

198. Prokesch, A., Hackl, H., Hakim-Weber, R., Bornstein, S. R. & Trajanoski, Z. Novel insights into adipogenesis from omics data. *Curr. Med. Chem.* **16**, 2952–64 (2009).

199. Baladrón, V. *et al.* The EGF-like homeotic protein dlk affects cell growth and interacts with growth-modulating molecules in the yeast two-hybrid system. *Biochem. Biophys. Res. Commun.* **291**, 193–204 (2002).

200. Urs, S. *et al.* Effect of soluble Jagged1-mediated inhibition of Notch signaling on proliferation and differentiation of an adipocyte progenitor cell model. *Adipocyte* **1**, 46–57 (2012).

201. Grochowski, C. M., Loomes, K. M. & Spinner, N. B. Jagged1 (JAG1): Structure, expression, and disease associations. *Gene* **576**, 381–4 (2016).

202. Ross, D. A., Rao, P. K. & Kadesch, T. Dual roles for the Notch target gene Hes-1 in the differentiation of 3T3-L1 preadipocytes. *Mol. Cell. Biol.* **24**, 3505–13 (2004).

203. Khoury, H., Suarez-Saiz, F., Wu, S. & Minden, M. D. An upstream insulator regulates DLK1 imprinting in AML. *Blood* **115**, 2260–3 (2010).

204. Sakajiri, S. *et al.* Dlk1 in normal and abnormal hematopoiesis. *Leukemia* **19**, 1404–10

(2005).

205. Charalambous, M. *et al.* DLK1/PREF1 regulates nutrient metabolism and protects from steatosis. *Proc. Natl. Acad. Sci. U. S. A.* **111**, 16088–93 (2014).

206. Ferrón, S. R. *et al.* Postnatal loss of Dlk1 imprinting in stem cells and niche astrocytes regulates neurogenesis. *Nature* **475**, 381–5 (2011).

207. Garcés, C., Ruiz-Hidalgo, M. J., Bonvini, E., Goldstein, J. & Laborda, J. Adipocyte differentiation is modulated by secreted delta-like (dlk) variants and requires the expression of membrane-associated dlk. *Differentiation.* **64**, 103–14 (1999).

208. da Rocha, S. T. *et al.* Gene dosage effects of the imprinted delta-like homologue 1 (dlk1/pref1) in development: implications for the evolution of imprinting. *PLoS Genet.* **5**, e1000392 (2009).

8 Appendices

8.1 List of Tables

8.2 List of Figures

8.3 Abbreviations

AGC1	Aggrecan
AML	Acute myeloid leukemia
BFU-E	Burst-forming unit erythrocyte
BM	Bone marrow
BSA	Bovine serum albumin
CAR	CXCL12-abundant reticular
CD	Cluster of differentiation
cDNA	Complementary DNA
CFU	Colony-forming unit
CFU-F	Colony-forming unit fibroblast
CFU-G	Colony-forming unit granulocyte
CFU-GEMM	Colony-forming unit granulocyte, erythrocyte, macrophage, megakaryocyte
CFU-GM	Colony-forming unit granulocyte, macrophage
CFU-M	Colony-forming unit macrophage
CLP	Common lymphoid progenitor
CMP	Common myeloid progenitor
CXCL12	C-X-C motif chemokine ligand 12
ddH_2O	Double distilled H_2O
Dlk1	Delta-like 1
DNA	Deoxyribonucleic acid
DTT	Dithiothreitol
ECL	Enhanced chemiluminescence
EDTA	Ethylenediaminetetraacetic acid
FA	Fatty acids
FACS	Fluorescence activated cell sorting
FAO	Fatty acid oxidation
Flt3 ligand	Fms-related tyrosine kinase 3 ligand
GMP	Granulocyte-monocyte progenitor
HSC	Hematopoietic stem cell
HSPC	Hematopoietic stem and progenitor cells
IL-1b	Interleukin 1 beta
IL-3	Interleukin 3
IL-6	Interleukin 6
ITGA11	Integrin subunit alpha 11
LDL	Low density lipoprotein
LepR	Leptin receptor
Lin	Lineage
LPL	Lipoprotein lipase
LSC	Leukemic stem cell
LTC	Long-term culture
LTC-IC	Long-term culture-initiating cell
LT-HSC	Long-term hematopoietic stem cells
MDS	Myelodysplastic syndromes
MEP	Megakaryocyte-erythrocyte progenitor

MNC	Mononuclear cell
MPN	Myeloproliferative neoplasms
MPP	Multipotent progenitors
mRNA	Messenger RNA
MSC	Mesenchymal stem cell
NGS	Next generation sequencing
NK cell	Natural killer cell
OCN	Osteocalcin
Osx	Osterix
PBS	Phosphate-buffered saline
PDGFRa	Platelet derived growth factor receptor alpha
pHPL	Pooled human platelet lysate
PPARγ	Peroxisome proliferator activated receptor gamma
PVDF	Polyvinylidene difluoride
qRT-PCR	Quantitative reverse transcription polymerase chain reaction
RNA	Ribonucleic acid
RNAseq	RNA sequencing
RUNX2	Runt related transcription factor 2
sAML	Secondary acute myeloid leukemia
SCF	Stem cell factor
SDS-PAGE	Sodium dodecyl sulphate polyacrylamide gel electrophoresis
SFM	Serum-free medium
Sfrp1	Secreted frizzled related protein 1
SOX9	SRY-box 9
SPP1	Secreted phosphoprotein 1
TACE	Tumor necrosis factor-α-converting enzyme
tAML	Therapy-induced AML
TBS	Tris-buffered saline
Tgln	Transgelin
TNFα	Tumor necrosis factor alpha
TPO	Thrombopoietin
Wnt10b	Wnt family member 10B
Wnt5a	Wnt family member 5A

8.4 List of Previous Publications

Wenk, C., Garz, A.-K., Grath, S., Huberle, C., Witham. D., **Weickert, M.-T.**, Malinverni, R., Niggemeyer, J., Kyncl, M., Hecker, J., Pagel, C., Mulholland, C. B. , Müller-Thomas, C., Leonhardt, H., Bassermann, F., Oostendorp, R. A. J., Metzeler, K. H., Buschbeck, M., Götze, K. S. (2018): Direct modulation of the bone marrow mesenchymal stromal cell compartment by azacitidine enhances healthy hematopoiesis, Blood Adv. 2018;2(23):3447-3461

Garz, A.-K., Wolf, S., Grath, S., Gaidzik, V., Habringer, S., Vick, B., Rudelius, M., Ziegenhain, C., Herold, S., **Weickert, M.-T.**, Smets, M., Peschel, C., Oostendorp, R. A. J., Bultmann, S., Jeremias, I., Thiede, C., Döhner, K., Keller, U., Götze, K. S. (2017): Azacitidine combined with the selective FLT3 kinase inhibitor crenolanib disrupts stromal protection and inhibits expansion of residual leukemia-initiating cells in *FLT3*-ITD AML with concurrent epigenetic mutations, Oncotarget 2017;8(65):108738-108759

Weickert, M.-T.; Garz, A.-K.; Hecker, J.; Ziegenhain, C.; Grath, S.; Strunk, D.; Peschel, C.; Enard, W.; Oostendorp, R. A. J.; Goetze, K. S. (2017): Significantly Reduced CFU-F Frequency and Increased Adipogenic Differentiation of Mesenchymal Stem Cells (MSC) in Myelodysplastic Syndromes (MDS) and Acute Myeloid Leukemia (AML), Annals of Hematology, Vol. 96: S52-S52, Acute Leukemias XVI: Abstract 7

Hannus, M., Beitzinger, M., Engelmann, J. C., **Weickert, M.-T.**, Spang, R., Hannus, S., Meister, G. (2014): siPools: highly complex but accurately defined siRNA pools eliminate off-target effects, Nucleic Acids Res. 2014;42(12):8049-8061

9 Acknowledgements

First, I would like to thank my supervisor Katharina Götze for her support and guidance throughout this project, sharing her scientific and clinical expertise and greatly broadening my knowledge in the hemato-oncology field.

Furthermore, I want to thank Christian Peschel, Head of the Department of Medicine III at Klinikum rechts der Isar (TUM), and his successor Florian Bassermann for giving me the opportunity to conduct my Dr. rer. nat. thesis at their department.

I also want to thank my mentor Robert Oostendorp for his support, stimulating discussions and helpful feedback. My thanks go also to Bernhard Küster for his support as my second examiner.

In addition, I want to acknowledge the support and contributions of our collaborators: Martin Nolde, who provided us with fresh femoral heads from hip replacement surgery in the SANA-Klinik München-Solln, and the whole team of Aktion Knochenmarksspende Bayern in Gauting, who provided us with residuals in BM filter bags from healthy donors after stem cell transplantation; Dirk Strunk and his team at the Institute of Experimental & Clinical Cell Therapy of Paracelsus Medical University in Salzburg for instructions and advice on isolation and culture of primary MSC; Lynette Henkel, Immanuel Andrä, and Matthias Schiemann from the CyTUM-MIH facility for their support with the cell sorting experiments; Christoph Ziegenhain, who constructed RNA libraries and performed RNAseq, as well as Wolfgang Enard and his team, Sonja Grath, Ines Hellmann, and Beate Vieth (all members of the Department Biology II, LMU), who performed bioinformatic analyses; Christoph also supported with the bioanalyzer assays together with Johanna Geuder. My project was supported by grants from FOR2033 and SFB1243 of the DFG.

Special thanks go to my wonderful colleagues and friends Judith Hecker, Michèle Buck, and Theresa Sippenauer for their practical, scientific, and emotional support in- and outside of the lab.

A big thank you to all members of the Götze, Oostendorp and Keller research groups for your practical support, fruitful scientific discussions, and great working environment.

To my family and my boyfriend Julius: Thank you so very much for your continuous support, encouragement, love, and patience. Without you, I wouldn’t be where I am today.